2015-08-07

Exploring New Strategies to Overcome Resistance in Glioblastoma Multiforme: A Dissertation

Yulian P. Ellis
University of Massachusetts Medical School

EXPLORING NEW STRATEGIES TO OVERCOME RESISTANCE IN GLIOBLASTOMA MULTIFORME

A Dissertation Presented

By

YULIAN PAOLA ELLIS

Submitted to the Faculty of the

University of Massachusetts Graduate School of Biomedical Sciences, Worcester

in partial fulfillment of the requirements for the degree of

DOCTOR OF PHILOSOPHY

August 7, 2015

CANCER BIOLOGY

EXPLORING NEW STRATEGIES TO OVERCOME RESISTANCE IN GLIOBLASTOMA MULTIFORME

A Dissertation Presented
By

YULIAN PAOLA ELLIS

The signatures of the Dissertation Defense Committee signifies completion and approval as to style and content of the Dissertation

Alonzo Ross, Ph.D., Thesis Advisor

Arthur Mercurio, Ph.D., Member of Committee

Nicholas Rhind, Ph.D., Member of Committee

Daniel Jay, Ph.D., Member of Committee

The signature of the Chair of the Committee signifies that the written dissertation meets the requirements of the Dissertation Committee

Leslie Shaw, Ph.D., Chair of Committee

The signature of the Dean of the Graduate School of Biomedical Sciences signifies that the student has met all graduation requirements of the school.

Anthony Carruthers, Ph.D.,
Dean of the Graduate School of Biomedical Sciences

Cancer Biology Program
August 7, 2015

Acknowledgements:

I want to begin by thanking my mentor, Dr. Alonzo Ross, as he has been instrumental in my graduate development. Rarely will you find a professor who has his student's best interest in mind, 100% of the time. Alonzo provided me with constant support and guidance while allowing independence needed to grow as a researcher. He was kind, patient, and always encouraging.

I am grateful to my lab mate, Jessica Weatherbee. Thank you for always listening and offering your advice. The last three years of school, away from my husband and daughters, were made easier with your company, the constant trips back and forth from the airport, and your willingness to help when I was out of town.

I want to acknowledge and thank Dr. Richard Moser for supplying numerous tumor samples and his insightful discussions during our lab meetings.

My time at UMASS and in Massachusetts would not have been the same without my amazing group of friends. Christine, Candace, Ryan, Nate, Jay, and Mike, I found myself far from family, or any support system, when I first moved to MA but you all became my family. There was never a time I could not count on you, whether it was to help move, babysit, or simply be there to talk and grab coffee.

I would like to thank my family who has never faltered in their support, love, and encouragement. Mom and dad, all the sacrifices you have made throughout the years have not gone unnoticed! Katheryn, you are so self-giving; thank you for all those late nights you stayed up with me while I wrote my dissertation. Steven, despite you being so far away in Mozambique, your encouraging words always found their way to me.

To my husband Kyle and my daughters Isabella, Katheryn, and Alexandra; you are my all! Kyle, I would not have gotten this far without your support. I cannot count the number of times you told me not to give up; always reassuring me I could do this. You sacrificed day in and day out so that I could go to school and our family was provided for. To my smart, funny, kind daughters you inspire me every day. Thank you for making this journey fun.

ABSTRACT

Glioblastoma multiforme (GBM) tumors are highly malignant in nature and despite an aggressive therapy regimen, long–term survival for glioma patients is uncommon as cells with intrinsic or acquired resistance to treatment repopulate the tumor. This creates the need to investigate new therapies for enhancing GBM treatment outside of the standard of care, which includes Temozolomide (TMZ). Our lab focused on two novel strategies to overcome resistance in GBMs. In our first approach, the cellular responses of GBM cell lines to two new TMZ analogues, DP68 and DP86, are reported. The efficacy of these compounds was independent of DNA repair mediated by Methyl Guanine Methyl Transferase (MGMT) and the mismatch repair (MMR) pathway. DP68 or DP86 treated cells do not give rise to secondary spheres, demonstrating that they are no longer capable of self-renewal. DP68-induced damage includes interstrand DNA crosslinks and exhibits a distinct S-phase accumulation before G2/M arrest; a profile that is not observed for TMZ-treated cells. DP68 induces a strong DNA damage response and suppression of FANCD2 expression or ATR expression/kinase activity enhanced the anti-GBM effects of DP68. Collectively, these data demonstrate that DP68, and to a lesser extent DP86, are potent anti-GBM compounds that circumvent TMZ resistance and inhibit recovery of cultures. Our second approach stems from a previous discovery in our lab which demonstrated that the combination of TMZ with Notch inhibition, using a gamma secretase inhibitor (GSI), enhances GBM therapy. Efficacy of TMZ + GSI treatment is partially due to GBM cells shifting into a permanent senescent state. We sought to identify a miR signature that mimics the effects of TMZ + GSI as an alternative

approach to enhance GBM therapy. MiR-34a expression was highly upregulated in response to TMZ or TMZ + GSI treatment. Exogenous expression of miR-34a revealed that it functions as a tumor suppressor and mimicked the *in vitro* effects of TMZ + GSI treatment. Additionaly, miR-34a overexpression leads to the downregulation of Notch family members. Together these two studies contribute to our understanding of the complex mechanisms driving resistance in GBM tumors and suggest strategies to develop more effective therapies.

Table of Contents

List of Tables

List of Figures

List of Abbreviations

7-AAD,	7 aminoactinomycin D
APNG,	alkylpurine-DNA-N-glycosylase
ATM,	ataxia telangiectasia mutated
ATR,	ataxia telangiectasia and Rad-3 related
BBB,	blood brain barrier
BCNU,	bis-chloroethylnitrosourea, Carmustine
bFGF,	basic fibroblast growth factor
BiSEQ,	bisulfite sequencing
BRCA1,	breast cancer susceptibility gene 1
BRCA2,	breast cancer susceptibility gene 2
BSA,	bovine serum albumin
CHK1,	checkpoint kinase 1
CHK2,	checkpoint kinase 2
CTNNBIP1,	β-catenin, beta-catenin
DAPI,	4',6-diamidino-2-phenylindole
DAPT,	N-[N-(3,5-difluorophenacetyl)-L-alanyl]-S-phenylglycine t-butylester
DDR,	DNA damage response
DMEM,	dulbecco's modified eagle's medium
DMSO,	dimethylsulfoxide
DSB,	double strand breaks
ECL,	enhanced chemoluminescence

EGF, epidermal growth factor

EGFR, epidermal growth factor receptor

EGFRvIII, epidermal growth factor receptor variant III

EORTC, European Organization for Research and Treatment of Cancer

FA, Fanconi anemia

FANCD2, Fanconi anemia complementation group D2

FBS, fetal bovine serum

FL, full length

GBM, glioblastoma multiforme

GFP, green fluorescent protein

GSI, gamma secretase inhibitor

Gy, gray

H2AX, *H2A* histone family, member X

HRR, homologous recombination repair

ICD, intracellular domain

ICL, interstrand crosslinks

IHC, immunohistochemistry

IP, intraperitoneal

IR, ionizing radiation

IT, intratumoral

KAP1, KRAB associated protein 1

LDEV, lactate dehydrogenase elevating virus

LOH, loss of heterozygosity

LRP6, low density lipoprotein receptor-related *protein* 6

MGMT, O^6-methyl-guanine methyltransferase

miRNA, microRNA

MLH, mutL homolog

MMR, mismatch repair

MSH, mutS homolog

MSI, microsatellite instability

MSP, methylation-specific PCR

MTIC, 3-methyl-(triazen-1-yl)imidazole-4-carboxamide

MTT, 3-(4,5-Dimethylthiazol-2-Yl)-2,5-Diphenyltetrazolium Bromide

*N*7-G, *N*7-guanine

*N*3-A, *N*3-adenine

NABTT, New Approaches to Brain Tumor Therapy

NHA, normal human astrocytes

NHEJ, non-homologous end joining

NICD, notch intracellular domain

*O*6-BG, O6-benzylguanine

*O*6-meG, *O*6-methylguanine

OS, overall survival

PARP, Poly (ADP-Ribose) Polymerase

PaTrin-2, O6-(4-bromothenyl) guanine

PFS,	progression-free survival
PI,	propidium iodide
PMS,	postmeiotic segregation
pol II,	polymerase II
pre-miRNA,	precursor microRNA
pri-miRNA,	primary microRNA
PTEN,	phosphatase and tensin homolog
PVDF,	polyvinylidene difluoride
qRT-PCR,	quantitative real-time PCR
RIPA,	radioimmunoprecipitation assay buffer
RISC,	RNA-induced silencing complex
RT,	room temperature
RTK,	receptor tyrosine kinase
SEM,	standard error of the mean
TBS,	tris-buffered saline
TCGA,	The Cancer Genome Atlas
TMZ,	temozolomide
UTR,	untranslated region
WHO,	World Health Organization

CHAPTER I

INTRODUCTION

Parts of this chapter represent work submitted as:

Ramirez, Y.P.; Weatherbee, J.L.; Wheelhouse, R.T.; Ross, A.H. Glioblastoma Multiforme Therapy and Mechanisms of Resistance. *Pharmaceuticals* **2013**, *6*, 1475-1506, review

Dr. Wheelhouse is responsible for the figures depicting chemical structures and reactions.

Dr. Richard Moser provided MRI scans for Figure 1.1 A and Dr. Thomas Smith provided H&E photos in Figure 1.1 B-C.

CHAPTER I

Introduction

Gliomas

The annual incidence of primary and central nervous system tumors is 6.4 per 100,000 men and women per year. This year alone 22,850 new brain and central nervous system tumor cases are estimated, making up 1.4% of all new cancer cases (Institute 2015). Astrocytomas are a subtype of glioma derived from astrocytes, one of the major types of glial cells (Kimelberg and Nedergaard 2010). Clinically, astrocytomas are divided into four grades established by the World Health Organization (WHO). The classification is based on histology and tumors are given a grading of I-IV depending on presence and extent of nuclear atypia, mitosis, microvascular proliferation, and necrosis (Louis, Ohgaki et al. 2007). Grade I (pilocytic astrocytoma) and II (diffuse astrocytoma) tumors are considered low grade while Grade III (anaplastic astrocytoma) and IV (Glioblastoma Multiforme (GBM)) are high-grade, malignant tumors (**Figure 1.1 A**). These astrocytic tumors are rapidly proliferating, heterogeneous, have aberrant vascularization, and are diffuse infiltrative in nature (Veliz, Loo et al. 2015), meaning tumors grows intermingled with normal brain cells. This makes it hard to define tumor borders and makes surgical resection challenging and not curative. GBMs are different from the low grade tumors in that they have microvascular proliferation and necrosis (Louis, Ohgaki et al. 2007) (**Figure 1.1 B-C**). These tumors grow so quickly that the vasculature is unable to keep up, resulting in necrosis.

GBMs can be divided into de novo (primary) GBMs and secondary GBMs. Secondary GBMs progress from a lower grade astrocytomas (Ohgaki and Kleihues 2013). Primary GBMs are characterized by EGFR amplification, loss of heterozygosity (LOH) on chromosome 10q, and inactivation of PTEN. On the other hand, secondary GBMs exhibit PDGFR activation and p53 mutations, which are rare in de novo GBMs (Ohgaki and Kleihues 2013; Ahmed, Oborski et al. 2014).

Integrative genomic studies of GBM tumors have given us insights into the signaling networks driving this disease. Of those commonly altered are the p53 and RB pathways, and receptor tyrosine kinases (RTK)-activated pathways (Cancer Genome Atlas Research 2008). The p53 pathway was dysregulated in 85.3% of GBM, RB pathway dysregulated in 78.9%, and RTKs are altered in 67% of GBMs; most GBMs have alterations in all three pathways (Chen, McKay et al. 2012; Brennan, Verhaak et al. 2013). These large studies have elucidated the redundancy of signaling pathways within GBM cells. This is important as it gives us insight into how GBM cells can quickly evade targeted therapies.

The epidermal growth factor receptor (EGFR) is amplified or mutated in ~ 40% of tumors and critical for GBM signaling, contributing to anti-apoptotic, angiogenic, and invasive pathways (Chandramohan, Bao et al. 2013). In addition, PTEN which is frequently inactivated in GBMs (Cancer Genome Atlas Research 2008; Brennan, Verhaak et al. 2013) coupled with activated EGFR signaling, keeps tumors in a constant

proliferative state as a result of downstream activation of the growth and survival PI3K/Akt pathway. One well studied EGFR mutation is the EGFR variant III (EGFR*vIII*), which results from deletion of exons 2-7 of EGFR, leaving the receptor unable to bind to its ligand, and results in constitutively active EGFR signaling (Gan, Kaye et al. 2009). Lack of EGFR or EGFRvIII expression in normal cells makes it an attractive target for therapy. However, EGFR tyrosine kinase inhibitors (TKI), such as Gefitinib and Erlotonib, have shown very little promise in the clinic so far (Perry, Okamoto et al. 2012).

Using large-scale sequencing, novel GBM-associated mutations have been identified (Parsons, Jones et al. 2008). It was found that 50-80% of low-grade gliomas carried mutations of isocitrate dehydrogenase 1 (IDH1) or isocitrate dehydrogenase 2 (IDH2) while later studies showed that IDH mutants are more prevalent in secondary GBMs with 60-90% expressing mutant IDH proteins (Prensner and Chinnaiyan 2011; Zhang, Moore et al. 2013). Although a variety of other tumor types bear IDH mutations, the percentages of mutation-positive tumors are much less than for GBMs. The IDH1 and IDH2 enzymes catalyze the oxidative decarboxylation of isocitrate, producing α-ketogutarate (α-KG) and regenerating NADPH as part of the tricarboxylic (TCA) cycle. For both enzymes, arginines in the catalytic pocket (IDH1 R132 and IDH2 R140 or R172) are mutated. The uniqueness of these mutations suggested a gain-of-function mutation, and a subsequent study demonstrated that these mutated IDH enzymes reduced α-KG to an oncometabolite, 2-hydroxyglutarate (2-HG) (Dang, White et al. 2009).

Overexpression of these mutated IDH enzymes induces histone and DNA hypermethylation and blocks cellular differentiation.

A natural question is whether IDHs are targets for therapy. Although IDH is universally expressed, the unique IDH mutations could be specifically targeted, lowering levels of 2-HG and slowing tumor growth. In two recent studies, promising IDH inhibitors were described (Rohle, Popovici-Muller et al. 2013; Wang, Travins et al. 2013). Both the IDH1 and IDH2 inhibitors showed marked preferences for the cancer-mutated IDH enzymes. Wang et al (Wang, Travins et al. 2013) inhibited the mutated IDH2 enzyme in leukemia cells, slowing cell proliferation and inducing differentiation. Rohle et al (Rohle, Popovici-Muller et al. 2013) used the IDH1 inhibitor to slow proliferation of GBM cells, induce demethylation of histones and enhance astroglial differentiation. These results have exciting applications for the clinic. For example, a mutated IDH inhibitor with low toxicity might delay progression of low-grade to high-grade tumors.

Standard of Care: surgery, radiation, and chemotherapy

In 2000, a phase III study was carried out by the European Organization for Research and Treatment of Cancer (EORTC) and the National Cancer Institute of Canada with the objective of comparing the regimen of TMZ concurrent and adjuvant to radiotherapy versus radiotherapy alone. At the two year time point, a statistically significant increase in survival rate was observed; from 10% with radiation alone to 27%

when radiation was combined with TMZ. For patients, that translates to an increase in median overall survival (OS) of 14.6 months from 12.1 months (Stupp, Mason et al. 2005). As a result of the Stupp et al study, the standard of care now consists of surgical resection, coupled with ionizing radiation, and the chemotherapeutic agent TMZ (Temodar, Temodal) (Stupp, Mason et al. 2005; Stupp, Hegi et al. 2009). Patients receive 30 fractions of 200 cGy five days a week, for six weeks, for a total radiation therapy dose of 60 Gy. TMZ is orally available and treatment begins with a 75 mg/m^2 daily dose while patients are receiving radiation. Adjuvant dose of TMZ increases to 150-200 mg/m^2 for five consecutive days, every four weeks, for a total of 6 months (Grossman, Ye et al. 2011).

Despite aggressive surgical resection and chemotherapy, almost all GBM patients undergo tumor recurrence. Ninety percent of GBM tumors have been shown to recur within 2 cm of the original tumor (Wen and Kesari 2008; Milano, Okunieff et al. 2010). Many patients undergo further surgical resection and therapy options include: rechallenging with TMZ or other alkylating agents (carmustine, lomustine,), platinum drugs, or the VEGF inhibitor, bevacizumab (Avastin®). However, these measures are not curative and ultimately patients succumb to this disease.

Glioma Chemotherapy: TMZ and Gliadel

TMZ is an orally available alkylating drug that crosses the blood brain barrier (BBB) (Zhang, Stevens et al. 2012). It has excellent uptake and distribution behavior, and there is direct evidence of tumor localization (Spiro, Liu et al. 2001). TMZ is a prodrug, and its aqueous chemistry is typical of imidazotetrazine compounds (**Figure 1.2 A**). It undergoes hydrolytic ring opening at neutral or alkaline pH under purely chemical control, and the first significant intermediate is the open-chain triazene MTIC (**Figure 1.2 A**) (Wheelhouse and Stevens 1993).

The activated intermediate MTIC is shared with dacarbazine, a prodrug used against malignant melanoma, which in contrast, requires hepatic demethylation to release MTIC. From MTIC, methyldiazonium is released, which methylates DNA (**Figure 1.2 B**). The majority (70%) of the methyl groups transferred to DNA appear at *N*7-Guanine (*N*7-G) sites with only about 10% at *N*3-Adenine (*N*3-A) and 5% at *O*6-Guanine (*O*6-G) (Denny, Wheelhouse et al. 1994; Zhang, Stevens et al. 2012). P53 status impacts the response TMZ elicits within the cell. The classical prolonged G2/M arrest known to occur following TMZ treatment is characteristic of p53 wild-type cells. In contrast, p53 deficient cells have a minimal G2/M arrest (Hirose et al, Cancer Research 2001).

Gliadel is a biodegradable wafer impregnated with carmustine (bis-chloroethylnitrosourea (BCNU)), a small lipophilic alkylating and interstrand crosslinking nitrosourea (Perry, Chambers et al. 2007; Panigrahi, Das et al. 2011). There

are strong parallels between the mechanisms of prodrug activation and action of carmustine and TMZ (**Figure 1.3)** (Pratt, Ruddon et al. 1994). Under physiological conditions, spontaneous hydrolysis results in fragmentation of the nitrosourea to release an alkyldiazoinium ion (in this case chloroethyldiazonium) and an isocyanate (Bleasdale, Golding et al. 1991). Subsequent reaction of the isocyanate with biological macromolecules is not a major contributor to the pharmacology. Chloroethyldiazonium in aqueous systems has a complex fate (Lown and Chauhan 1981; Lown and Chauhan 1982), but the therapeutic activity is derived from guanine chloroethylation of DNA, in particular at *O*6-G positions, and further reaction of the monoalkylation adducts to form interstrand crosslinks.

Gliadel wafers are implanted in the cranial resection cavity prior to radiotherapy. The Gliadel wafers release high local concentrations of carmustine directly into the tumor bed after surgery when the tumor burden is low (Grossman, Reinhard et al. 1992; Fung, Ewend et al. 1998). The rationale for this approach is that the resection cavities are relatively avascular and Gliadel may target cells missed by systemically administered carmustine. Furthermore, the wafers release carmustine for several weeks. In contrast, systemically administered carmustine persists only for a few hours. Clinical trials demonstrated that Gliadel wafers are safe for both newly diagnosed and recurring GBMs (Kleinberg, Weingart et al. 2004; McGirt, Than et al. 2009). Radiotherapy plus Gliadel showed greater OS than radiotherapy alone. However, the combination of radiotherapy, TMZ and Gliadel did not show a statistically significantly increase in survival over

radiotherapy and TMZ. As a result, radiotherapy and TMZ continue to be the standard therapy for GBMs.

DNA Damage Repair

MGMT

The best-documented mechanism of resistance to TMZ is mediated by the DNA repair protein MGMT, which removes methyl groups from *O*6-meG lesions that arise from TMZ treatment (Park, Kim et al. 2012). During the repair process, the modified base is flipped out of the double helical stack so it can enter the MGMT active site; its position in the DNA duplex being taken by a lysine residue (Pegg 2000). In the active site, base-catalysis generates a reactive thiolate nucleophile from cysteine 145 (in the human form). This cleaves the C-O bond of *O*6-meG in a nucleophilic substitution reaction that results in a mixed thioether product, leading to the inactivation of the protein (**Figure 1.4)** (Daniels, Mol et al. 2000). MGMT is thus a reagent consumed stoichiometrically during the repair reaction, not an enzyme. In the context of TMZ antitumor activity, DNA repair by MGMT is the primary mechanism of drug resistance.

MGMT expression inversely correlates with sensitivity to the alkylating agents TMZ and carmustine in glioma cells and glioma stem-like cells (Gerson 2002; Hermisson, Klumpp et al. 2006; Sato, Sunayama et al. 2011). Differentiated cell lines with elevated levels of MGMT show increased chemoresistance (van Nifterik, van den Berg et al. 2010; Villalva, Cortes et al. 2012). This dependence has been demonstrated by

treating glioma, leukemia, ovarian, and breast cell lines with suicide inactivators of MGMT, *O6*-Benzylguanine (*O6*-BG) (Kanzawa, Bedwell et al. 2003) or 6-[(4-Bromo-2-thienyl) methoxy]-9*H*-purin-2-amine (PaTrin-2) (Barvaux, Ranson et al. 2004; Clemons, Kelly et al. 2005; Turriziani, Caporaso et al. 2006); MGMT inhibition increased sensitivity to TMZ treatment.

Methylation of the MGMT promoter occurs in approximately 45% of newly diagnosed GBM patients and is prognostic for response to TMZ treatment (Hegi, Diserens et al. 2004). Patients with MGMT promoter methylation have increased survival when treated with radiotherapy in combination with TMZ, while patients with MGMT-positive tumors do not benefit as greatly from this dual treatment (Hermisson, Klumpp et al. 2006; Stupp, Hegi et al. 2009). Several methods can be employed to determine MGMT status (mRNA levels, protein levels by immunohistochemistry (IHC), and promoter methylation); however, current evaluations in the clinic usually only assess MGMT protein expression and promoter methylation. It remains unclear which technique has the greatest prognostic value in the clinical setting. In a new retrospective study, Lalezari et al (Lalezari, Chou et al. 2013) focused on 418 patients with newly diagnosed GBMs, of whom 410 were treated with radiotherapy and TMZ. Tumors were analyzed for MGMT protein expression via IHC, promoter methylation by methylation-specific PCR (MSP), and individual CpG sites were analyzed by bisulfite sequencing (BiSEQ). Low MGMT protein expression (<30% positive cells) and high promoter methylation individually correlated with OS and progression-free survival (PFS). MGMT MSP

correlated with MGMT IHC, and IHC status stratified outcome in the methylated group. This data was further validated by BiSEQ analysis of 24 CpG sites within the differentially-methylated region 2 (DMR2) of the MGMT promoter. Protein levels inversely correlated with methylation density in the DMR2 and showed that hypermethylation (≥3 CpG sites) was correlated with higher OS and PFS. Combining analyses of protein expression and promoter methylation offers superior prognosis than individual analyses of these factors and is recommended for testing of newly diagnosed GBMs (Lalezari, Chou et al. 2013).

A subpopulation of GBM patients have low MGMT expression with no detectable promoter methylation (Park, Kim et al. 2012; Lalezari, Chou et al. 2013), indicating that other molecular mechanisms also regulate MGMT expression. Recently, Kreth et al (Kreth, Heyn et al. 2010) focused on the post-transcriptional regulation of MGMT and found that MGMT was subject to alternative polyadenylation, giving rise to transcripts with varying 3' untranslated region (UTR). The longer 3'UTRs were expressed in tumors and absent in normal brain tissue. MGMT protein levels were reduced when the elongated transcript was expressed. These results were independent of the promoter methylation and were attributed to decreased mRNA stability as a result of miRNA regulation. This study provides an explanation for tumors with unmethylated MGMT promoter and low MGMT expression and provides further insight into molecular mechanisms that regulate MGMT expression. Further studies are needed to evaluate

whether the long 3'UTR MGMT transcript is a prognostic factor for survival of GBM patients.

MGMT Therapeutic Targets

Inhibition of MGMT in combination with TMZ has been studied as an approach to improve treatment of GBMs in the clinic. *O6*-BG is a small-molecule pseudosubstrate that transfers a benzyl group to the MGMT active site cysteine 145 residue, thereby, inactivating MGMT and preventing removal of methyl groups from the DNA (Pegg 2000). Initial phase I clinical trials showed that *O6*-BG effectively inhibits MGMT in GBM tumors, but TMZ therapy in combination with *O6*-BG was limited by myelosuppression (Quinn, Desjardins et al. 2005). This enhanced toxicity is attributed to *O6*-BG inhibition of the low levels of MGMT in hematopoietic progenitor cells. Studies on MGMT-/- mice, also demonstrated that damage to bone marrow was the main source of toxicity. This effect can be averted by transplantation of wild-type bone marrow into MGMT-/- mice (Reese, Qin et al. 2001). A new clinical trial will explore the feasibility of infusing hematopoietic progenitors modified to express MGMT via a retroviral vector as a way to overcome the limitation of therapy-induced myelosuppression (Srinivasan and Gold 2012).

One therapeutic strategy that has been evaluated is the use of increased doses and prolonged scheduling of TMZ as a means of depleting MGMT. This approach was shown to decrease MGMT activity in peripheral blood mononuclear cells (Tolcher, Gerson et al.

2003). In addition, a recent phase II study of 58 patients, with first recurrences, evaluated the efficacy and safety of a 21 days on/7 days off regimen at 75-100 mg/m^2/day. Only patients whom had previously received TMZ concomitant and adjuvant radiotherapy were included, and the study was ended when second progressions occurred. This regimen proved to be safe, but none of the patients achieved a complete response. Partial responses for 13 % of patients were observed as well as 6 month PFS of 11 %, showing this regimen had little efficacy for recurrent tumors (Norden, Lesser et al. 2013).

Other approaches utilize RNAi to directly interfere with MGMT protein expression. Using MGMT-siRNAs and a novel liposome, LipoTrust EX Oligo, for delivery, MGMT was efficiently knocked down in glioma cells lines, GBM-stem like cells, and *in vivo* glioma tumors. *In vivo* delivery was effective whether administered intratumorally (IT) in a subcutaneous model or via an osmotic pump in an intracranial model. Both *in vitro* and *in vivo*, MGMT siRNA enhanced sensitivity to TMZ (Kato, Natsume et al. 2010). Another RNAi approach employed a lentiviral-based technology to target MGMT with a small hairpin RNA (Viel, Monfared et al. 2013). MGMT was successfully inhibited in TMZ-resistant glioma cultures, enhancing sensitivity to TMZ for tumors implanted into the flanks of nude mice. Efficient *in vivo* transduction of the shMGMT vector into GBM xenografts decreased MGMT expression and inhibited tumor growth following TMZ treatment. Although this seems a promising therapy, the efficacy and toxicity of these viral vectors require further evaluation.

Post-translational regulation of MGMT occurs by the 26S proteasome, making this a candidate for therapy. Bortezomib (BTZ, PS-341) is a boronic acid dipeptide that inhibits the proteasome and markedly reduces levels of MGMT mRNA and protein (Vlachostergios, Hatzidaki et al. 2013). MGMT is directly regulated by NF-κB. The proteasome activates NF-κB by degrading its inhibitor, IκB. Upon treatment with BTZ, the proteasome is inhibited, IκB is stabilized, NF-κB is not activated, and MGMT levels are reduced. Efficacy of combined BTZ and TMZ therapy differed between glioma lines and was schedule-dependent. MGMT-negative U87MG cell line showed decreased viability and increased apoptosis when TMZ was administered before BTZ, while the opposite was true for MGMT-positive T98G cells. This effect was partially mediated through MGMT downregulation (Vlachostergios, Hatzidaki et al. 2013) and speaks to the importance of sequence of therapy in combination treatments. Primary glioma stem-like cells were more sensitive to proteasome inhibition by BTZ than normal neural stem and progenitor cells due in part to the lower proteasome activity (Gong, Schwartz et al. 2011), making it an attractive therapy to combat recurrence. Phase I studies showed BTZ to be well tolerated with thrombocytopenia being the most common toxicity (Dy, Thomas et al. 2005; Phuphanich, Supko et al. 2010). BTZ is now clinically approved for hematopoietic malignancies (Phuphanich, Supko et al. 2010).

MMR

The MMR pathway is made up of Mut S homologs (MSH) (MSH2, MSH3, and MSH6), MutL homologs (MLH) (MLH1, MLH3), and post meiotic segregation (PMS)

(PMS1, PMS2) (Pal, Permuth-Wey et al. 2008). Important for the repair of mismatch is: the MutSα heterodimer consisting of MSH2 and MSH6, as well as the MutLα heterodimer, made up of MLH1 and PMS2. MutSα recognizes the mispaired nucleotide and subsequently leads to the recruitment of MutLα, displacement of DNA polymerase and PCNA, and recruitment of an exonuclease (EXO1) (Rodrigues, Gomes et al. 2013).

Deficiencies in MMR contribute to TMZ resistance

The response to TMZ treatment does not absolutely correlate with MGMT levels, leading us to believe that additional mechanisms are at play. One mechanism thought to mediate resistance is loss of MMR (Ghosal and Chen 2013). *O*6-meG lesions mismatched with thymine bases are recognized by the MMR. The thymine residue is excised; however, in the absence of MGMT, the *O*6-meG remains, and, thymine is reinserted opposite the *O*6-meG. These futile cycles of repair result in activation of ATR and Chk1, generation of double-strand breaks (DSBs) and eventually apoptotic cell death (Zhang, Stevens et al. 2012). Cells with MMR deficiencies do not process the mismatch, DNA replication proceeds, and no cell cycle arrest or apoptosis occurs.

In vitro and *in vivo* analysis shows that resistance to alkylating agents is mediated by loss of MMR pathway protein such as MLH1 and MSH2 (Fink, Aebi et al. 1998; Shinsato, Furukawa et al. 2013; McFaline-Figueroa, Braun et al. 2015). In contrast, Rellecke et al (Rellecke, Kuchelmeister et al. 2004) showed that the source of resistance was high MSH2 expression in 25 primary *de novo* glioma cultures. The sensitivity of

these primary GBM cells to a panel of chemotherapeutic agents, including carmustine, cisplatin, and taxol, was evaluated with 36% of the cultures showing insensitivity to all of the agents tested. Expression levels of MMR across the 25 glioma cultures showed no differences between the lines, with the exception of MSH2. MSH2 expression was high in 48% of the tumors while the remaining 52% has low to undetectable levels. Interestingly, all the multiresistant tumors showed high MSH2 transcript.

However, clinical studies examining MMR have failed to show that MMR deficiency is responsible for TMZ resistance. In one study, 52 glioma patient samples were assessed for microsatellite instability (MSI), which is thought to be a result of MMR gene inactivation (Martinez, Schackert et al. 2005). Zero patients exhibited high MSI, defined as instability in three of five loci analyzed. Direct sequencing of MSH6 identified mutations, many of which did not hinder generation of wild-type protein. In this study MMR deficiency does not appear to contribute to resistance to TMZ therapy (Maxwell, Johnson et al. 2008). A low MSI rate of 8.5 % was found in a larger panel of 129 GBM patients and a higher presence of MSI was detected amongst the 20 GBMs that had recurred. Consistent with the previous studies, no high MSI was detected, and IHC for MMR proteins showed aberrant expression in only one tumor with MSI (Martinez, Schackert et al. 2005). A larger scale analysis of 624 gliomas further validated the lack of high MSI with an incidence of 0.16 % (Eckert, Kloor et al. 2007). Paired analysis of primary and recurrent tumors, noted no differences in PMS2, MLH1, MSH2, and MSH6 expression, and promoters of these genes remained unmethylated in both instances (Park,

Kim et al. 2012). Similarly, another study saw no apparent correlation between MSH2, MSH6, and PMS2 protein and sensitivity to TMZ (Hermisson, Klumpp et al. 2006). Single nucleotide polymorphism (SNPs) analysis of patient samples treated with radiation alone or with TMZ showed that 50 % harbored MSH6 G268A polymorphisms. However, no OS benefit was noted between samples harboring or lacking MSH6 G268A (Pei, Chen et al. 2013). Yip et al (Yip, Miao et al. 2009) focused their studies on a cohort of The Cancer Genome Atlas (TCGA) recurrent tumors, which had been previously found to have MSH6 mutations. Analysis of samples pre and post exposure to alkylating agents showed the MSH6 mutations were not present in pre-treatment samples; indicative that these mutations arose as a result of therapy. This same observation carried over to *in vitro* work with an A172 glioma line cultured to be resistant to TMZ. The TMZ resistant line, A172TR3, had reduced sensitivity to TMZ, decreased expression of MSH6 and a MSH6 somatic mutation. Similarly, knockdown of MSH6 in the glioma U251 line reduced sensitivity to TMZ. All these results were independent of MGMT as the glioma lines and the TCGA recurrent samples, were all MGMT negative. However, in agreement with previous studies high MSI was not detected (Yip, Miao et al. 2009). Some of the contradictory reports may be explained by the continued use of high levels of MSI as readout for MMR deficiency, despite reports indicating no correlation between the two (Maxwell, Johnson et al. 2008; Yip, Miao et al. 2009). One hypothesis is that the low levels of MSI observed in some cases might indeed be the result of MMR but of minor MMR players, which were not tested in these analyses (Martinez, Schackert et al. 2005).

Despite the complex interpretation of MSI, we conclude that both the MGMT and MMR pathways contribute to the tumor response to TMZ treatment. A tumor low in MGMT will respond well to initial TMZ therapy but at the cost of accumulated mutations. Surviving tumor cells are likely to have acquired MMR mutations, resulting in acquired tolerance to further TMZ therapy: a situation typical of GBMs in the clinic.

Fanconi Anemia Pathway and FANCD2

The Fanconi Anemia (FA) pathway is involved in the repair of interstrand cross-links (ICLs) generated by cross-linking agents such as platinums, nitrogen mustards, and mitomycin C (Deans and West 2011). ICLs are extremely toxic to cells as they covalently link both DNA strands and prevent unwinding coordinated by DNA helicases; thus, replication does not progress. Currently 17 FA genes make up the FA pathway and mutations in any of these renders the cell unable to resolve ICLs (Wang and Smogorzewska 2015). FANDA, FANCB, FANC, FANCE, FANCF, FANCG, FANCL, and FANCM assemble into what is known as the FA core complex which has E3 ubiquitin ligase activity attributed to FANCL (Meetei, de Winter et al. 2003). In response to DNA damage, ATR is activated and serves as the signal for the cell to activate the FA pathway (Andreassen, D'Andrea et al. 2004). FA complex is recruited to the site of damage where it monoubiquitinates FANCD2 and FANCDI. Monoubiquitinated FANCD2/FANCDI dimer localizes to chromatin foci that contain repair factors such as: FANCD1 (BRCA2), FANCJ (BACH1), Rad51, and PCNA which work together to

resolve the cross-link. The role of each FA protein within this pathway remains poorly undefined.

Recent studies implicate the FA pathway in repairing DSBs and stalled replication forks by homologous recombination repair (HRR.)(Kee and D'Andrea 2010). HRR is an error-free repair mechanism that uses homologous DNA from a sister chromatid as a template for DNA polymerase to extend past the breaks. FANCG has been shown to complex with FANCD1 (BRCA2), FANCD2, and XRCC3, a Rad51 paralog. This complex is proposed to function in HRR, independent of the FA complex (Wilson, Yamamoto et al. 2008).

FANCD2 and GBMs

Analysis of FANCD2 expression in GBM tumors has only been carried out in one published study (Patil, Sayal et al. 2014). FANCD2 was found to be upregulated in 93 % of the GBM samples analyzed and correlates with tumor grade. Additionally, cultures derived from fresh GBM samples expressed monoubiquinated FANCD2 and formed FANCD2 foci in response to TMZ; indicating that the FA pathway is not only expressed but activate in GBM cells. Similarly FANCD2 expression is higher in primary melanoma samples compared to controls (Kao, Riker et al. 2011).

FANCD2 and TMZ Resistance

The role of FANCD2 and the FA pathway in mediating TMZ resistance has not been extensively studied. In the absence of functional MGMT and MMR, *O*6-meG lesions go unresolved, and following futile cycles of repair, give rise to DSBs (Zhang, Stevens et al. 2012). DSBs can be repaired by both error-prone non homologous end joining (NHEJ) and HRR (Kondo, Takahashi et al. 2010). However, it has been demonstrated that cells are protected from *O*6-meG-induced DSBs by BRCA2/XRCC2 mediated HRR and not NHEJ (Roos, Nikolova et al. 2009). Thus, FANCD2, through its role in HRR, could mediate resistance to TMZ.

Chen et al demonstrated that resistance to alkylating agents, TMZ and BCNU, is mediated in part by the FA pathway (Chen, Taniguchi et al. 2007). In this study, HT16 GBM cells (FA-deficient) were more sensitive to TMZ or BCNU treatments, than FA-proficient GBM lines. Similarly, inhibition of FANCD2, via siRNA, sensitizes U87MG cells to BCNU and TMZ treatment. Inhibition of MGMT in FANCD2 knockdown lines further sensitizes the cells to TMZ treatment. In a similar study, the FA pathway in GBM lines was inhibited with commercial small molecule inhibitors (Patil, Sayal et al. 2014). Treatment of U87MG (FA-proficient) or primary GBM cells with FA inhibitors led to a decrease in monoubiquitinated FANCD2 and FANCD2 nuclear foci. Reduction of FA pathway activity sensitizes cells to TMZ treatment and this activity was independent of MGMT. Examination of individual components of the FA pathway shows that FANCD2 -/- cells and to a greater extent, FANCD1 (BRCA2) mutant, and FANCG -/- cells are

more sensitive to TMZ exposure than parental cells (Kondo, Takahashi et al. 2011). An *in vitro* recombination assay to assess HRR demonstrated that frequency of HRR was greatest following treatment with TMZ. Subsequently, knock down of FANCD1 (BRCA2) in A172MG cell line sensitizes the cells to TMZ and ACNU, and does not give rise to Rad51 foci. Therefore, targeting FANCD1 (BRCA2) in combination with TMZ might be of use for the treatment of GBMs. While FANCD2 -/- was more sensitive than the parental line, it was not to the same magnitude as FANCD1 (BRCA2) mutant cells.

MicroRNAs

MicroRNAs (miRNAs) are 18-25 nucleotide long non-coding double stranded RNA molecules known to regulate the stability and translation of target mRNA (Bartel 2004). Thousands of human miRNAs have been identified and are thought to regulate as many as 60 % of human transcripts (Friedman, Farh et al. 2009); playing a role in many of the cells processes including development (Alvarez-Garcia and Miska 2005), invasion (Ma, Creanga et al. 2006), DNA damage (Hu, Du et al. 2010), cell-cycle control, proliferation, and apoptosis (Ivanovska, Ball et al. 2008). Recent studies have shown that aberrant expression of miRNAs occurs in many human cancers, including GBMs. This dysregulation of expression has shown that miRNAs themselves can serve as oncogenes or tumor suppressors. Furthermore, recent studies support the involvement of miRNAs in modulating radiotherapy and chemotherapy resistance (Blower, Chung et al. 2008; Shi, Zhang et al. 2013).

MiRNA discovery, biogenesis, and mode of action

In 1993, studies examining the development of *Caenorhabditis elegans* (*C. elegans*) led to the discovery of lin-4, a small non-coding RNA that regulates the translation of LIN-14 protein (Lee, Feinbaum et al. 1993; Wightman, Ha et al. 1993). Analysis of lin-4 demonstrated that it did not encode a protein, transcript size was small, and was complementary to a site within the 3'UTR of lin-14 mRNA. Seven years later, another small non-coding RNA molecule, let-7, was found to regulate the transition from late larval to adult fate (Pasquinelli, Reinhart et al. 2000). Subsequent studies found let-7 to be conserved across species, including humans, where its expression is cell-type specific (Pasquinelli, Reinhart et al. 2000). By 2001 the term microRNA was established (Lagos-Quintana, Rauhut et al. 2001; Lau, Lim et al. 2001; Lee, Kermani et al. 2001). Fast forward 14 years and 2,588 human miRNAs have been identified and are being functionally validated (Griffiths-Jones 2014).

Transcription of miRNAs by the RNA polymerase II (pol II) promoter give rise to long primary miRNA transcripts (pri-miRNA) that are capped, polyadenylated, and spliced. These long transcripts are processed by a RNAse III endonuclease known as Drosha to form a 70 bp precursor miRNA (pre-miRNA). The Ran-GTP-dependent transporter, Exportin-5, transports the stem-looped pre-miR from the nucleus into the cytoplasm, where it interacts with another RNAse III molecule, Dicer. The endonuclease activity of Dicer leads to the formation of a miRNA:miRNA duplex consisting of a passenger strand and a mature miRNA strand . The double-stranded RNA duplex is

unwound, allowing for the subsequent specific incorporation of one of the strands into the RNA-induced silencing complex (RISC). Activated RISC is guided to complementary regions within the 3'UTR of target mRNA and either cleaves the mRNA or inhibits translation (Winter, Jung et al. 2009). Additionally, miRNAs can bind to the 5'UTR of target mRNA, resulting in enhanced translation (Orom, Nielsen et al. 2008).

Role in GBM resistance

MiRNAs are thought to mediate resistance through their regulation of cellular processes that allow malignant cells to evade apoptosis, invade, and grow. More recently involvement of miRNAs in regulating DNA damage repair pathways has been demonstrated. MiR-221 influences GBM cell's response to TMZ treatment by targeting MGMT. Overexpression of miR-221 increases TMZ-induced apoptosis and DSBs (Quintavalle, Mangani et al. 2013). MiR-181d also post-transcriptionally regulates MGMT in GBMs (Zhang, Zhang et al. 2012) and expression of miR-181d is inversely correlated with patient OS. Like MGMT, miR-181d could serve as a predictive biomarker. Another miRNA, miR-21, is upregulated in GBMs and its expression correlates with sensitivity to radiation (Chao, Xiong et al. 2013). The MMR protein, MSH2, was found to be directly regulated by miR-21. Similarly, miR-21 was shown to directly target both MSH2 and MSH6 in colorectal tumors (Ahmad, Patel et al. 2011). In an *in vivo* xenograft model, high levels of miR-21 contributed to resistance to 5'-fluorouracil (5'-FU). Other miRNAs target DNA damage sensors as shown by miR-421 mediated regulation of ATM in neuroblastomas (Hu, Du et al. 2010). Overexpression of

miR-421 allows cells to overcome ionizing radiation-induced S-phase block and survive. Hu et al, found that N-Myc regulates miR-421 expression; thus provides a mechanism for N-Myc to indirectly regulate ATM.

TCGA data analysis identified a miRNA signature of 25 miRNAs associated with survival in GBMs. The 25 miRNAs were classified as risky or protective (Wong, Fatimy et al. 2015). Among the risky miRNAs were miR-221, miR-222, miR-31, miR-148a, miR-34a, and miR-34b. The authors chose miR-31 and miR-148a for further evaluation. Despite no effect *in vitro*, delivery of miR-31 or miR-148a inhibitors to orthotopic GBM xenografts decreased proliferation, reduced a CD133+ population within the tumor, provided a normalized vasculature, and minimized invasion. Both miRNAs target the factor inhibiting hypoxia-inducible factor 1 (HIF1) and thus affect downstream pathways involved with HIF1 and Notch which promote growth of the tumor. MiR-34a, another miRNA identified as risky, has been previously identified as a regulator of growth signaling as it regulates hundreds of transcripts involved in growth factor signaling and cell cycle regulation (Lal, Thomas et al. 2011). Among the list of miR-34a validated targets are: CDK4/6, CCND1 (Cyclin D1), and E2F3, all of which participate in cell cycle regulation. Among miRNAs with protective phenotypes is miR-21 which, as discussed earlier, is upregulated in GBMs. MiR-21 has been shown to protect GBM cells from TMZ-induced apoptosis by decreasing the ratio of Bax:Bcl-2 as well as caspase activity (Shi, Chen et al. 2010).

Glioma Cancer Stem Cells (CSCs)

Another layer contributing to the complexity of resistance in GBMs is the subpopulation of cancer stem cells within tumors. These cells have proliferative and self-renewal capacities, and are capable of multi-lineage differentiation. When transplanted into immunodeficient mice, GBM CSCs recapitulate the parental tumor (Singh, Clarke et al. 2003; Park and Rich 2009). GBM CSCs are resistant to the cytotoxic effects of radiation and chemotherapy (Altaner 2008), leading many to conclude that this population of cells must be targeted in order to achieve complete responses.

GBM CSCs Markers

One of the challenges facing the study of GBM CSCs is the lack of reliable markers for the identification and subsequent isolation of these cells. Several influential studies found that GBM CSCs defined by expression of the marker CD133 (Prominin-1) are more tumorigenic than bulk tumor cells (Singh, Clarke et al. 2003; Singh, Hawkins et al. 2004). And these CD133+ populations have been shown to be resistant to TMZ, carboplatin, Taxol, and etoposides (Liu, Yuan et al. 2006). However, CD133 has proven to be a controversial marker. CD133 expression is stress- and cell cycle-dependent (Platet, Liu et al. 2007; Jaksch, Munera et al. 2008). Most GBMs have a small fraction of CD133+ cells, but others have no CD133+ cells or a high percentage of CD133+ cells (Nakano, Masterman-Smith et al. 2008; Wang, Sakariassen et al. 2008; Mihaliak, Gilbert et al. 2010). Despite this variation in CD133 expression, all GBMs are highly tumorigenic. Anti-CD133 antibodies vary in tissue staining, and one of the most

commonly used anti-CD133 antibody is dependent on protein glycosylation (Bidlingmaier, Zhu et al. 2008). As a result, it is now common to assess multiple stem cell markers (CD133, Nestin, Musashi-1, Sox2, and SSEA among others) (Christensen, Schroder et al. 2008) as well as carrying out functional assays such as neurosphere formation (Iacopino, Angelucci et al. 2014). Cell sorting experiments reveal that selection for one stem cell marker, does not pull out all of the cells with other stem cell markers. These results suggest that the GBM CSCs are heterogeneous, and there is not a single marker signature for CSCs (Chen, Nishimura et al. 2010; Venere, Fine et al. 2011; Antoniou, Hebrant et al. 2013). Suva et al (Suva, Rheinbay et al. 2014) proposed a novel model to explain these results. They found that CSCs require expression of four transcription factors (POUF3F2, SOX2, SALL2 and OLIG2). Many GBM cells express three or fewer of these transcription factors, express some stem cell markers, but are not CSCs.

CSCs and GBM resistance

It has been proposed that CSCs contribute to resistance and subsequently are responsible for regrowth after therapy (Chen, Li et al. 2012). CSCs may be resistant to therapy by multiple mechanisms, including over expression of DNA repair proteins such as MGMT and overexpression of ABC-transporters such as BCRP1 (Bao, Wu et al. 2006; Liu, Yuan et al. 2006). In addition, the role of the CSCs may be complicated by epigenetic changes that allow differentiated cells to undifferentiate and become CSCs

(Safa, Saadatzadeh et al. 2015). However, interpretation of these data is complicated by the lack of specific cell-surface CSC markers.

One molecular mechanism being examined involves the histone-lysine N-methyltransferase (EZH2), an enzyme within the polycomb repressive complex 2 (PRC2) which tri-methylates histone H3 and aids in the silencing of differentiation genes (Simon and Lange 2008). EZH2 is of interest to the study of GBMs as it is located on chromosome 7, which is often amplified in GBMs (Brennan, Verhaak et al. 2013). Depletion of EZH2 in GBM CSCs decreases self-renewal and tumors formation following transplantation into mice (Suva, Riggi et al. 2009). Recently it was shown that EZH2 is regulated by a complex made up of the kinase, MELK, and the transcription factor, FOXM1 (Kim, Joshi et al. 2015). MELK is enriched in GBM stem cells (CD133+) and its expression is inversely correlated with survival of GBM patients (Liu, Yuan et al. 2006; Nakano, Masterman-Smith et al. 2008). Knockdown of MELK via siRNA influences proliferation of GBM CSCs and decreases the number of neurospheres. Another study by the same lab showed that radioresistance of GBM cells can be attributed to MELK expression. Cells without MELK are radiosensitive, and sensitivity is diminished in cells overexpressing MELK (Kim, Joshi et al. 2015). Post-radiation recurrent tumors analyzed in that study were also found to contain more MELK and EZH2 positive cells than naïve therapy GBMs. Interestingly, EZH2 is highly expressed in established TMZ-resistant cultures and knockdown of EZH2 in these lines sensitized cells to TMZ and decreased expression of multiple ATP-binding cassette (ABC)

transporters (Fan TY 2014). These studies elucidate one of many mechanisms by which GBM CSCs are radiation- and chemotherapy-resistant.

Emerging Approaches to Therapies

Development of Novel TMZ-like Drugs

TMZ is a successful drug with oral administration, manageable side effects and enhanced survival for patients with GBMs (Stupp, Mason et al. 2005; Stupp, Hegi et al. 2009; Zhang, Stevens et al. 2012). However, its most toxic product, *O*6-meG, is readily reversed by MGMT, and methylation of DNA at other sites is reversed by BER. A drug with less readily repaired products would enhance therapy in the clinic. Fortunately, TMZ and related compounds have been extensively studied, and this information will facilitate design of TMZ-like drugs with increased anticancer activity and good pharmacokinetics.

Two approaches are currently being taken to develop new TMZ derivatives that are resistant to, or avoid the two principal constraints on the ability of a tumor to respond to TMZ therapy, via, MGMT and MMR dependence. One approach has been to modify the imidazotetrazine 3-substituent so that the group transferred to DNA *O*6-G sites is either not recognized or not repaired by MGMT. A range of neutral polar and charged *O*6-G substituents resistant to cleavage by MGMT has been characterized (Pletsas, Wheelhouse et al. 2006). Several such substituents have been incorporated into experimental imidazotetrazines 2, 3 (**Figure 1.5**). Other than the free carboxylic acid (**2**, R = H), these compounds have all been shown active against GBM and colorectal cell

lines that are resistant to TMZ, whether because of proficient MGMT or having deficiency or mutation in the MMR components hMLH1 or hMSH6. Onset of repair processes was slower than for TMZ and replication-independent (*i.e.*, MMR-independent) DSBs were implicated in the cellular mechanism.

In the second approach a complete switch of chemical mechanism has been achieved with the dual aims of avoiding MGMT and MMR dependence and making the drug more efficient than TMZ by generating pharmacological activity from the major reaction site on DNA, *N*7-G (70% for TMZ), rather than the minor (5%) *O*6-G site. This advance employs a neighboring group participation mechanism to control the behavior of the released alkyldiazonium ions (**Figure 1.6**). This serves the dual functions of controlling reactivity, so giving the electrophile time to locate its reaction site on DNA, and delivering an alternative form of damage to DNA. Since the response of tumors to TMZ is determined by the interaction of DNA repair systems with modified DNA, altering the electrophile would necessarily alter the profile of tumor responses. In these respects, the potential of the imidazotetrazines as acid-stable precursors of aziridinium ions was explored as these are reactive intermediates of proven clinical utility, widely found in or generated by synthetic and natural product anti-tumor drugs, e.g., nitrogen mustards. The bifunctional agent DP68 and its analogous monofunctional form DP86 are currently under preclinical investigation.

The aqueous chemistry of diazonium ions is beset by problems of competing hydrolysis, elimination and re-arrangement reactions, which are reduced for aziridinium ions. In a ^{13}C labeling study, DP86 was shown to be an efficient precursor of aziridinium ions (**Figure 1.6**). At the stage of the diazonium ion, there was 96% conversion to the aziridinium form with only 4% direct hydrolysis. Products of further reaction had the labeled atom scrambled so that it appeared equally at both positions of the ethyl chain: confirming that they were entirely derived via the aziridinium route. Highly effective control of the diazonium ions had been achieved—in sharp contrast to other agents designed as precursors of aminoethyldiazonium ions (Garelnabi, Pletsas et al. 2012).

Rationale for Thesis

Despite advances in the treatment of GBMs with a three prong approach of surgery, radiotherapy, and TMZ, tumors with intrinsic or acquired resistance to TMZ persist and repopulate. Recurrent tumors have been shown to be genetically diverse from the primary tumor (Kim, Joshi et al. 2015; Mazor, Pankov et al. 2015), hindering therapy as a drug regimen effective in a naïve tumor will likely be ineffective in the subsequent recurrence. This necessitates drug regimens that bypass DNA repair mechanism and eliminate all cells within the initial tumor, including those with self-renewal capability, in an attempt to overcome recurrence.

Our first approach involves the characterization of two TMZ-analogues, DP68 and DP86. The rationale for this research project was developed from knowledge that the

efficacy of TMZ is dependent on the MGMT and MMR pathways (Fink, Aebi et al. 1998; Hegi, Diserens et al. 2004; Hermisson, Klumpp et al. 2006). Prior clinical strategies to overcome resistance utilized MGMT inhibitors such as *O*6-BG and PaTrin-2(Pegg 2000; Barvaux, Ranson et al. 2004; Quinn, Desjardins et al. 2005; A and H 2011). However, these inhibitors gave rise to bone marrow toxicity and were not optimal for use in the clinic. Our collaborator, Dr. Richard Wheelhouse took a different approach: developing drugs that deliver *O*6-G modifications not recognized or repaired by MGMT (Pletsas, Wheelhouse et al. 2006). He demonstrated that MGMT-mediated drug resistance may be bypassed through agents that deliver polar groups to DNA, rather than the current simple alkyl groups (methyl, chloroethyl). Bulkier groups are also hard for MGMT to clear. Our hypothesis is that the TMZ analogues, DP68 and DP86, whose response is independent of MGMT, will be more efficacious agents for GBM therapy. We investigated the biological effects of these novel alkylating agents in a GBM model in the context of resistance mediated by DNA repair mechanisms. Chemotherapeutic agents whose damage cannot be repaired by the classic DNA repair pathways are desirable not only for de novo GBM patients but for those with TMZ-resistant tumors.

Our second approach involved miRNA replacement therapy for GBMs. The rationale for this research project came from a previous preclinical study in our lab. Gilbert et al (Gilbert, Daou et al. 2010) demonstrated that blocking the Notch pathway with GSIs enhanced TMZ treatment. TMZ + GSI treated cells are no longer capable of self-renewal and survival was enhanced in a GBM xenograft model compared to TMZ or

GSI alone. TMZ + GSI treatment leads to therapy-induced senescence in glioma cells, which in turn prevented regrowth of GBM cultures (Gilbert 2011). Because therapy-induced senescence is one mechanism currently being investigated to target cancer cells we wanted to identify miRNAs whose expression could be modulated to induce senescence. MiR-34a is an appealing miRNA to study as it is downregulated in GBMs and has predicted seed matches to Notch family members. Our hypothesis is that miR-34a alone has therapeutic benefits by inhibition of Notch signaling. The study described herein focuses on the effects of miR-34a on GBM biology and the study of its potential targets.

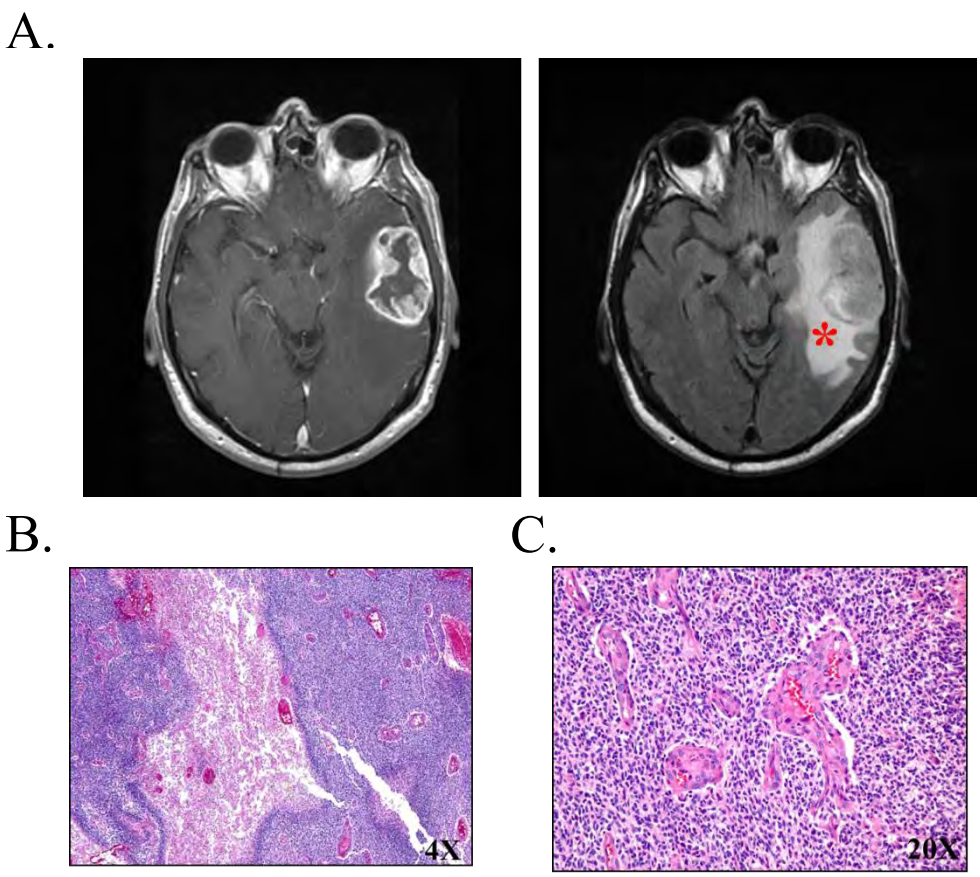

Figure 1.1 Glioblastoma: pre-operative scan and histology.
GBMs appear as contrast enhancing lesions on MRI scans (A). Left Scan: Tumor is enhanced with Gadolinium Chloride, Right scan: flair (*) in this scan shows the vasogenic edema, which results from disruption of the blood brain barrier, and infiltration beyond the enhanced mass. Matched H&E stain of patients GBM tumor depicting large areas of necrosis (B) and vascular proliferation (C).

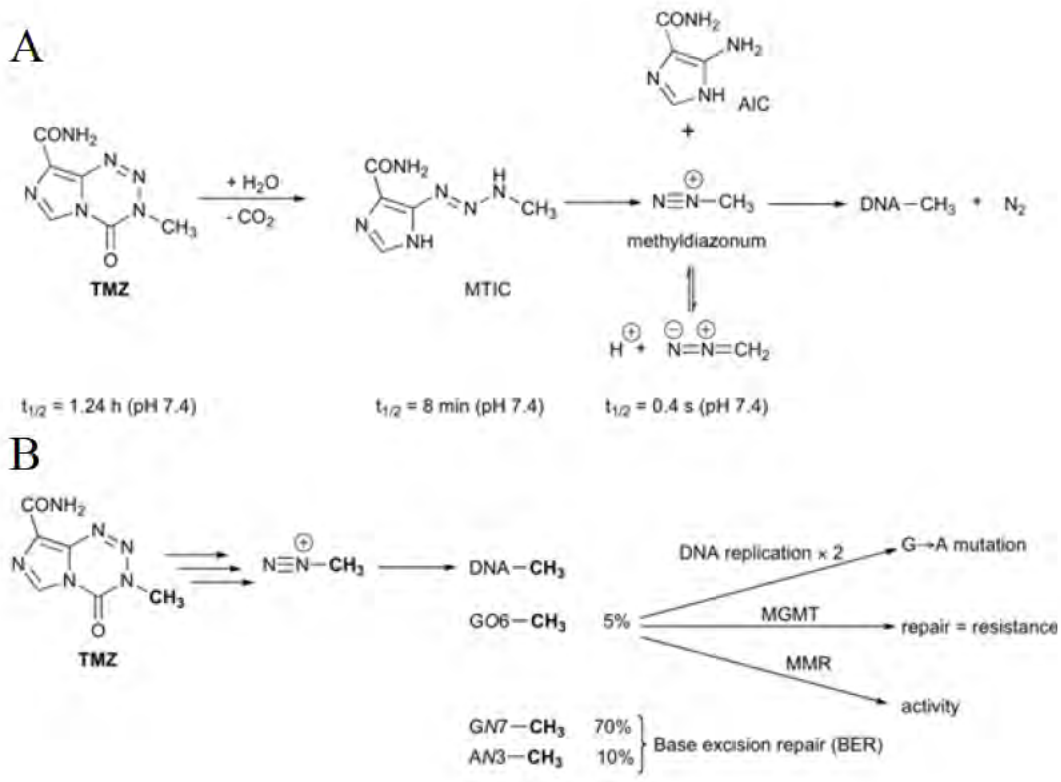

Figure 1.2 Activation and mode of action of TMZ.
Prodrug activation of TMZ (A) and biological fate of methyldiazonium ions (B).

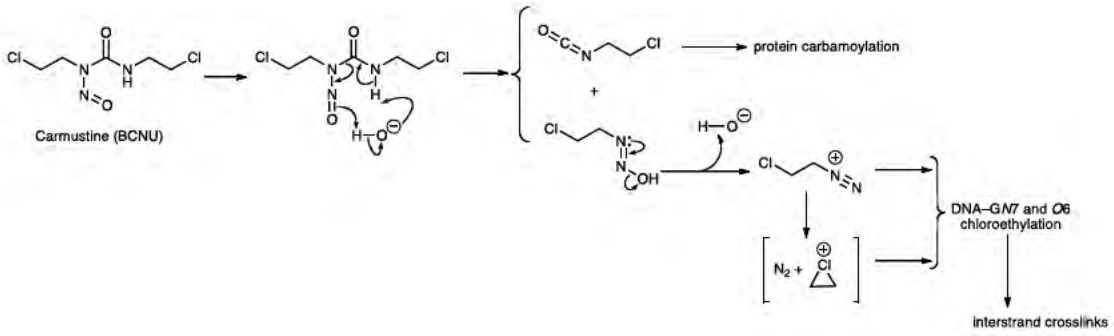

Figure 1.3. Mechanism of prodrug activation and action of carmustine. Mechanisms of carmustine activation resembles that of TMZ. Under physiological conditions, spontaneous hydrolysis results in release of reactive chloroethyldiazonium. Therapeutic activity is derived from guanine chloroethylation of DNA and form of interstrand crosslinks.

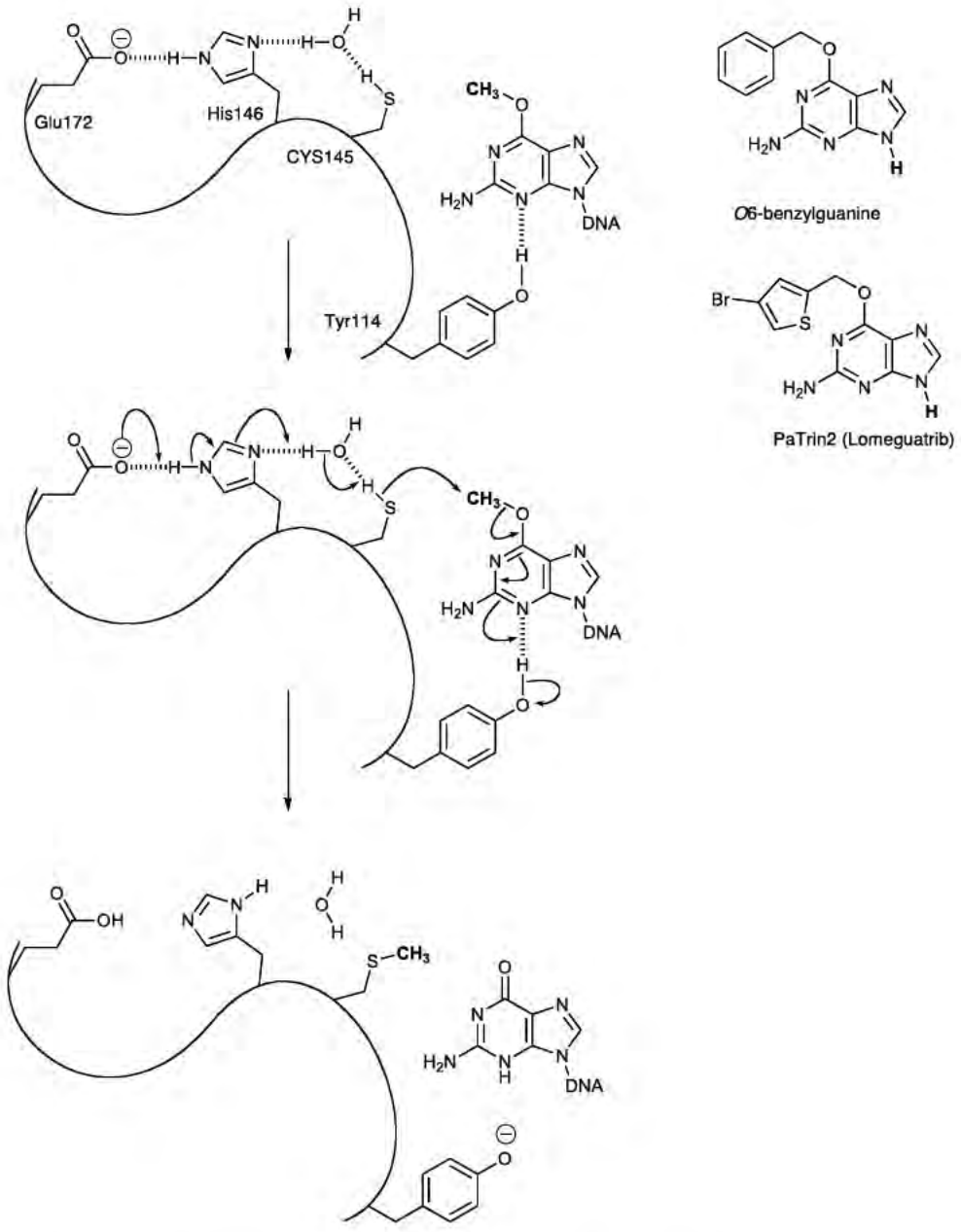

Figure 1.4 Mechanism of action of MGMT and structures of the two clinically tested MGMT inactivators.
Mechanism by which MGMT removes *O*6-meG and the structures of *O*6-BG and PaTrin-2.

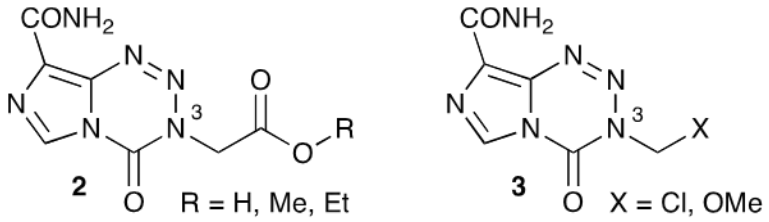

Figure 1.5 Novel TMZ-like drugs.
Experimental imidazotetrazines 2 and 3 and the substituents that have been incorporated into the compounds.

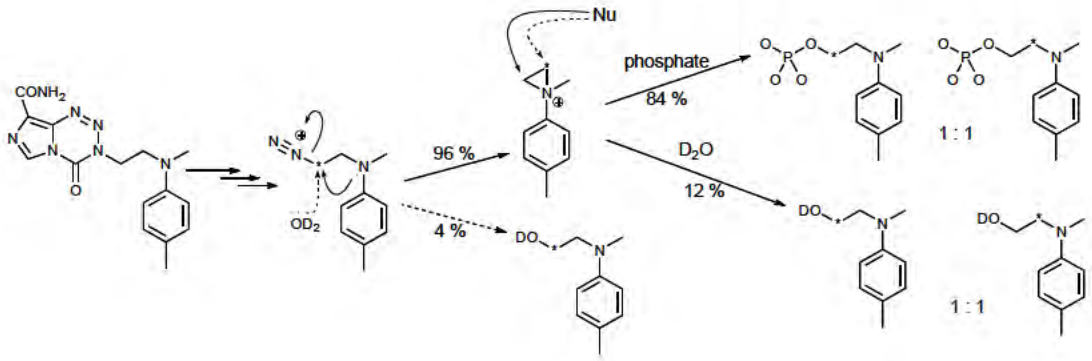

Figure 1.6 Reaction of DP86 in phosphate buffer, pH = 7.4. * Sites of ^{13}C labelling.

Reaction of monofunctional DP86 and the generation of the diazonium ion.

CHAPTER II

EVALUATION OF NOVEL IMIDAZOTETRAZINE ANALOGUES DESIGNED TO OVERCOME TEMOZOLOMIDE RESISTANCE AND GLIOBLASTOMA REGROWTH

CHAPTER II

Preface

The contents of this chapter stem from research carried out in Alonzo Ross's lab from the end of 2011 until 2014. It is a collaboration with Dr. Wheelhouse from the University of Bradford, who supplied us with TMZ analogues he and his colleagues synthesized. As the project proceeded, the project expanded to include Dr. Phillips of the University of Bradford, Dr. Sakaria from the Mayo Clinic and Dr. Rautio from the University of Eastern Finland. Parts of this chapter represent work that resulted from our collaboration, published as: Ramirez YP, Mladek AC, Phillips RM, Gynther M, Rautio J, Ross AH, Wheelhouse RT, Sakaria JN. *Mol Cancer Ther*. 2015 Jan;14(1):111-9.

In this chapter, I carried out the following: generation and characterization of the U87NSTMZ line, IC_{50} studies for U87NS, U87MG, U118MG, U118NS, and U87NSTMZ lines, all secondary sphere assays, knockdown of MLH1 in T98G and U87MG and subsequent experiments, PMS2 western, limiting dilution assays and all *in vivo* mouse work. First co-author Ann C. Mladek (Mayo Clinic) performed all GBM6, GBM12, and GBM12TMZ work, westerns for DNA damage response, *O*6-BG experiments, flow cytometry with U251 and T98G, and knockdown/inhibition of ATM/ATR/FANCD2 experiments. Dr. Phillips performed the comet assays. Dr. Gynther and Dr. Rautio performed pharmacokinetic experiments. Dr. Wheelhouse supplied the schematics depicting compound structure and chemistry.

Abstract

The cellular responses to two new TMZ analogues, DP68 and DP86, acting against GBM cell lines and primary culture models are reported. Dose-response analysis of cultured GBM cells revealed that DP68 is more potent than DP86 and TMZ and that DP68 was effective even in TMZ-resistant models. Based on a secondary neurosphere formation assay, DP68 inhibits repopulation of these cultures even at low concentrations. The efficacy of these compounds was independent of MGMT expression and the MMR pathway protein, MLH1. We characterized DP68-induced damage in H_2O_2-treated cells and found that DP68 formed interstrand DNA crosslinks. Furthermore, DP68 induced a distinct cell cycle arrest with accumulation of cells in S phase that is not observed for TMZ. Consistent with this biological response, DP68 induces a strong DNA damage response, including phosphorylation of ATM, Chk1 and Chk2, KAP1, and histone variant H2AX. Suppression of FANCD2 expression or ATR expression/kinase activity enhanced anti-GBM effects of DP68. Initial pharmacokinetic analysis revealed rapid elimination of these drugs from serum. In line with this, efforts to demonstrate efficacy of compounds *in vivo* were unsuccessful. Collectively, these data demonstrate that DP68 is a novel and potent anti-GBM compound that circumvents TMZ resistance, likely as a result of its independence from MGMT and MMR and its capacity to crosslink strands of DNA. These results will guide Dr. Wheelhouse in the preparation of additional TMZ analogues with the potential to treat GBMs *in vivo*.

Introduction

The imidazotetrazine prodrug TMZ (**Figure 2.1**) concurrent and adjuvant to radiotherapy is now the first line of treatment for GBM in North America and Europe; however, intrinsic and acquired resistance ultimately limit the efficacy of therapy (Stupp, Hegi et al. 2009; Zhang, Stevens et al. 2012). It is stable under acidic conditions and is orally available. At neutral pH, TMZ is moderately unstable ($t_{1/2}$ = 1.24 h, pH 7.4) (Stevens, Hickman et al. 1987) and is hydrolyzed in a ring-opening reaction to the open chain triazene MTIC (**Figure 1.2 A**; $t_{1/2}$ = 8 min, pH 7.4) (Shealy and Krauth 1966) that fragments to the reactive electrophile, methyldiazonium ($t_{1/2}$ = 0.39 s, pH 7.4) (McGarrity and Smyth 1980; Wheelhouse and Stevens 1993; Saleem, Brown et al. 2003). The methyldiazonium ion reacts with nucleophilic groups on DNA, resulting in DNA methylation. Approximately 70% of the methyl groups are located on *N*7-G, 10% on *N*3-A and 5% at *O*6-G sites (Denny, Wheelhouse et al. 1994; Zhang, Stevens et al. 2012). Products of *N*-methylation are readily repaired by the base-excision repair pathway and are not thought to be major contributors to cytotoxicity (Svilar, Dyavaiah et al. 2012). In contrast, *O6*-methylguanine (*O*6-meG) lesions are reversed by the DNA repair gene, MGMT, and failure to remove these lesions can lead to cytotoxicity and accumulated G→A transition mutations (**Figure 1.2 B**) (Pegg 2000). The MGMT gene is silenced by promoter methylation in approximately 35% of GBMs and is believed to be a predictive marker for TMZ response (Park, Kim et al. 2012). In these tumors, persistent *O*6-meG lesions form wobble base-pairs with thymidine during replication. These *O*6-meG:T pairings trigger futile cycles of mismatch repair by the MMR machinery, stalled

replication forks and lethal DNA DSBs. Disruption of MMR through mutation or suppressed expression results in a TMZ-tolerant phenotype, while high-level expression of MGMT protein is a major mechanism of inherent TMZ resistance (Ramirez, Weatherbee et al. 2013).

The short lifetime of the methyldiazonium ion can limit the efficiency of DNA methylation by TMZ; furthermore, of the methyl groups transferred to DNA, only a small fraction is the therapeutically-beneficial *O*6-MeG lesion. In an attempt to overcome these limitations, new TMZ derivatives with modified spectra of activity have been engineered. One strategy is to modify DNA at *O*6-G in a manner that is not recognized or repaired by MGMT, which is known to occur by addition of a polar or bulky adduct (Pletsas, Wheelhouse et al. 2006; Zhang, Stevens et al. 2011). In addition, the design of the imidazotetrazine compounds investigated herein sought a switch of chemical mechanism with the aims of avoiding known mechanisms of TMZ resistance and generating therapeutic benefit from the major reaction site, *N*7-G (70% for TMZ), rather than the minor (5%) *O*6-G site (Garelnabi, Pletsas et al. 2012).

In this study, we focus on two of the most promising compounds developed: the mono-functional DP86 and the bi-functional DP68 imidazotetrazines (**Figure 2.1**) (Garelnabi, Pletsas et al. 2012; Pletsas, Garelnabi et al. 2013). These compounds are precursors of aziridinium ions, which are reactive intermediates of proven clinical utility related to those generated by nitrogen mustard drugs (**Figure 2.2 A-B**). The bi-functional,

DP68, and monofunctional, DP86, have been previously screened in the ovarian cancer cell line, A2780, and its cisplatin resistant counterpart, A2780-cp70. Chemosensitivity to both compounds was measured in the A2780 (MMR+) and A2780-cp70 (MMR-) cell lines with and without the MGMT inhibitor PaTrin-2. DP68 is the most potent compound and has the least dependence on MGMT function and MMR status. Further evaluation showed activity of novel analogues is independent of p53, unlike TMZ (Pletsas, Garelnabi et al. 2013). The bi-functional molecules would be expected to generate DNA crosslinks, which would not be processed by MMR and should overcome that mechanism of resistance. This analogue was selected for detailed investigation; the mono-functional analogue, DP86, was evaluated for comparison.

The novel analogues were screened against the NCI-60 panel of human tumor cell lines, which includes six gliomas, four of which are the GBM lines SF-295, SF-539, SNB-19 and U251 (Shoemaker et al, nature reviews, 2006). In matrix COMPARE analysis of the NCI-60 data, the new compounds showed no significant correlation with another TMZ analogue, mitozolomide, ($0.46 \geq P \geq 0.35$). So these are distinct new members of the imidazotetrazine class. The putative DNA lesion of the bifunctional agent is a five-atom crosslink, related in structure to those formed by the nitrogen mustard prodrugs; however, no drugs of this class showed strong correlations ($0.59 \geq P \geq 0.29$). Notably, there was also no similarity to the nitrosoureas, which are also diazonium ion precursors ($0.45 \geq P \geq 0.05$), or cisplatin, another *N*7-G reactive agent ($0.42 \geq P \geq 0.27$) (Pletsas, Garelnabi et al. 2013).

These data describe the biological effects of these novel DNA alkylating agents in GBM models and their relative activities in the context of MGMT-overexpression and other mechanisms of TMZ resistance.

Results

MGMT expression correlates with TMZ sensitivity but not DP68 or DP86

Because MGMT expression is associated with TMZ resistance (Gerson 2002; Hermisson, Klumpp et al. 2006; Sato, Sunayama et al. 2011), we analyzed the sensitivity of a panel of glioma cells following exposure to various concentrations of TMZ and novel analogues, DP68 and DP86 (**Table 2.1**). A correlation between MGMT expression (**Figure 2.3D**) and TMZ sensitivity was observed in all lines examined. MGMT-negative lines, U87MG and U251 (U87MG, IC_{50} =43 μM; U251, IC_{50} =60 μM), showed the greatest sensitivity to TMZ treatment, while the MGMT-positive lines were the least sensitive (U118MG, IC_{50} =135 μM; T98G, IC_{50}= 340 μM). In contrast to TMZ, DP68 was efficacious in both MGMT-negative (U251, IC_{50}= 5.2 μM; U87MG, IC_{50} =14 μM) and MGMT-positive (T98G, IC_{50} = 11.3 μM; U118MG, IC_{50}=10 μM) cell lines. The bi-functional agent DP68 was significantly more potent than TMZ in all cell lines with IC_{50} ratios (TMZ:DP68) ranging from 3 to 85 (**Table 2.1**). The mono-functional agent DP86 was approximately 10-fold less potent than DP68 in all lines studied, but similar to DP68, the activity of DP86 was independent of MGMT expression (U251, IC_{50}= 68 μM; U87MG, IC_{50} =67 μM; T98G, IC_{50} = 110 μM; U118MG, IC_{50}=42 μM). To validate that

the efficacy of the novel imidazotetrazine analogues was not limited to long-term monolayer glioma cultures alone, U87NS and U118NS neurosphere cultures as well as neurospheres derived from the Mayo xenograft panel were treated with TMZ, DP86, and DP68. All neurosphere cell lines showed similar trends in the sensitivities to DP68 and DP86 (**Figure 2.3**). Interestingly, while U87NS and U118NS had similar DP86 IC_{50} to their adherent counterparts (U87NS IC_{50} = 61 μM vs U87MG IC_{50} = 67 μM; U118NS IC_{50} = 42 μM vs U118MG IC_{50} = 42 μM), sensitivity to DP68 was 2-fold increased in the neurosphere cultures (U87NS IC_{50} = 5.9 μM vs U87MG IC_{50} = 14 μM; U118NS IC_{50} = 2.7 μM vs U118MG IC_{50} = 5.2 μM). Patient-derived GBM6 and GBM12 lines showed similar elevated sensitivity to DP68 (GBM6, IC_{50} = 1.3 μM; GBM12, IC_{50} = 0.8 μM).

Generation of TMZ resistance models

In order to study the effects of DP86 and DP68 in TMZ-mediated resistance, we exposed U87MG cells to increasing doses of TMZ and generated the line U87MGTMZ with a resistant phenotype. Neurosphere culture, U87NSTMZ, was generated by culturing the U87MGTMZ line in serum-free media. Changes in morphology included enlarged cells observed with U87MGTMZ and U87NSTMZ cultures (**Figure 2.4**). U87MGTMZ cultures contained cells that had "flattened" out with processes extended outwards in all directions. TMZ-resistant neurospheres grew in spheres that were not as compact as the parental line. Attempts to propagate U87NSTMZ line *in vivo* failed; subcutaneous injection ($1x10^6$ cells) into the flank of Nu/Nu mice did not give rise to tumors (n=10 mice, zero tumors). Our collaborators in the Sarkaria lab simultaneously

generated the U251TMZ-resistant line along with a resistant primary line, GBM12TMZ (Giannini, Sarkaria et al. 2005; Kitange, Mladek et al. 2012). GBM12TMZ was developed from a primary line GBM12 propagated *in vivo* and repeatedly treated *in vivo* with TMZ. U87MGTMZ and U251TMZ lines remained MGMT negative like their parental lines (**Figure 2.3 D**). In contrast, GBM12TMZ showed expression of MGMT at high levels.

DP68 is efficacious in models of TMZ resistance

In our three models of acquired TMZ resistance, the sensitivity of the cells to TMZ decreased significantly (**Table 2.1, Figure 2.5** green circles): U251TMZ, U87NSTMZ, and GBM12TMZ showed 5.1-fold, 20.3-fold, and 156-fold less sensitivity to TMZ, respectively, than the corresponding parental cell lines. TMZ IC_{50} values for all three resistant lines (U87NSTMZ, IC_{50} = 153 μM; U251TMZ, IC_{50} = 306 μM; GBM12TMZ, IC_{50} = 500 μM) are substantially greater than the concentrations achieved in the clinic. In contrast, the efficacy of DP68 was essentially unchanged compared to the parental lines with an IC_{50} for DP68 in U251TMZ of 3.6 μM and in U87NSTMZ of 4.1 μM. In the third TMZ-resistant model, GBM12TMZ, DP68 was highly effective (IC_{50} = 1.4 μM). DP86 was approximately 10-fold less potent than DP68 with IC_{50}s ranging from 19– 43 μM. However, these IC_{50}s were similar to the responses measured for the parental cell lines.

Efficacy of DP68 is not an artifact of neurosphere plating density

Because plating density affects the efficiency of neurosphere formation (Pastrana, Silva-Vargas et al. 2011), limiting dilution assays were carried out with GBM12, GBM12TMZ, and GBM6 cells plated at various densities (1, 10, 30, 100, and 1000 cells/well) and treated with TMZ, DP68, or DMSO. GBM12 was the only line that formed spheres at all of the tested densities. TMZ and DP68 have similar potencies for inhibition of neurosphere formation in this line regardless of cell density. DP68 demonstrated greater inhibition of neurosphere formation than TMZ (**Figure 2.6**). While GBM12TMZ and GBM6 were unable to form spheres at the single cell level, sphere formation was observed at the higher densities (10 cells/well and 30 cells/ well). The potency of TMZ and DP68 agrees with our other assays.

Efficacy of DP68 and DP86 in human glioma cultures is independent of MGMT and MMR expression

To assess the impact of MGMT activity on DP68 and DP86 activity, T98G and GBM6 cells were co-treated with the MGMT suicide inhibitor *O*6-BG. *O*6-BG is a synthetic derivative of guanine and works by transferring a benzyl group to the active site of MGMT, thus inactivating it. Consistent with previous data, co-treatment with *O*6-BG increased sensitivity to TMZ in MGMT-expressing T98G and GBM6 cells (**Figure 2.7 A, C**), while *O*6-BG had no impact on the efficacy of DP68 and DP86 in these cells (**Figure 2.7 B, D**).

Cytotoxicity of TMZ also depends on the integrity of the MMR system, which is activated in response to *O*6-meG lesions that mismatch with thymine. To assess the importance of this pathway, we infected T98G (MGMT+) and U87MG (MGMT-) cells with shRNA lentiviruses targeting MLH1 (**Figure 2.8 A-B**). In the T98G line, knockdown of MLH1 had no impact on activity of DP86 or DP68 while decreasing the sensitivity to TMZ (empty vector IC_{50}=982 μM, sheGFP IC_{50}=1077 μM, shMLH1 #1 IC_{50}= 2005 μM, shMLH1 #2 IC_{50}= 1748 μM) (**Figure 2.8 C**). The MGMT-negative line, U87MG, had a similar response to TMZ treatment but larger in magnitude with 2.6-fold (shRNA#1), 4.9-fold (shRNA#2), and 5.2-fold (shRNA#3) changes in sensitivity compared to sheGFP control (empty vector IC_{50}=230 μM, sheGFP IC_{50}=153 μM, shMLH1 #1 IC_{50}= 396 μM, shMLH1 #2 IC_{50}= 756 μM, shMLH1 #3 IC_{50}= 791 μM). Responses to DP68 and DP86 were not altered despite the efficacy of MLH1 knock down. Because MLH1 affects protein stability of another MMR pathway protein, PMS2, (Trojan, Zeuzem et al. 2002) T98G MLH1 knockdown lines were analyzed for PMS2 expression and both shMLH lines shows substantial decrease in expression (**Figure 2.8 E**). Collectively, these data confirm that activity of the new imidazotetrazine compounds is independent of cellular MGMT and MMR expression in the panel of glioma cell lines tested.

DP68 and DP86 inhibit recovery and secondary sphere formation

The effects of imidazotetrazines on long-term cell growth were evaluated in a secondary neurosphere formation assay (**Figure 2.9**) with MGMT non-expressing glioma

line U87NS and MGMT expressing line U118NS. Treatment of U87NS and U118NS with TMZ (100 μM) showed similar reductions in the number of neurospheres at day 7 ('Treatment' – **Figure 2.10 A**) with 95% and 96% reductions, respectively. By day 14, U118NS cultures recovered, showing similar number of neurospheres as the DMSO treated culture ('Recovery' – **Figure 2.10 A**), while there were few spheres present for U87NS cells. The neurospheres were dispersed and replated. By day 21, U87NS and U118NS cultures formed secondary spheres with marked recovery from TMZ treatment ('Secondary' – **Figure 2.10 A**). In contrast, DP68 treatment greatly reduced neurosphere formation after a single treatment and prevented the subsequent recovery of spheres (**Figure 2.10 B**); secondary sphere formation was completely repressed by 10 to 30 μM DP68. Similar results were seen with DP86 at approximately 10-fold higher concentrations than DP68 (**Figure 21.0 C**). Thus, in comparison to TMZ, DP68 and DP86 provide more durable inhibitory effects on primary and secondary neurosphere formation.

DP68 Induces DNA Crosslinks in Glioma Cells

To evaluate the DP68-induced lesions we examined damage to nuclear DNA by single cell electrophoresis (comet assay). This assay detects single and DSBs and alkali labile sites and has been adapted to measure DNA inter-strand cross-linking. Pre-treatment with DNA cross-linking agents retards the migration of DNA fragments generated by H_2O_2 treatment (Collins, Oscoz et al. 2008). In this assay, a decreased comet tail moment indicates DNA cross-linking. The cross-linking agent melphalan

(positive control) and DP68 showed significant and comparable, concentration-dependent cross-linking of nuclear DNA in U251 cells (**Figure 2.11**), while DP86 and TMZ showed no evidence of cross-linking (**Figure 2.11**). These data show that DP68 is equipotent with melphalan at DNA cross-linking; in contrast, the mono-functional agents do not form crosslinks.

S-phase accumulation and G2/M arrest by DP68

The effects of DP68 and TMZ on cell cycle distributions were compared in U251 (MGMT non-expressing) and T98G (MGMT expressing) cells (**Figure 2.12 A**). In U251 cells, treatment with 30 μM TMZ had relatively minimal effects on cell cycle until 72 h after treatment, when there was an accumulation of cells in G2/M, which is characteristic of TMZ treatment. In contrast, DP68 induced a marked S-phase accumulation within 16–24 h, and by 72 h the majority of cells accumulated in G2/M. In contrast, TMZ treatment has no significant effects on cell cycle distribution in TMZ-resistant T98G cells, while DP68 treatment results in a similar cell cycle distribution as in U251 with marked accumulation in S and G2/M 24 h after treatment and significant accumulation in sub-G1 by 72 h after treatment. A preliminary experiment with another MGMT negative line, U87MG, showed similar responses to TMZ (**Figure 2.12 B**) with arrest at G2/M phase 72 h following TMZ treatment. Marked S-phase accumulation was observed by 24 h with doses as low as 5 μM, which is less than half of U87MG's IC_{50} of 14 μM. However, this low concentration did not lead to the G2/M arrest observed with 10 μM DP68. Thus,

DP68 has a cell cycle arrest profile distinct from TMZ, with an early accumulation of cells in S-phase followed by G2/M arrest.

Activation of DNA damage response by low concentrations of DP68

Consistent with the flow-cytometry data, DP68 activated DNA damage signaling pathways within hours of treatment. As seen in **Figure 2.13 A**, phosphorylation of ATM (S1981) and the canonical ATM substrate Chk2 (T68) were detected 4 to 8 h after treatment with 30 μM DP68, while phosphorylation of the canonical ATR substrate Chk1 was later with reproducible phosphorylation induction at 8 to 16 h. Both ATM and ATR can phosphorylate KAP1 (S824) in response to DNA damage (White, Negorev et al. 2006), and consistent with activation of these pathways, phosphorylation of KAP1 was evident within 8 h of DP68 treatment and maintained for at least 72 h. In contrast, TMZ-induced damage signaling was evident only in U251 cells and only at a late 72 h time-point. DP68-induced phosphorylation of this DNA damage response network (p-ATM, p-Chk2, p-Chk1, and p-KAP1) and histone variant H2AX (S139; γ-H2AX) at concentrations as low as 3 μM in MGMT-negative U251 and MGMT-positive T98G cells (**Figure 2.13 B**). Collectively, these data are consistent with robust activation of ATM- and ATR-dependent DNA damage signaling at concentrations associated with significant chemosensitivity.

Impact of ATM, ATR and FANCD2 suppression on imidazotetrazine sensitivity

The Fanconi's Anemia pathway is important for repairing DNA inter-strand crosslinks, and DP68 forms DNA inter-strand crosslinks, activating the ATM and/or ATR damage responses. To assess functional importance, these pathways were evaluated using siRNAs and small molecule inhibitors. U251 cells were electroporated with siRNAs directed against ATM, ATR and a core Fanconi Anemia pathway gene, FANCD2 (**Figure 2.14 A**). Knockdown of ATM had no impact on sensitivity to TMZ, DP68, or DP86 (**Figure 2.14 B**), while ATR knockdown significantly enhanced the responses to TMZ, DP86 and DP68. FANCD2 knockdown resulted in a significantly enhanced activity only with DP68 treatment (relative fluorescence of 0.16 vs. 0.51, $p \leq 0.001$), but had no significant effect on TMZ (0.37 vs. 0.44, respectively; $p=0.26$) or DP86 (0.87 vs. 0.96, respectively; $p=0.11$) treated cells. The impacts of ATR and ATM signaling on cytotoxicity were confirmed using small-molecule inhibitors of ATM (KU-60019) and ATR (VE-821) kinase activity in U251 (**Figure 2.15 A**) and T98G (**Figure 2.15 B**) cells. In both lines, co-treatment with VE-821 markedly enhanced the efficacy of DP68, and to a lesser extent DP86 in T98G cells. In contrast, KU-60019 was less effective than VE-821 when combined with DP68 in T98G cells (p-value ≤ 0.001) and in U251 cells (p-value ≤ 0.01). Similarly, co-treatment with the ATR inhibitor VE-821, but not KU-60019, enhanced the efficacy of DP68 and DP86 in a neurosphere assay with GBM12 or GBM12TMZ (**Figures 2.15 C-D**). These data are consistent with the induction of DNA crosslinks by DP68 and suggest that ATR and FANCD2 aid recovery following treatment with DP68.

GBM tumors fail to respond to novel imidazotetrazine compounds in vivo

The efficacy of DP68 and DP86 was evaluated *in vivo* in xenografts of U87NS (**Figure 2.16 and Figure 2.17**). Mice were injected with $1x10^6$ U87NS single cells and drug treatments began when tumor volumes reached 250-350 mm^3 (**Figure 2.16 A**) or 300-450 mm^3 (**Figure 2.16 B**). Treatment groups consisted of: vehicle control, TMZ (20 mg/kg), DP86 (20 mg/kg), DP68 (10 mg/kg), or DP68 (20 mg/kg) and drug was delivered via intraperitoneal (IP) injection on two consecutive days. Following TMZ treatments, tumor growth continued but leveled off around day five, showing a delay in tumor growth for an additional 10 days (**Figure 2.16 A**). However, with the exception of one mouse, TMZ-treatment did not completely inhibit tumor progression and eventually tumor growth resumed. DP86- and DP68-treated mice failed to show any effect on tumor growth. Survival data (**Figure 2.16 C, Table 2.2**) shows that DP86- and DP68-treated mice had median survival times equivalent to DMSO:PBS treated mice. TMZ-treated mice showed a 2-fold increase in survival (**Table 2.2**). Concerns regarding the solubility of the novel imidazotetrazines in PBS, as was used in the initial *in vivo* work, led us to repeat the mouse experiments with drugs dissolved in 100% DMSO, but there was still no *in vivo* response to DP86 and DP68 (**Figure 2.16 B and D, Table 2.3**). We next attempted to improve the efficacy of DP86 and DP68 with different drug delivery methods and changes to the treatment schedule (**Figure 2.17**). U87NS subcutaneous xenografts were treated with DMSO, 25 mM TMZ, 25 mM DP86, or 25 mM DP68 via IT injection on five consecutive days. IT injections allow for higher doses of drug delivered to the tumor with less systemic toxicity. TMZ-treated tumors showed strong inhibition of

tumor growth with four of the six tumors failing to progress and even regressing in some cases (**Figure 2.17**). Finally, DP86 and DP68 failed to demonstrate an effect on tumor growth compared to DMSO control in this model. Tumors were removed and examined once the mice were sacrificed (**Figure 2.18**). DP68 tumors displayed areas where drug precipitated. This was not seen for tumors treated with any of the other drugs, including DP86.

Evaluation of pharmacokinetic properties of imidazotetrazine compounds

The pharmacokinetic properties of DP68 and DP86 were evaluated in mice for potential dosing strategies. Following a single IP injection, DP86 peaked rapidly with a T_{max} of 10 min, C_{max} of 3230 nM and $t_{1/2}$ = 14 min (**Figure 2.19 A**). DP68 had similar pharmacokinetic properties except that absorption was much more limited with a C_{max} of 206 nM (**Figure 2.19 B**). No adverse clinical effects were noted in the mice for up to 6 h after drug injection. However, because of the very short half-life for both drugs and the relatively limited absorption for DP68, further *in vivo* characterization of these compounds was not pursued.

We investigated whether the fast elimination could be due to enzymatic degradation using published techniques (Gynther, Laine et al. 2008). The half-lives of DP68 and DP86 were determined in mouse liver homogenate (DP68 $t_{1/2}$ = 1.73 ± 0.05 h (n=3); DP86 $t_{1/2}$ = 1.62 ± 0.18 h (n=3)), and the half-lives were roughly the same as those in aqueous buffer at pH 7.4 (DP68 $t_{1/2}$ = 1.75 ± 0.04 h (n=3); DP86 $t_{1/2}$ = 1.74 ± 0.08 h

(n=3)). Therefore, it is likely that DP68 and DP86 are not susceptible to enzymatic degradation in the liver.

Conclusion and discussion

TMZ is a key component of therapy for GBM, but resistance limits the ultimate benefit. Expression of the MGMT DNA repair protein accounts for profound TMZ resistance in the majority of chemotherapy-naïve GBM patients, and inactivation or down-regulation of MMR can lead to acquired tolerance of TMZ-induced lesions. Therefore, developing therapeutic agents based on the TMZ structure that circumvent mechanisms of TMZ resistance may provide significant therapeutic gains. In this study, the anti-glioma activity was evaluated for two novel imidazotetrazine analogs: the bivalent DP68 and monovalent DP86. Both compounds exhibited activity in established glioma lines maintained in both serum-containing medium and as neurospheres in defined medium. In short-term explant cultures from primary GBM xenograft lines, these compounds were equipotent in TMZ-sensitive and -resistant GBM models. The bivalent DP68 induced a rapid and profound S-phase accumulation, and was associated with early activation of DNA damage signaling. These data provide a proof-of-concept that novel TMZ analogs can circumvent TMZ resistance in GBM models.

TMZ chemotherapy provides significant benefit to a subset of patients, although eventual emergence of TMZ resistance and progressive tumor growth are almost universal. Stem-like cells express drug efflux transporters, have higher DNA repair capacities and may be responsible for re-populating tumors with therapy-resistant clones (Bao, Wu et al. 2006; Chen, Li et al. 2012; Kreso, O'Brien et al. 2013). They grow as neurospheres in serum-free media, and in this study, the effects of the imidazotetrazine

analogs on neurosphere growth were evaluated in cell line- and patient-derived neurospheres.

The neurosphere recovery assay provides a 3-dimensional tumor model that measures acute responses to drug therapy and the clonogenic potential of cells following treatment. Both U87NS (TMZ sensitive) and U118NS lines (TMZ resistant), cells were initially responsive to TMZ treatment, but outgrowth of secondary neurospheres was only inhibited at TMZ concentrations greater than 100 μM (**Figure 2.10**), which is at the limit of clinically achievable levels of TMZ (Middlemas, Stewart et al. 2000). A similar pattern of regrowth was observed with DP68, but at a 10-fold lower concentration. The impact of drug therapy also was evaluated in neurosphere cultures derived directly from patient-derived xenograft lines. In both GBM12 (TMZ sensitive) and GBM6 (TMZ resistant) models, DP68 effectively suppressed neurosphere formation at a log-lower dose of drug than TMZ. Although other criteria for defining tumor stemness were not tested in this study, we have demonstrated tri-lineage differentiation, self-renewal and tumorigenicity in animals for multiple Mayo GBM xenograft lines (Higgins, Wang et al. 2013). Thus, these data suggest that DP68 effectively kills stem-like cells and reduces the emergence of TMZ resistance mechanisms.

Three models of acquired TMZ resistance were evaluated in this study. The dose responses for DP68 and DP86 were similar for GBM12 and GBM12TMZ, while the latter line was markedly resistant to TMZ. Resistance in GBM12TMZ has been linked to

high-level MGMT expression (Kitange, Carlson et al. 2009). Co-administration of the MGMT suicide inhibitor *O*6-BG significantly sensitized MGMT overexpressing cells lines to TMZ (GBM6 and T98G), but had no impact on responses to DP68 or DP86. The U87NSTMZ and U251TMZ lines have distinct mechanisms of TMZ resistance unrelated to MGMT. Previous studies linked mutational inactivation of MSH2 or MSH6 in the MMR pathway to tolerance of cytotoxic *O*6-MeG lesions, resulting in TMZ resistance in GBM patients (Zhang, Stevens et al. 2011; Zhang, Stevens et al. 2012). Further analysis of TMZ-resistant line U87NSTMZ (**Figure 2.20**) showed an increase in MLH1 and a decrease in MSH2 levels compared to parental U87NS. In the FA/BRCA pathway, we observed FANCD2 overexpression and BRCA1 downregulation in U87NSTMZ. FANCD2 data is consistent with studies demonstrating FANCD2 overexpression in chemotherapy-resistant lines (Chen, Taniguchi et al. 2007) while FANCD2 loss sensitizes multiple cell types to chemotherapy drugs (Lyakhovich and Surralles 2007). The mechanism of resistance in the U251TMZ line was not evaluated. Regardless of mechanism, the data demonstrate equal efficacy of DP68 and DP86 in parental tumor lines (U251, U87NS) and derivative models of acquired TMZ resistance (U251TMZ, U87NSTMZ). Thus, DP68 and DP86 are highly effective in models with diverse mechanisms of TMZ resistance and support our hypothesis that these compounds can overcome a major clinical problem, TMZ resistance.

The aqueous chemistry of DP68 and DP86 is subtly different from that of TMZ (**Figure 2.2**). All three compounds undergo pH-dependent hydrolytic ring-opening

reactions to generate reactive diazonium ions. For TMZ these are the final reactive intermediates that covalently modify *N*7-G, *O*6-G, and *N*3-A. In contrast, the diazonium ions from DP68 and DP86 undergo an efficient, intra-molecular trapping reaction to form aziridinium ions, and these intermediates react with DNA, predominantly at *N*7-G sites (Garelnabi, Pletsas et al. 2012). These new agents are designed to generate anticancer activity from *N*7-G adducts, but in addition, adducts at *O*6-G are resistant to repair by MGMT (Pletsas, Garelnabi et al. 2013). Consistent with either mechanism, sensitivity to both compounds was unaffected by MGMT expression in the TMZ-resistant T98G, GBM6, or GBM12TMZ models, and a similar MGMT-independence was observed in A2780 ovarian carcinoma cells (Pletsas, Garelnabi et al. 2013). The early arrest in S-phase with DP68 treatment is consistent with DNA adducts that cannot be bypassed by the replication machinery, thereby, stalling replication forks. Consistent with these observations, DP68 triggered robust DNA damage signaling to the Chk1 and Chk2 checkpoint kinases and the chromatin remodeling protein KAP1 within 4 to 8 h of treatment, and ultimately phosphorylation of H2AX (Ghosal and Chen 2013). These damage-inducible modifications are typically mediated by ATM in response to DNA DSBs and by ATR in response to replication-induced DNA damage. Consistent with signaling triggered by replication-induced damage, disruption of ATR signaling enhanced the potency of DP68 and DP86, while ATM inhibition had less significant and inconsistent effects (**Figure 2.14 and 2.15).** Collectively, these data suggest that DP68 and DP86 induce DNA lesions that disrupt DNA replication.

Despite likely similar nucleotide targets, DP68 and DP86 trigger significantly different patterns of DNA damage processing compared to TMZ. DP68 is a bivalent molecule that could generate two reactive aziridinium ions. Given the propensity of aziridinium ions to react with *N*7-G, we speculated that DP68 would insert five-atom, 3-azapentylene *N*7-G–*N*7-G intra- and/or inter-strand crosslinks. The marked suppression of H_2O_2-induced comet tail moment following treatment with DP68, but not DP86, is consistent with formation of DNA inter-strand crosslinks. Moreover, the Fanconi's anemia DNA repair pathway specifically repairs cross-link damage (Chen, Taniguchi et al. 2007), and disruption of this repair function, via siRNA suppression of FANCD2, sensitized U251 cells to DP68 but not DP86 or TMZ. These data indicate formation of inter-strand crosslinks by DP68, and the 10-fold greater potency compared to DP86 likely reflects this DNA cross-linking activity.

The present study provides proof-of-concept for novel imidazotetrazine analogs that induce DNA adducts insensitive to TMZ-resistance mechanisms. Specifically, bi-functional DP68 with DNA cross-linking activity provided significant gains in potency and was highly effective against cells with the most common mechanism of TMZ resistance: MGMT overexpression. While *in vivo* studies failed to demonstrate efficacy of either DP86 or DP68, preliminary pharmacokinetic studies gave us better insight into the lack of *in vivo* efficiency. These pharmacokinetic studies showed that the half-life for DP68 and DP86 (14 min) are significantly shorter than TMZ (55 min). Based on these data, medicinal chemistry approaches are being used to optimize the drug-like properties

for improved biodistribution. Essentially all GBM patients treated with TMZ develop refractory disease and ultimately die from progressive tumor growth. Thus, developing novel chemotherapies specifically effective against, or indeed averting the evolution of TMZ-resistant tumors is a critical unmet clinical need (Johnson, Mazor et al. 2014). The data presented suggest that mono- and bi-functional imidazotetrazines may be a compound class for treating TMZ-resistant tumors. Future studies with optimized second-generation molecules will focus on defining the *in vivo* efficacy in orthotopic GBM xenograft models and defining the toxicity profile and therapeutic window for this promising class of agents.

Materials and Methods

Cells and Reagents

The glioma cell lines U87MG, T98G, and U251 were purchased from the ATCC in 2011, 2001, and 2001, respectively. U118MG was a kind gift from Dr. Larry Recht (Stanford University, 2003). U251 (ATCC), T98G (ATCC), U118MG (IDEXX RADIL) and U87MG (IDEXX RADIL) were authenticated by short tandem repeat analysis in 2013. These cell lines are representative of the diverse GBM genotypes (**Table 2.1**). Adherent lines were maintained as monolayer cultures in DMEM supplemented with 10% FBS and 1% penicillin/streptomycin. U87MG and U118MG were converted to neurosphere cultures, U87NS and U118NS, by lifting cells from plates with 0.05%Trypsin-EDTA (Gibco), washing cells three times with PBS to remove traces of FBS, and plating 500,000 cells/75 cm^2 flask. U87NS and U118NS were maintained in serum-free media consisting of DMEM/F12 1:1 (Gibco), B27 supplement (Gibco), 15 mM HEPES (Gibco) supplemented with 20 ng/mL EGF (Invitrogen) and 20 ng/mL bFGF (Invitrogen). Short-term explant cultures, GBM6 and GBM12, were established from Mayo GBM xenograft lines by mechanical disaggregation followed by culture in neurobasal serum-free media (StemPro NSCSFM; Invitrogen Cat#A1050901) supplemented with 20 ng/mL EGF (Invitrogen) and 20 ng/mL bFGF (Invitrogen).

TMZ-resistant culture, U87MGTMZ, was established from U87MG cells by incrementally increasing TMZ twice-weekly to a final concentration of 325 μM. U87MGTMZ cells were then converted to the neurosphere culture, U87NSTMZ. TMZ-

resistant cells were maintained with a single weekly dose of TMZ and passaged every 14 days. GBM12TMZ (#3080) from the Mayo GBM xenograft panel and U251TMZ have been described (Giannini, Sarkaria et al. 2005; Kitange, Mladek et al. 2012).

DP68 and DP86 were synthesized as described previously (Garelnabi, Pletsas et al. 2012), and TMZ was bought from Schering-Plough Corp and Sigma-Aldrich. All 3 agents were prepared as 25 mM stocks in dimethyl sulfoxide (DMSO). *O*6-benzylguanine (*O*6-BG) was obtained from Sigma-Aldrich, the ATR inhibitor VE-821 from ChemieTek and the ATM inhibitor KU-60019 from Selleck Chemicals.

Antibodies against ATM (ab10939), p-ATM S1981 (ab81292), p-KAP1 (ab70369), and MSH2 were purchased from Abcam; Chk1 (#04-207), Chk2 (#05-649) and ATR (#PC538) from Millipore; PMS2 from B.D. Bioscience, p-Chk1 Ser345 (#MA5-15145) and MGMT (#MS-470-P) from Thermo Scientific; p-Chk2 Thr68 (#2661), KAP1 (#4123), p-H2A.X Ser139 (#2577), MLH1 (#3515), and BRCA1 from Cell Signaling; and FANCD2 (#2986-1) from Epitomics. Levels of FANCD2 in U87TMZ lines were measured using antibody from Santa Cruz Technologies. β-actin antibody was purchased from Sigma-Aldrich and Cell signaling (8H10D10, #3700). Secondary anti-rabbit IgG, peroxidase-linked and anti-mouse IgG, peroxidase-linked were purchased from Cell Signaling Technologies and Pierce, respectively.

Western Blotting

Cells were lysed in RIPA lysis buffer (R0278, Sigma-Aldrich) supplemented with a protease inhibitor cocktail (Roche). Total proteins were isolated from flash frozen flank xenografts or short-term explant cultures, separated by SDS-PAGE, and electro-transferred onto PVDF membranes. Membranes were blocked in Tris-buffered saline (TBS) containing 5% powdered milk and 0.1% Tween-20 at room temperature. All primary antibodies were incubated overnight at 4 ºC followed by room temperature incubation with a secondary antibody conjugated with horseradish peroxidase for 1 h. Detection was performed with Super Signal Chemiluminescent reagent according to the manufacturer's protocol (Pierce).

CyQUANT cell proliferation assay

A cell proliferation assay was performed using the CyQUANT Cell Proliferation kit (Invitrogen) according to manufacturer's recommendations. Cells were seeded (1,000 cells/well) in triplicate in 96-well plates, exposed to various concentrations of DP68, DP86, or TMZ, and incubated for 5 days. In experiments where MGMT was inhibited, *O*6-BG (10 μM) was added 1 h before DP68, DP86, or TMZ treatment. On day 5, medium was removed, cells were washed once with PBS, and plates were stored at –80^{o} C. The plates were thawed and lysed in CyQUANT GR dye-containing lysis buffer (200 μL/well). After 4 min incubation at room temperature, the fluorescence intensity of the DNA-binding dye was measured using a TECAN plate reader with excitation at 480 nm and emission at 520 nm.

Flow cytometry analysis

Cell cycle distribution was analyzed by flow cytometry. Cells were harvested, washed with PBS, and fixed with ice-cold 70% ethanol/30% PBS. Cells were re-suspended in PBS containing propidium iodide (40 μg/ml), RNase A (100 μg/ml) and Triton X-100 (0.05%), and incubated at 37 ºC for 30 min. DNA content was determined using a FACScan flow cytometer system (Becton Dickinson), and results were analyzed with Modfit software (Verity Software).

Neurosphere assays

Chemosensitivity (sphere IC_{50}) of GBM cells to TMZ, DP86, and DP68 was analyzed by seeding U87NS and U118NS cells in triplicate in 96-well plates (1,000 cells/100 μL/well) (BD Falcon). After 24 h, vehicle, TMZ, DP86, or DP68 was added to the wells, and primary neurospheres were quantified after 7 days. Primary xenograft cultures (GBM6, GBM12, and GBM12TMZ) were plated (500 cells/well), treated, and neurospheres were quantified at day 14. For the limiting dilution experiments in Figure 2.6, GBM12, GBM12TMZ, and GBM6 cells were plated at 1, 10, 30, 100, 300 or 1000 cells/well, drug treated after 24 hrs, and counted at day 14. Recovery and secondary sphere assay (Gilbert, Daou et al. 2010), cells were plated at clonal density (3,000 cells/mL; 2 mL total) in 6-well plates (BD Falcon) and treated with TMZ, DP86, DP68, or vehicle. Primary spheres were counted on day 7 and cells were fed with neurosphere medium (2 mL). Spheres for the recovery phase were counted on day 14, dissociated

using a basic pH dissociation method (Sen, Kallos et al. 2004), and a fraction of the culture re-plated. Secondary spheres were counted on day 21. Spheres with 10 cells or more were counted.

siRNA and shRNAs

Transient knockdown of ATM, ATR, and FANCD2 was achieved using siRNAs from Thermo Scientific/Dharmacon: ATM- AAG CAC CAG TCC AGT ATT GGC; ATR- C CTC CGT GAT GTT GCT TGA; FANCD2- GGU CAG AGC UGU AUU AUU C; control luciferase siRNA- CTT ACG CUG AGU ACU UCG A. siRNAs were mixed with 5-8 million U251 cells and electroporated with two 280 V pulses of 10 ms. The cells were plated, incubated overnight and again electroporated. After a 24 h recovery, cells were plated for subsequent studies.

For MLH1 knockdown experiments, lentiviral (TRC) shRNAs against eGFP and MLH1 (TRCN0000040053, TRCN0000040056) as well as the empty pLK0.1 vector construct were purchased from UMASS RNAi Core (Open Biosystems), and lentiviruses were produced using HEK293T. T98G and U87MG cells were infected by lentivirus using 10 μg/mL polybrene, followed by selection using 2 μg/mL puromycin for two weeks to generate stable lines.

Analysis of DNA cross-linking in single cells using alkaline comet assay

U251 cells in exponential growth were exposed to DP68, DP86, TMZ, or melphalan (positive control for cross-linking) for 24 h and subsequently treated with 100 μM hydrogen peroxide for 20 min. As described previously (Phillips and Ward 2001), cells then were embedded in 0.5% low melting point agarose, spread on agarose coated glass slides, and lysed in ice cold lysis buffer before being transferred to electrophoresis buffer (pH >13). After a 30 min incubation to allow DNA unwinding and expression of alkali labile sites, cells were subjected to electrophoresis at 0.6 V/cm for 25 min. Neutralization buffer was added drop-wise to the slides followed by rinsing in distilled water, fixation in 100% ice-cold ethanol and drying overnight. Slides were stained with SYBR^{TM}Gold solution (Molecular Probes Inc.), and the comets were visualized using an epi-fluorescent microscope (Nikon Eclipse E800). Tail moments were measured on 50 randomly selected comets using Comet Assay III software (Perceptive Instruments, UK). Percentage DNA cross-linking was calculated from (TM_C-TM_T) / TM_C where TM_C and TM_T represent the tail moment of control and drug treated cells respectively (Phillips and Ward 2001).

Subcutaneous xenografts and *in vivo* drug treatments

U87NS neurospheres were pH dissociated, counted, and injected ($1x10^6$/100 μL PBS) into the right flanks of Nu/Nu male mice (Charles River Labs). For the *in vivo* work in **Figure 2.17**, tumor volumes were measured with calipers, and drug treatments were initiated when tumor volumes reached 250-350 mm^3. Volume was calculated as (4/3) x

(π) x (length/2) x (width/2)^2. Mice were randomly assigned into treatment groups consisting of: 150 μL DMSO:PBS (1:1) (n=3), 20 mg/kg TMZ (5 mg/kg working stock) (n=4), 20 mg/kg DP86 (5 mg/mL working stock) (n=4), 10mg/kg DP68 (5 mg/mL working stock) (n=3), and 20 mg/kg DP68 (10 mg/mL working stock) (n=4). All drugs were prepared in DMSO and diluted in PBS to a working stock for injection. Drug was delivered via IP on two consecutive days. Tumor growth was monitored, and mice were sacrificed when tumor volumes reached 1000-1200 mm^3. For the *in vivo* work in Figure 2.18, drug treatments were initiated when tumor volumes reached 250-450 mm^3. Mice were divided into four treatment groups consisting of: DMSO IT (n=7), TMZ IT (25 mM stock) (n=6), DP86 IT (25 mM stock) (n=6), and DP68 IT (25 mM stock) (n=6). All drugs were prepared in DMSO. Drug was delivered on five consecutive days and drug volumes used to treat used were based on tumor volumes (1/10th of tumor volume). Tumor volumes were monitored for 25 days before remaining mice were sacrificed.

Pharmacokinetic analysis of imidazotetrazine compounds

DP68 and DP86 were formulated in 0.9% NaCl, 10% (w/v) HP-β-cyclodextrin, and C57B2/6 mice were dosed with a single 25 μmol/kg IP. Groups of 3 mice were euthanized at times up to 6 h after injection, and plasma was harvested for analysis. Drug levels were assessed by the LTQ quadrupole ion trap mass spectrometry method (Gynther, Laine et al. 2008).

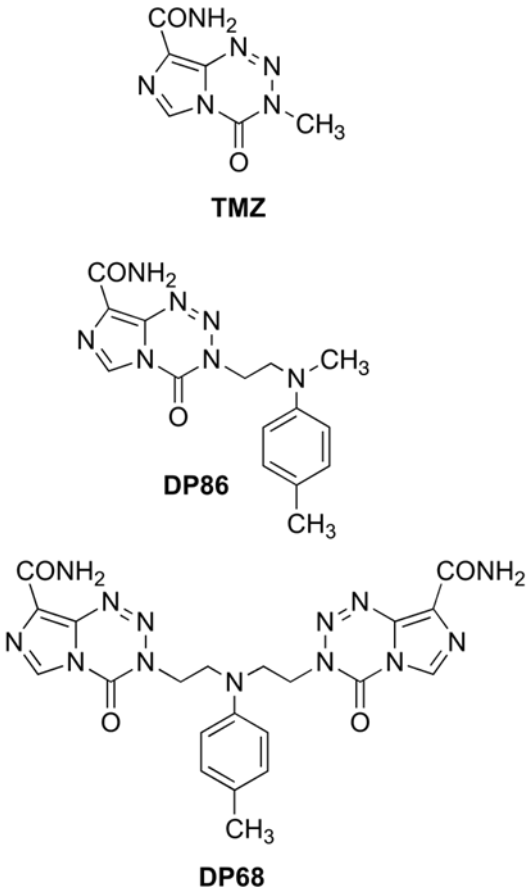

Figure 2.1 Structures of TMZ, DP68, and DP86.

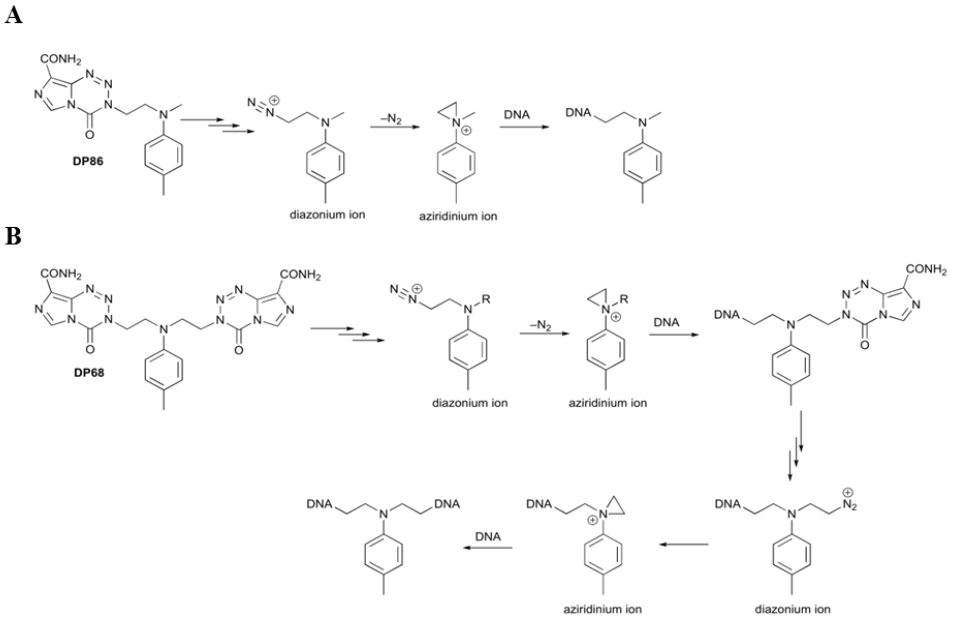

Figure 2.2 Summary of prodrug activation.
Summary of prodrug activation and drug mechanisms of action for DP68 and DP86 highlighting the roles of diazonium and aziridinium ion intermediates. DP86 monoalkylation (A) and DP68 crosslink formation (B).

Table 2.1 Activity of TMZ, DP68, and DP86 in glioma cultures.

CELL LINE	MGMT	EGFR AMPLIFIED	P53	PTEN ACTIVITY	IC50 (μM)			TMZ/DP68
					TMZ	DP86	DP68	
Established glioma cell line CyQuant assay								
T98G	+++	–	mutant	–	340 ± 21	110 ± 9	11.3 ± 2.2	30
U118MG	+	–	mutant	–	135 ± 41	42 ± 7	10 ± 3.0	14
U251	–	–	mutant	–	60 ± 21	68 ± 7	5.2 ± 0.6	12
U251TMZ	–	–	ND	–	306 ± 21	70 ± 13	3.6 ± 0.5	85
U87MG	–	–	WT	–	43 ± 23	67 ± 20	14 ± 5	3
Established glioma line neurosphere assay								
U118NS	+	–	mutant	–	71 ± 11	42 ± 9	2.7 ± 0.2	26
U87NS	–	–	WT	–	7.5 ± 1.0	61 ± 2	5.9 ± 0.5	1.3
U87NSTMZ	–	–	ND	ND	153 ± 8	33 ± 3	4.1 ± 0.2	37
Patient-derived xenograft neurosphere assay								
GBM6	+++	EGFRvIII	mutant	WT	187 ± 38	43 ± 24	1.3 ± 0.6	144
GBM12	–	mutant	mutant	WT	3.2 ± 0.3	19 ± 3	0.8 ± 0.1	4
GBM12TMZ	+++	ND	ND	ND	500 ± 132	25 ± 2	1.4 ± 0.1	357

ND: not determined
WT: wild type

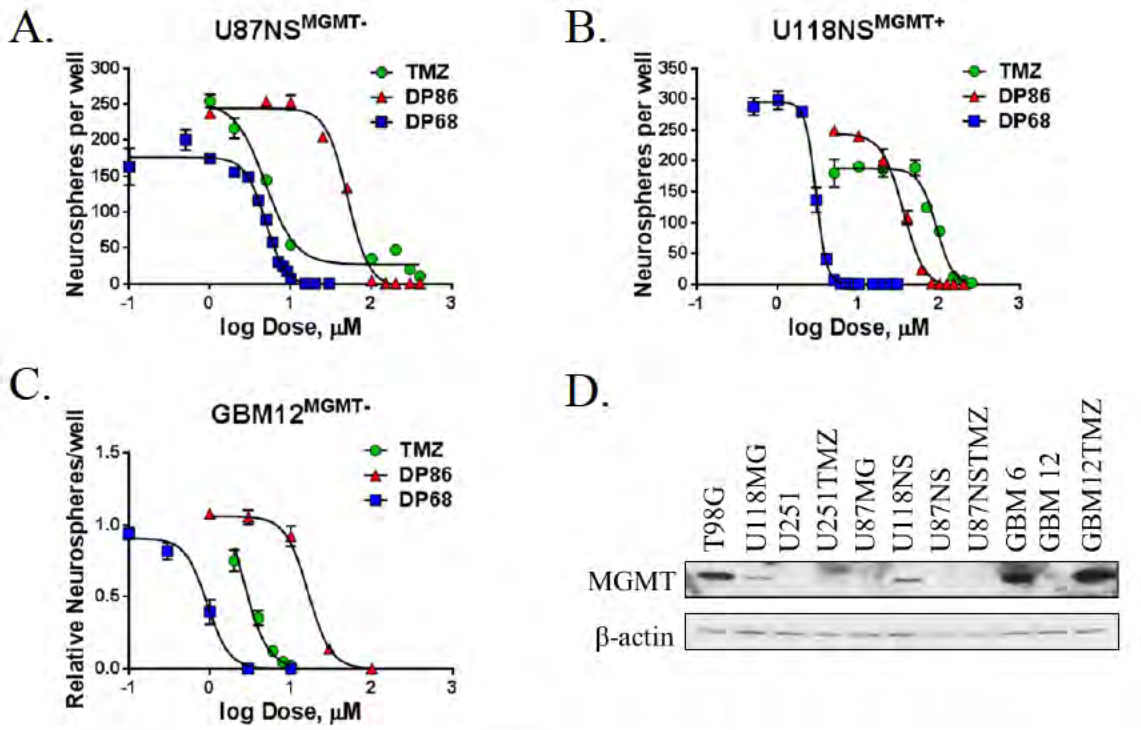

Figure 2.3 Glioma cell sensitivity to TMZ, DP86, and DP68.
The effects of TMZ, DP68, and DP86 were assessed in neurosphere formation assays for U87NS (A), U118NS (B) and GBM12 (C). All neurosphere lines were plated in triplicate and exposed to varying concentrations of each agent. Following a 7-day incubation neurospheres were counted. Mean ± SEM is plotted and representative results from at least three independent experiments are shown. Western blot analysis shows MGMT expression in glioma lines (D). Whole cell lysates were collected and analyzed by western blotting for expression of MGMT. β-actin was used as a loading control.

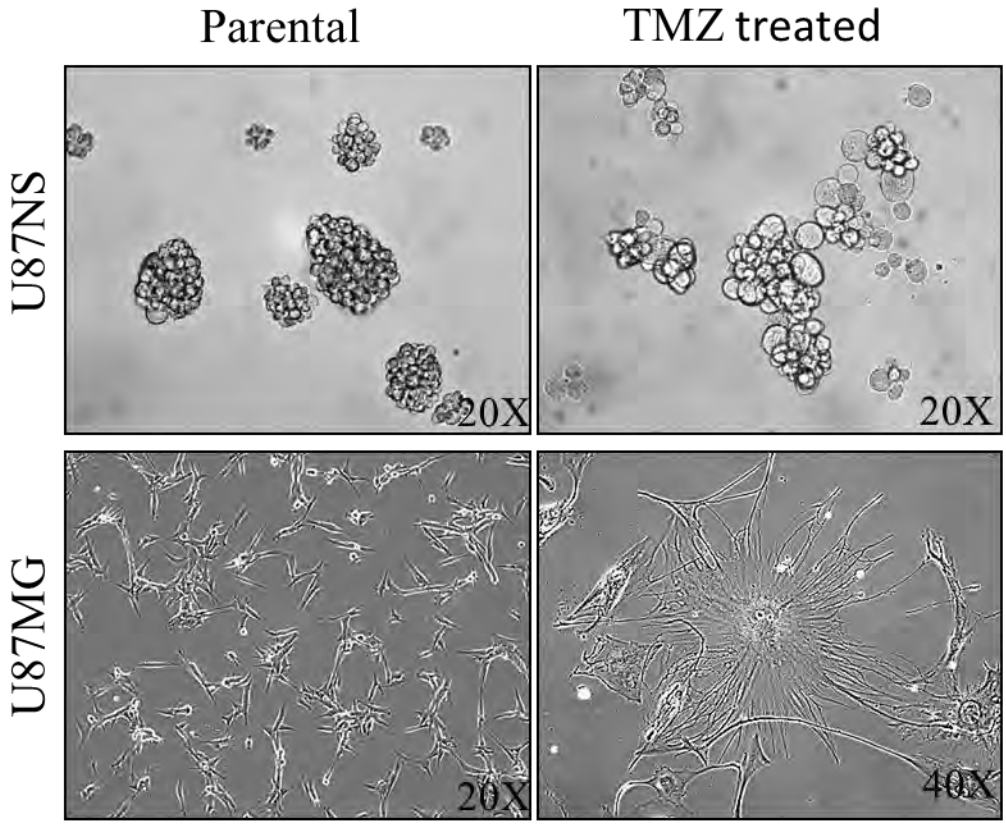

Figure 2.4 TMZ-resistant lines are morphologically different from parental. Phase-contrast microscopy of TMZ-resistant lines, U87MGTMZ and U87NSTMZ, and their respective parental lines. Morphological differences between the resistant and parental lines can be noted.

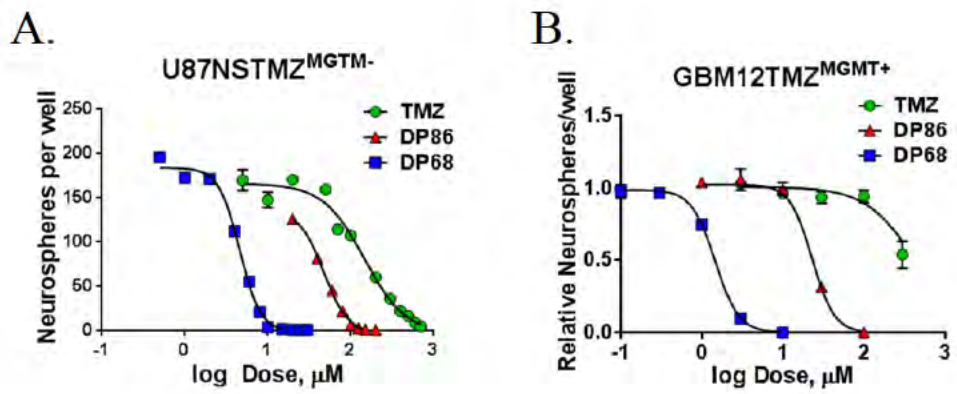

Figure 2.5 DP68 and DP86 efficacy unchanged in models of acquired-TMZ resistance.

The effects of TMZ, DP68, and DP86 were assessed in TMZ-resistant lines, U87NSTMZ (A) and GBM12TMZ (B). All neurosphere lines were plated in triplicate and exposed to varying concentrations of each agent. Following a 7-day incubation neurospheres were counted. U87NSTMZ and GBM12TMZ cell lines sensitivity to TMZ decreased while sensitivity to DP68 and DP86 remained comparable to parental lines. Mean ± SEM is plotted. Representative results from at least three independent experiments are shown.

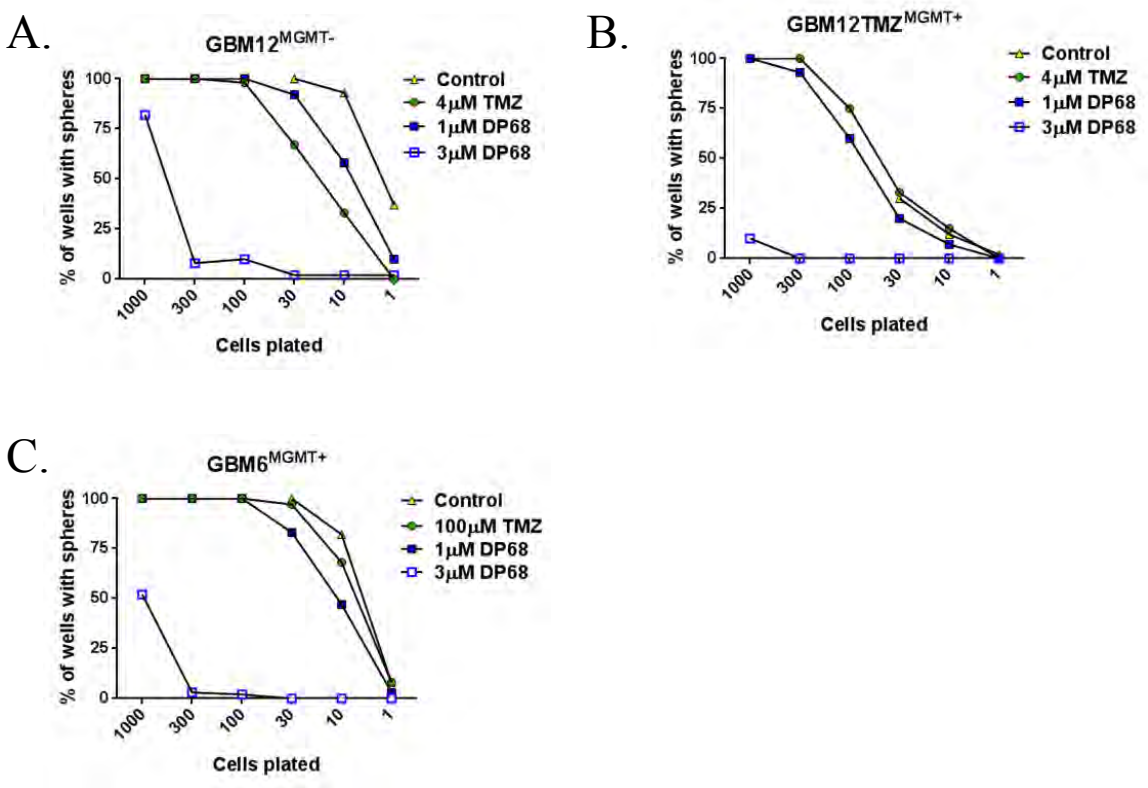

Figure 2.6 Cell density does not affect efficacy of DP68.
Primary cell lines GBM12 (A), GBM12TMZ (B), and GBM6 (C) were plated at various cells densities with the lowest being 1 cell/well. Cells were treated with TMZ, DP68, or control DMSO. Neurospheres were counted14 days later. GBM12 is capable of neurosphere formation following single cell plating while the other two primary lines do not have this capability. However, DP68 efficacy was maintained in all three lines at lower cell densities. Mean ± SEM is plotted. A is a representative of two independent experiments plated in triplicate while B-C is one experiment plated in triplicate.

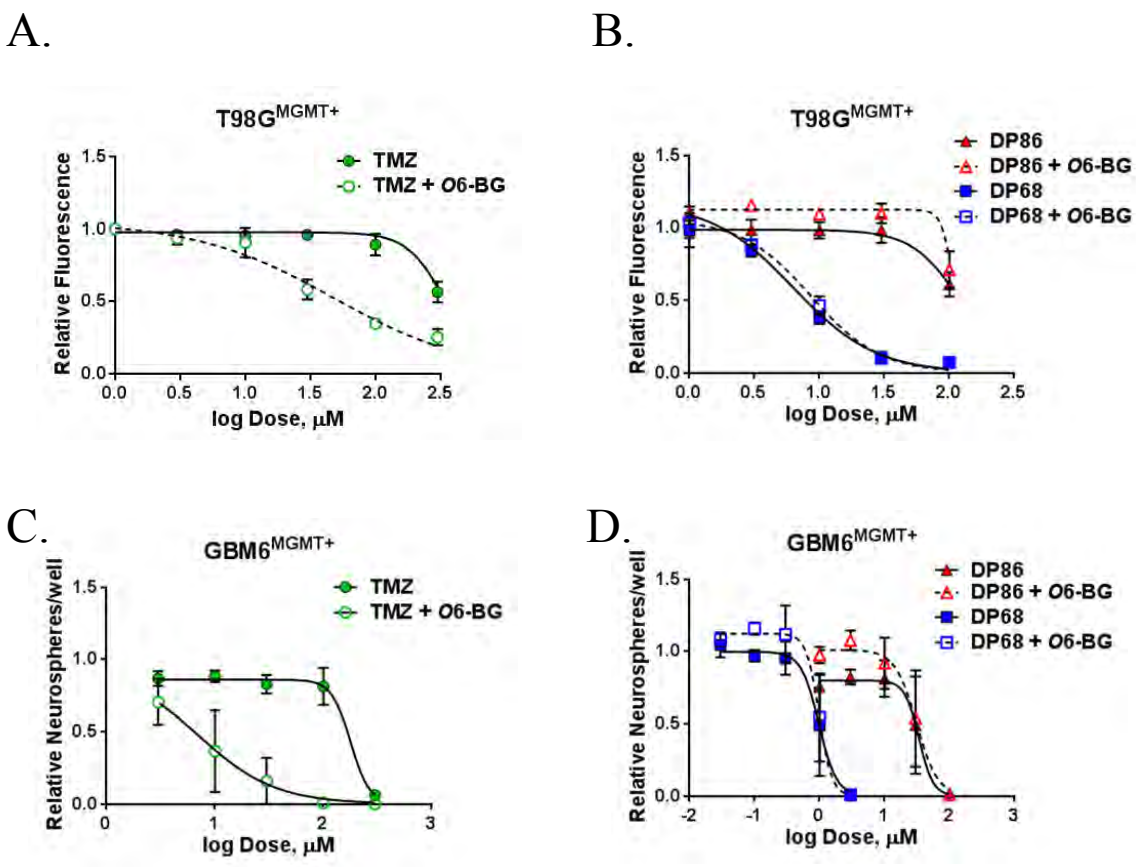

Figure 2.7 Activity of novel TMZ analogues is independent of MGMT.
T98G (A-B) and GBM6 (C-D) co-treated with TMZ (A,C), DP86 (B,D), or DP68 (B,D) and 0 or 10 µmol/L *O*6-BG were evaluated by a CyQUANT assay (A-B) or neurosphere formation (C-D). Inhibition of MGMT by *O*6-BG had no impact on GBM cell line response to DP86 or DP68. Mean ± SEM of three independent experiments are shown.

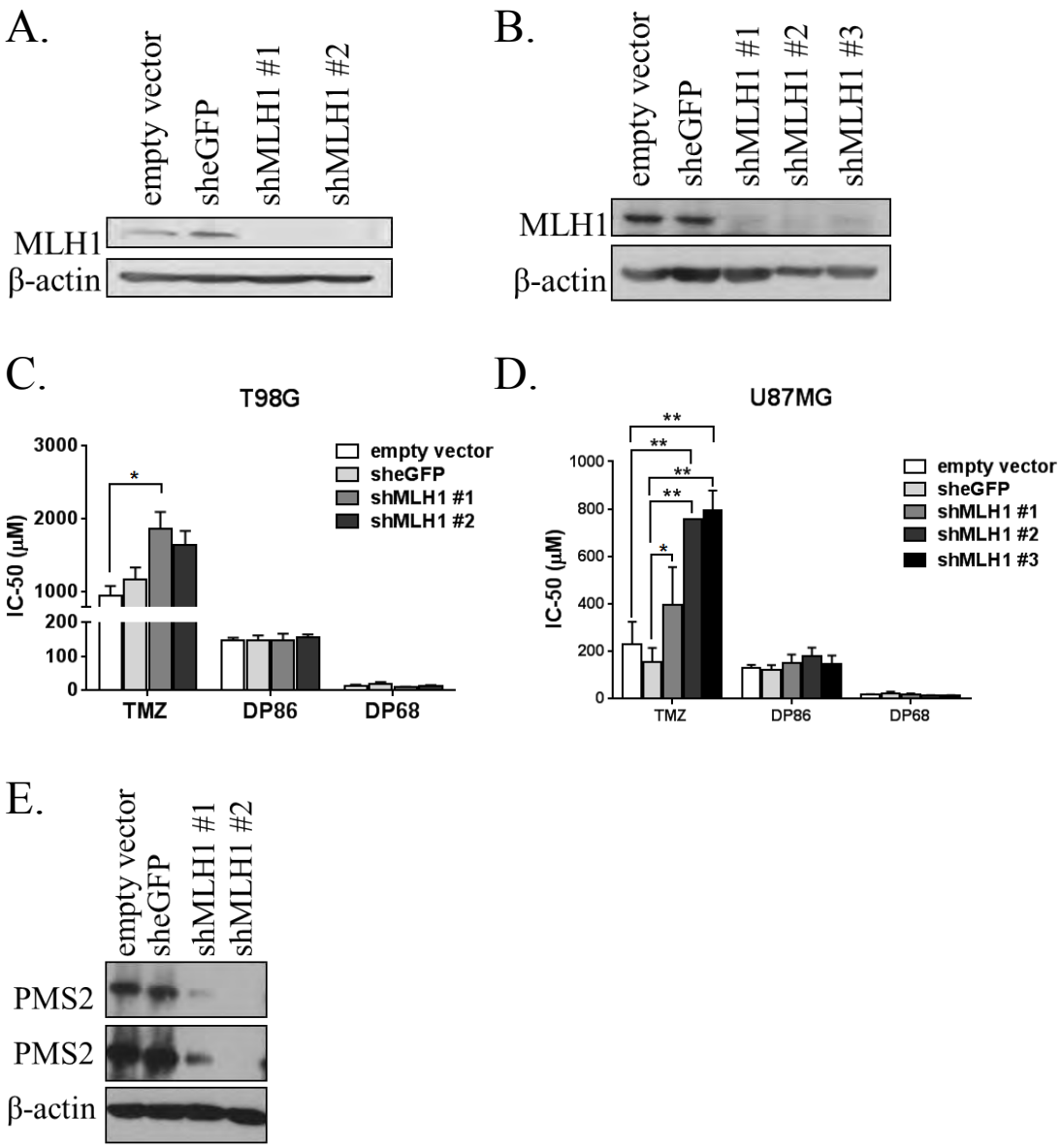

Figure 2.8 DP86 and DP68 activity is independent of MMR expression.
Western blot confirming knockdown in T98G (A) and U87MG (B) cells infected with empty vector, sheGFP, and shRNAs targeting MLH1. Infected T98G (C) and U87MG (D) cells were treated with TMZ, DP86, or DP68 and cell survival was analyzed via CyQUANT assay. Mean IC_{50} ± SEM from at least three independent experiments are graphed. *p<0.05, **p<0.01. Western blot shows decrease of PMS2 (E) expression in T98G MLH1 knockdown cells.

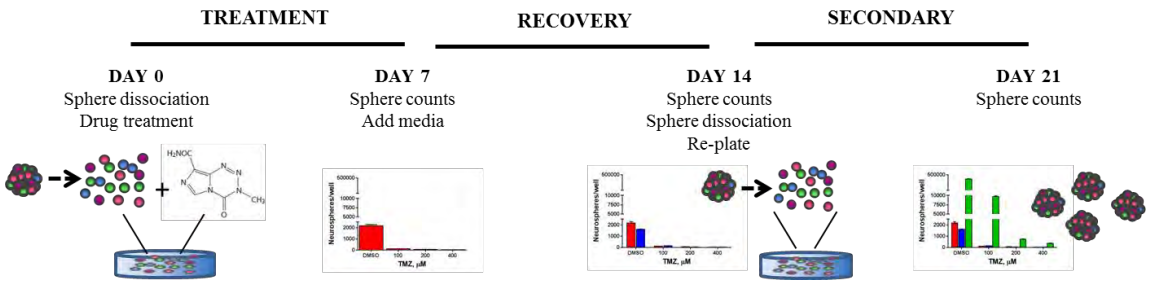

Figure 2.9 Schematic of neurosphere secondary assay.
Neurosphere secondary assay is used to evaluate the treatment, recovery, and secondary sphere formation potential of our GBM lines following treatment with TMZ or novel analogues, DP86 and DP68. On Day 0 GBM neurospheres are dissociated, plated at clonal density, and treated with a single dose DMSO, TMZ, DP86, or DP68. During the course of the assay neurospheres are quantified at day 7 (treatment phase), day 14 (recovery phase), and day 21 (secondary sphere formation phase).

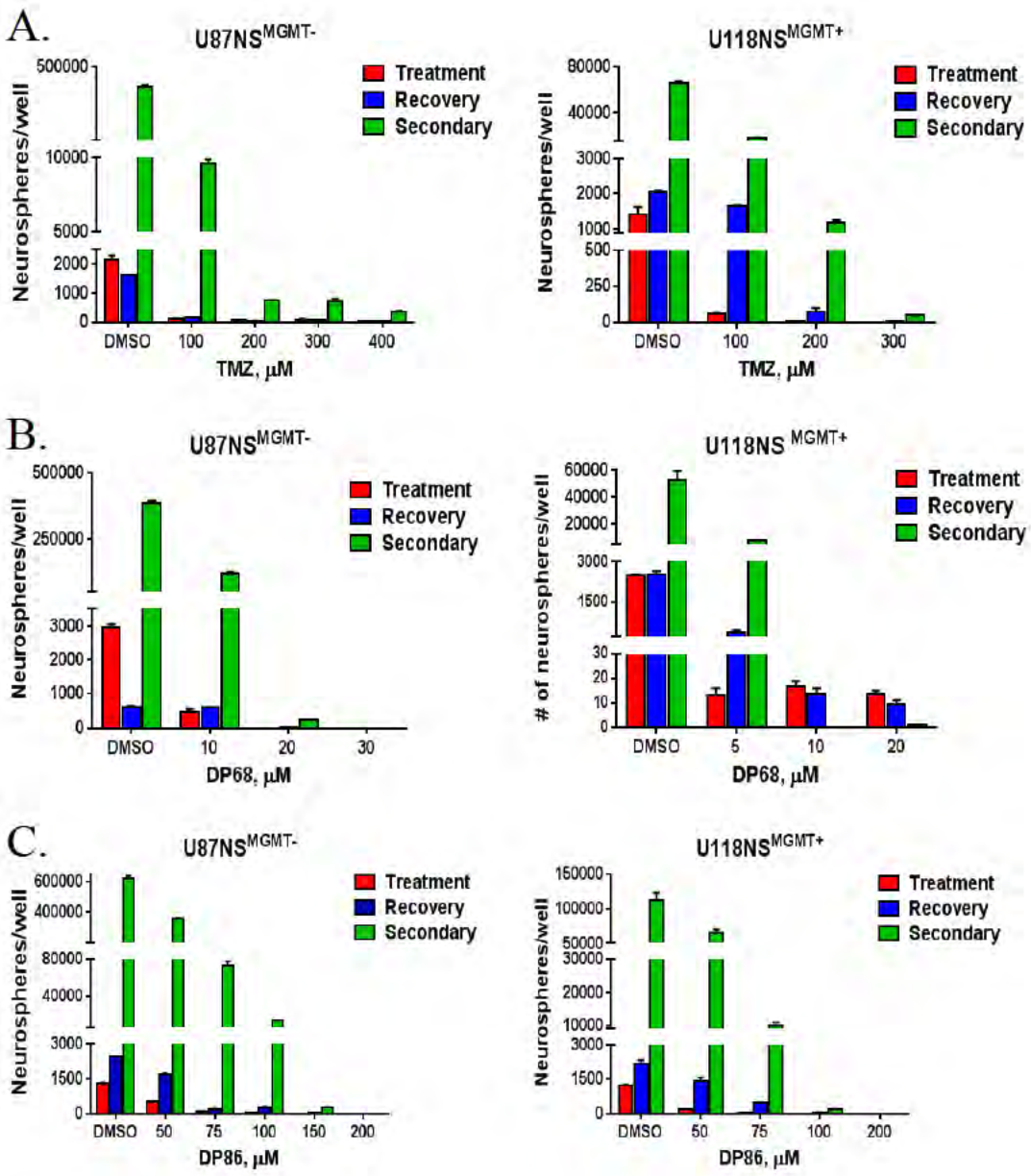

Figure 2.10 Single treatment of GBM neurospheres with DP68 or DP86 leads to a reduction of neurospheres and inhibition of secondary sphere formation.
U87NS or U118NS neurospheres were treated with TMZ (A), DP68 (B), or DP86 (C). Bars show the number of neurospheres counted following treatment on day 7 (red), recovery at day 14 (blue), and secondary spheres at day 21 (green). Representative results from at least three independent experiments are shown.

A.

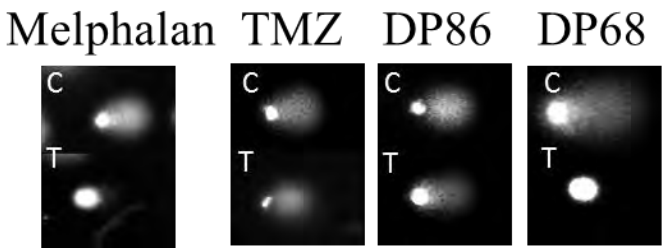

B.

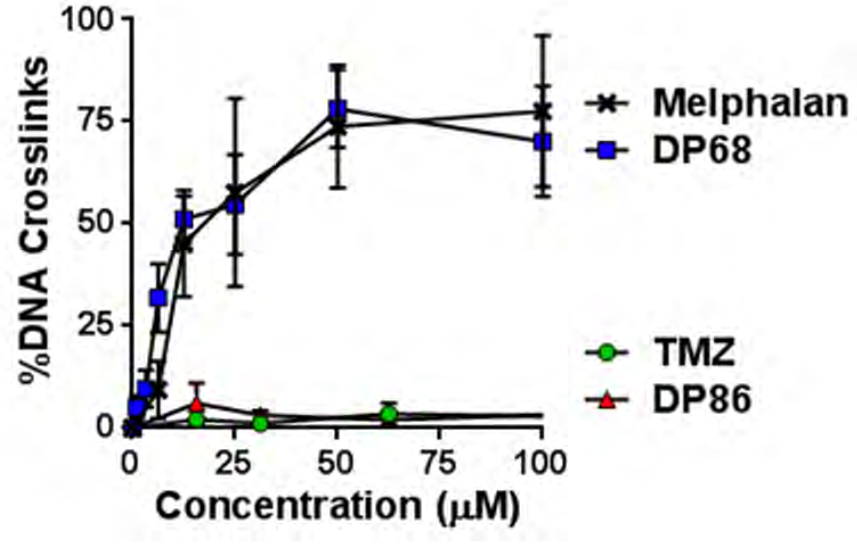

Figure 2.11 DP68 induces DNA damage in the form of crosslinks.
U251 cells were treated with Melphalan, TMZ, DP68 and DP86 for 24 h and then H_2O_2 for 20 min prior to analysis in an alkaline comet assay (A). C= control, T= treated. Relative amount of DNA cross-linking (B) was calculated from $(TM_C\text{-}TM_T)/TM_C$. TM_C= tail moment of control, TM_T= tail moment of drug treated cells. The tail moments of 50 randomly selected comets were measured using Comet Assay III software. % DNA cross-linking ± SD from three independent experiments.

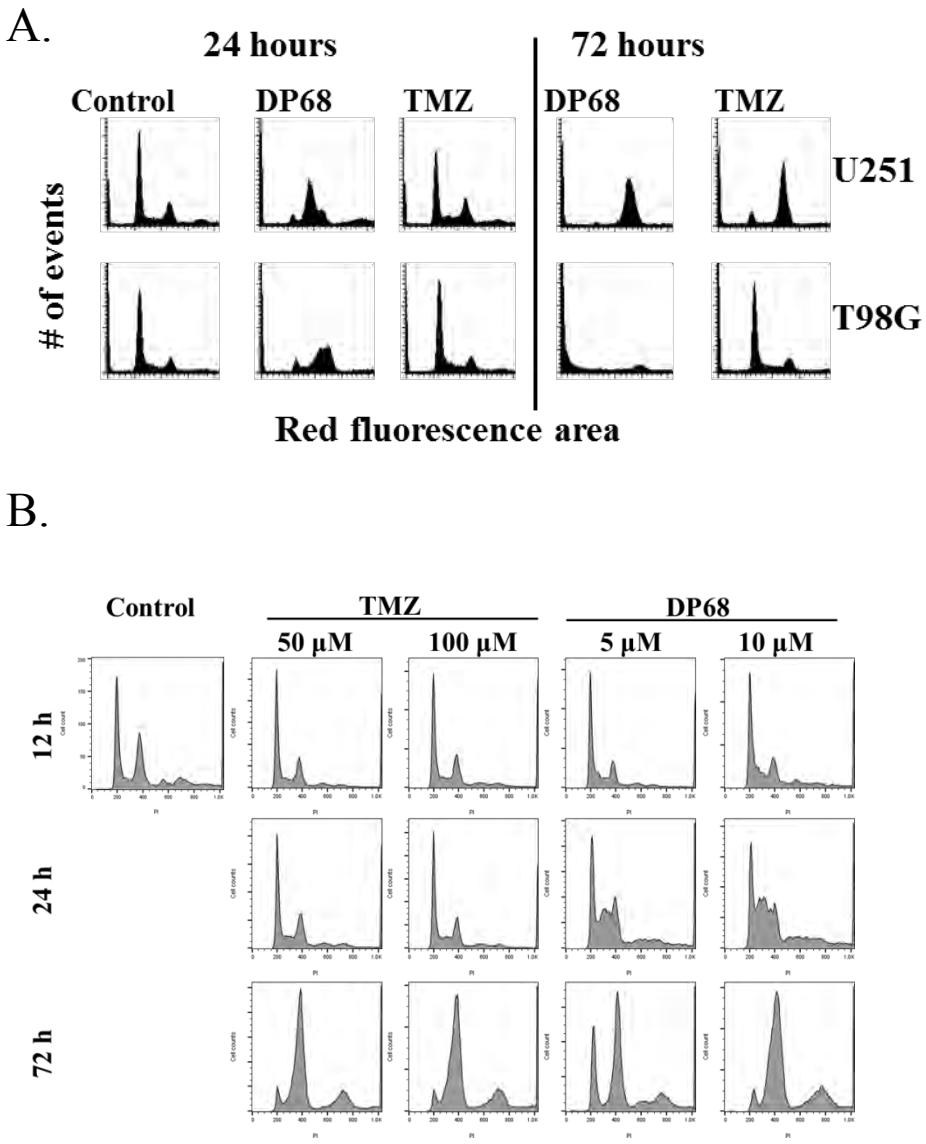

Figure 2.12 Cellular response of GBM lines to TMZ and DP68.
U251 and T98G (A) cells were treated with vehicle, 10 µM DP68, or 30 µM TMZ for 24 or 72 h, and then fixed. Histograms are representative of three independent experiments. Similarly U87MG (B) were treated with vehicle, TMZ, or DP68, stained with propidium iodide, and changes to cell cycle profiles were analyzed by flow cytometry.

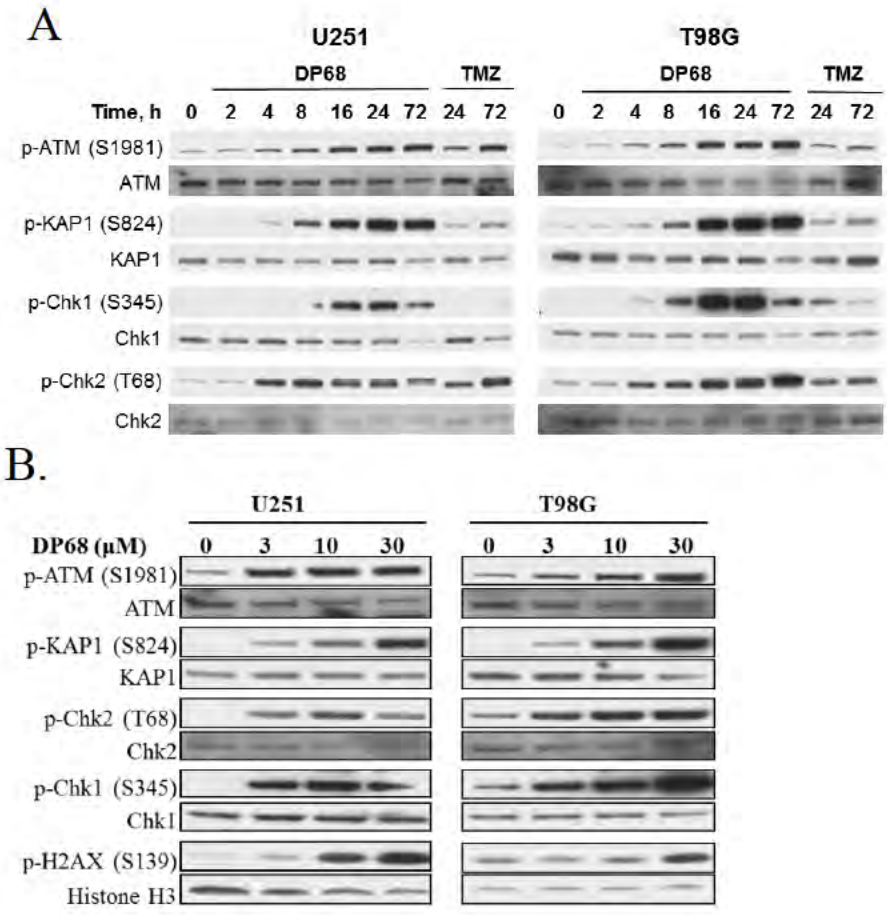

Figure 2.13 DNA damage signaling activated by low concentrations of DP68. U251 and T98G cells were treated with 0 or 30 μM DP68 or 100 μM TMZ and processed for Western blotting at various time points (A). U251 and T98G cells were exposed to various doses of DP68 for 24 h and whole cell and nuclear extracts were processed for western blotting (B). Representative blots from three independent experiments are shown.

A.

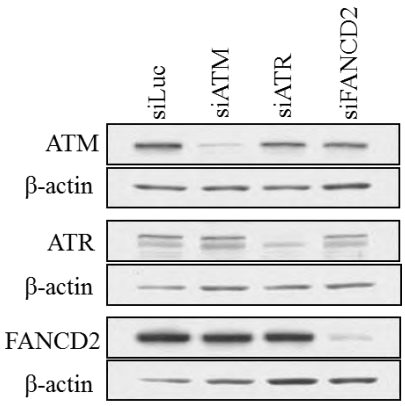

B.

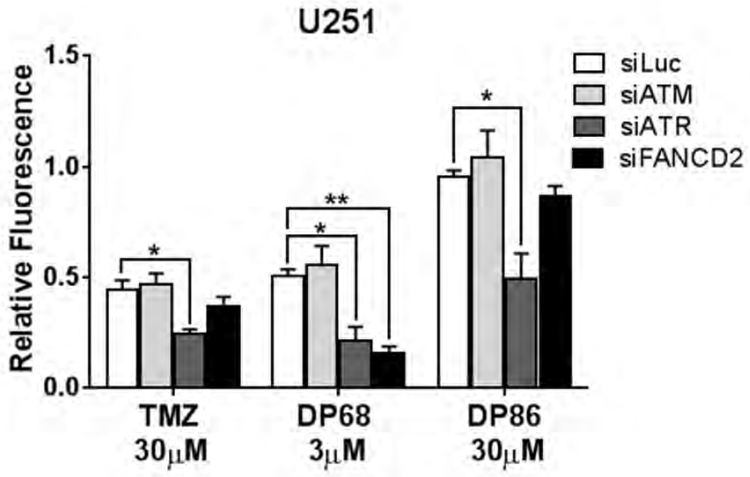

Figure 2.14 Recovery from DP68 induced DNA damage is ATR and FANCD2 dependent.

Western blot confirming knockdowns in U251 cells double electroporated with control (fLuc), ATM, ATR, or FANCD2 siRNA (A). Transfected cells were treated with 0 or 30 μM TMZ, 3 μM DP68 or 30 μM DP86 and assessed for cell growth using a CyQUANTassay (B). Mean ± SEM from three independent experiments. * $p<0.05$, ** $p<0.001$

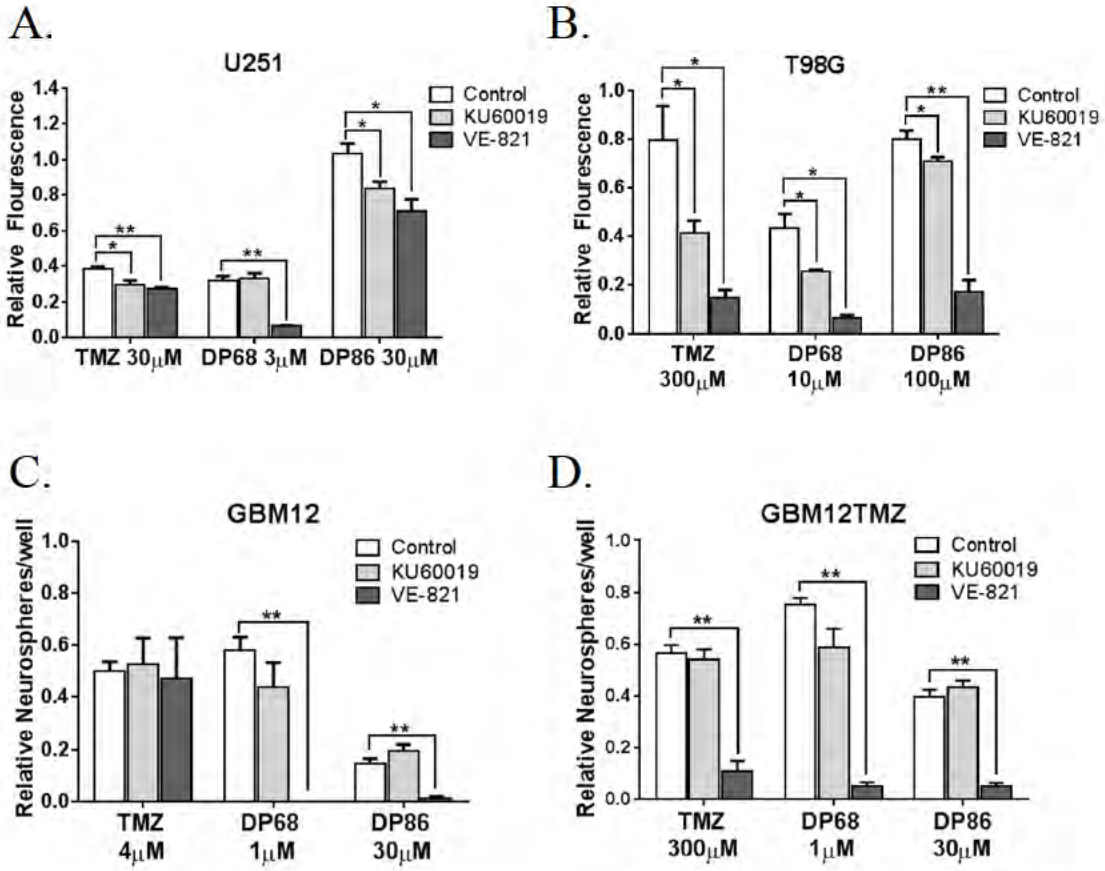

Figure 2.15 DP68's ATR dependence confirmed with small molecule inhibitors. U251 (A) and T98G (B) cells were treated with an ATR-inhibitor (1 μM VE-821), an ATM-inhibitor (1 μM KU60019), or vehicle with or without TMZ, DP68, or DP86, and cell survival was analyzed in a CyQUANT assay. Mean ± SEM from three independent experiments. A neurosphere assay was performed in parental GBM12 (C) and TMZ-resistant GBM12TMZ (D) explant cultures treated with 0, 1 μM VE-821, or 1 μM KU60019 in combination with TMZ, DP68, or DP86. Mean relative neurosphere number ± SEM from three independent experiments. * $p<0.05$, ** $p<0.001$

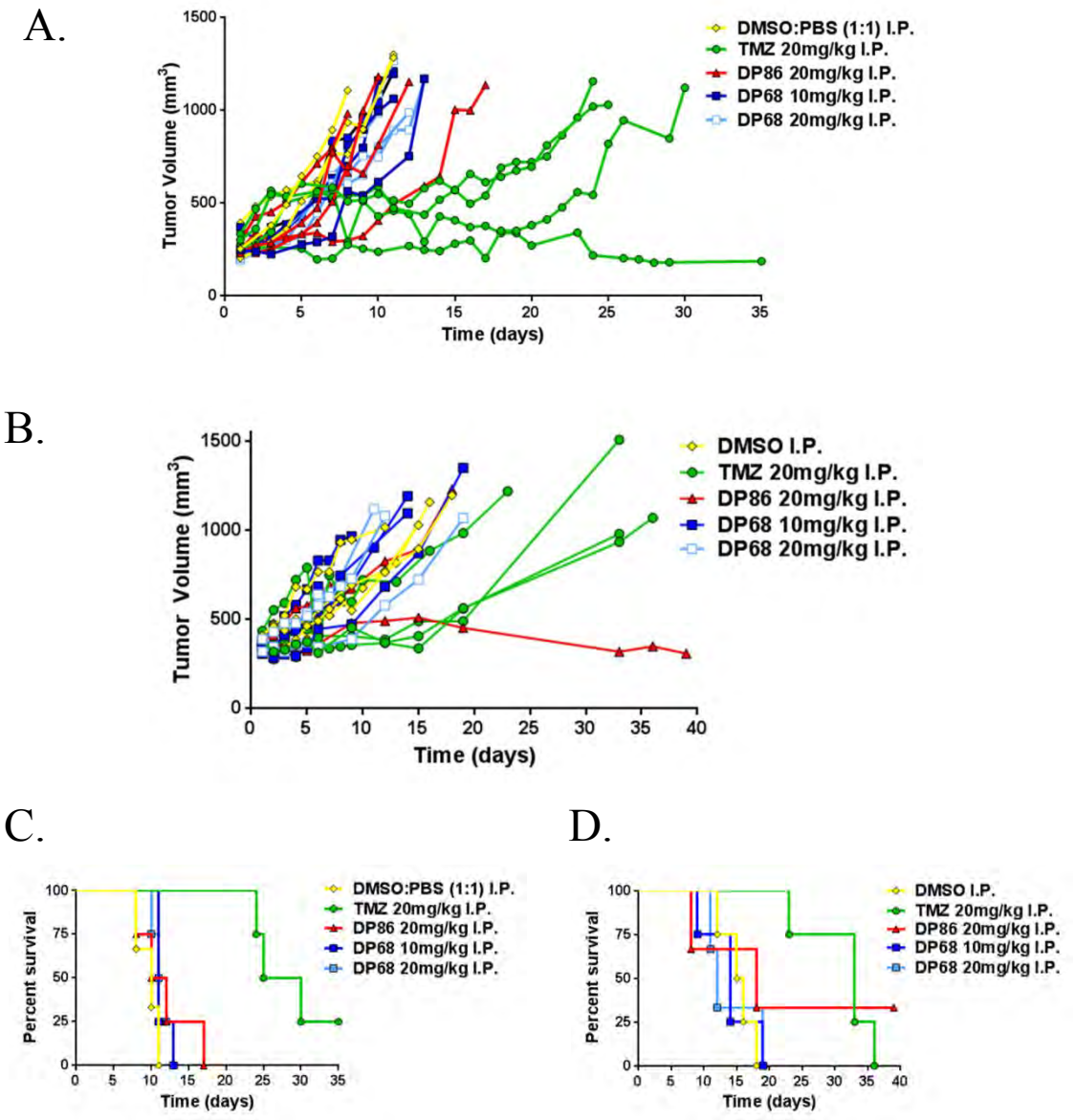

Figure 2.16 Efficacy of DP68 and DP86 *in vivo*.
U87NS were subcutaneously injected into Nu/Nu male mice and tumors allowed to progress. Mice were treated with vehicle control, TMZ, DP86, or DP68 via IP injections on two consecutive days (A-B). Drugs were diluted in either DMSO:PBS 1:1 mix (A, C) or 100% DMSO (B, D) to address solubility problems. Tumor volume was monitored and measured with calipers. Data plotted as percent survival (C-D). TMZ-treated tumors showed decreased tumor volumes and increased median survival. In contrast, DP86 and DP68 failed to show any apparent effect *in vivo* independent of solvent drug was diluted in.

Table 2.2 Median survival of U87NS xenografts drug treated via IP injection with drugs diluted in DMSO:PBS (1:1).

Median Survival of *in vivo* Treated Xenografts (days) ± SEM	
DMSO:PBS (1:1), n=3	10 ± 1
TMZ (20mg/kg), n=3	27.5 ± 3
DP86 (20mg/kg), n=4	10 ± 3
DP68 (10mg/kg), n=4	11 ± 1
DP68 (20mg/kg), n=4	11.5 ± 1

Table 2.3 Median survival of U87NS xenografts drug treated via IP injection with drugs diluted in 100% DMSO.

Median Survival of *in vivo* Treated Xenografts (days) ± SEM	
100% DMSO, n=4	15.5 ± 1
TMZ (20mg/kg), n=4	33 ± 3
DP86 (20mg/kg), n=3	18 ± 10
DP68 (10mg/kg), n=4	14 ± 4
DP68 (20mg/kg), n=3	12 ± 3

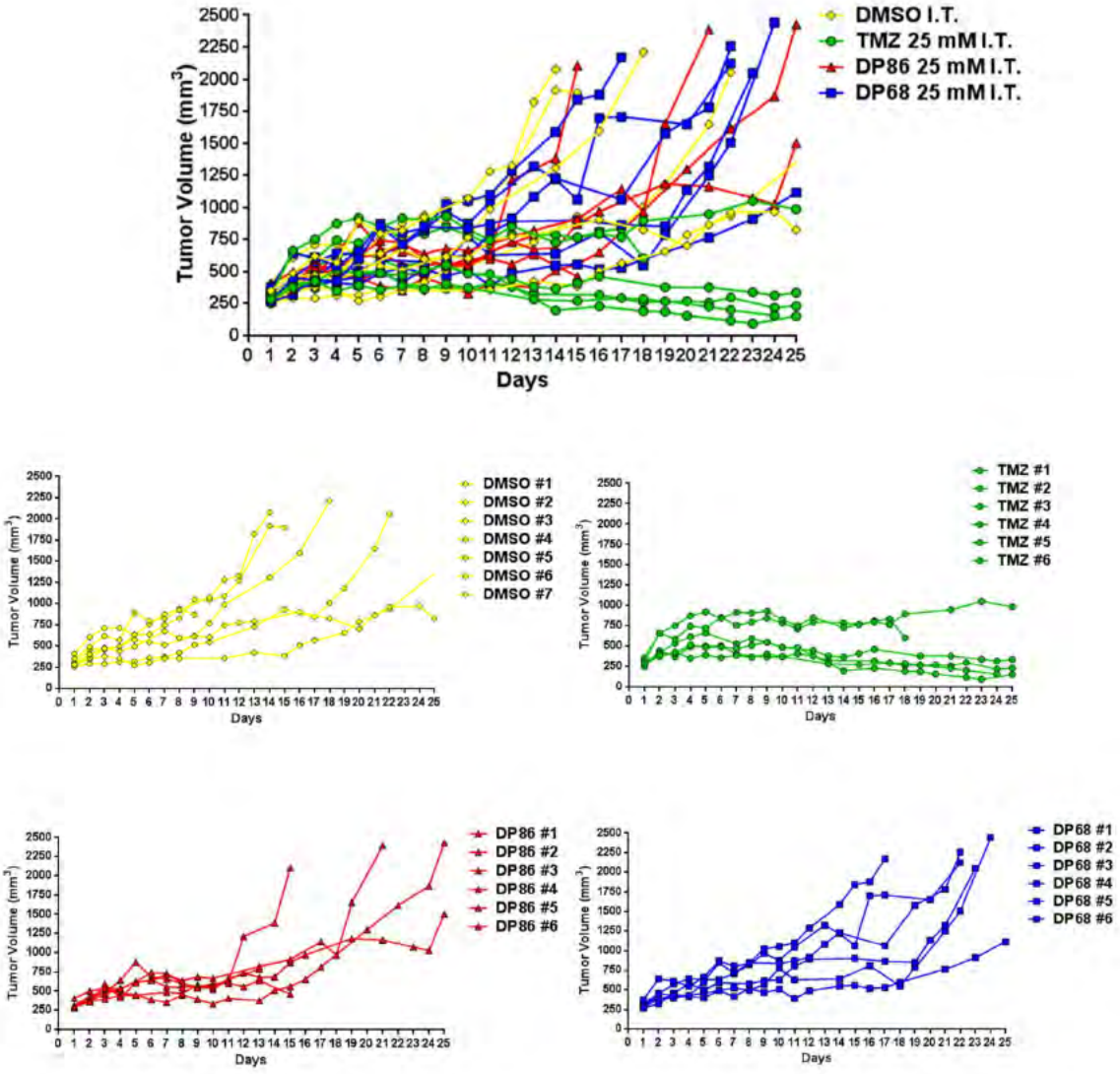

Figure 2.17 IT delivery of DP68 and DP86 *in vivo*.
Mice with flank tumors were treated *in vivo* with DMSO, TMZ, DP86, and DP68. Individual graphs for each treatment are shown. Drug was delivered via IT injection and tumor growth was monitored for 25 days and measured with calipers. TMZ treated tumor showed significant effects on tumor growth while DP86 and DP68 failed to demonstrate an effect *in vivo*.

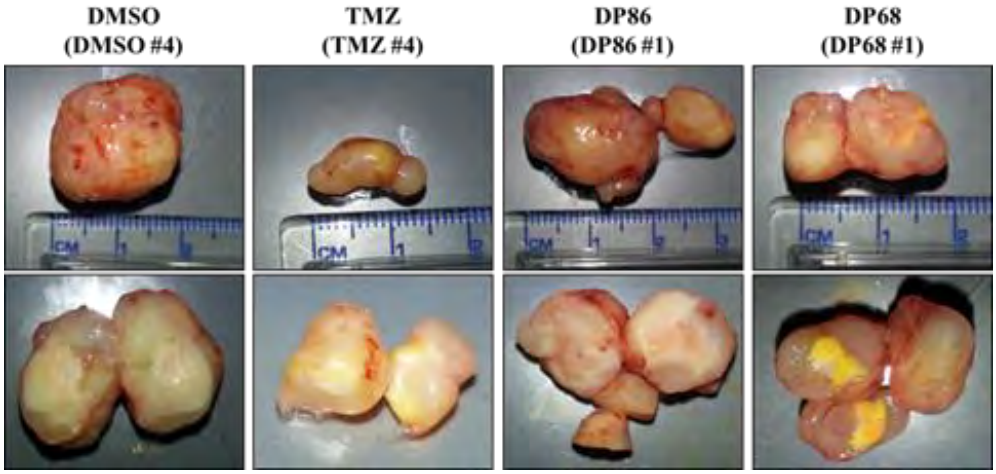

Figure 2.18 DP68 shows poor distribution following IT injections.
Tumors were removed after mice were euthanized and examined. DP68 tumors show precipitation of drug (yellow) within the tumor.

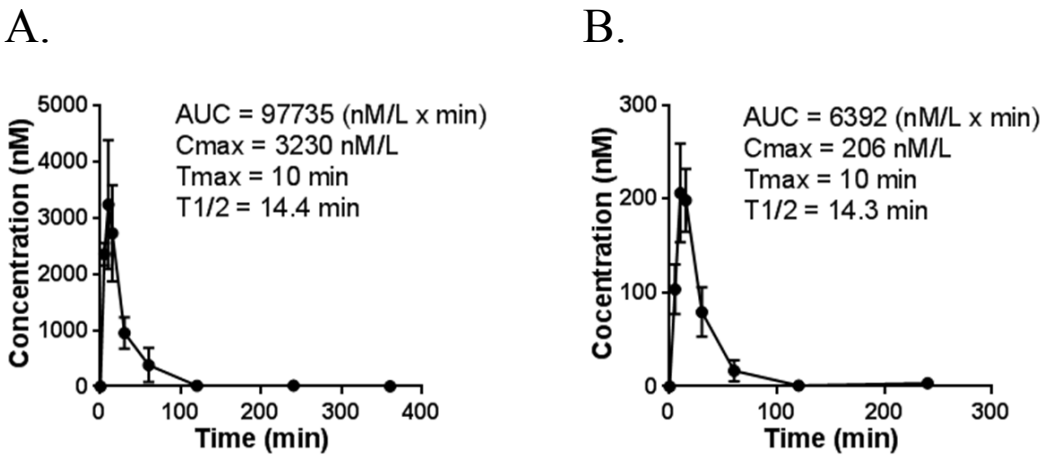

Figure 2.19 Pharmacokinetic evaluation of DP86 and DP68.
Following a single IP injection of DP86 (A) or DP68 (B), plasma drug levels were determined at times up to 6 h post-injection by LTQ quadrupole ion trap mass spectrometry. Results shown are mean ± SD at each time-point (n=3 mice per time-point).

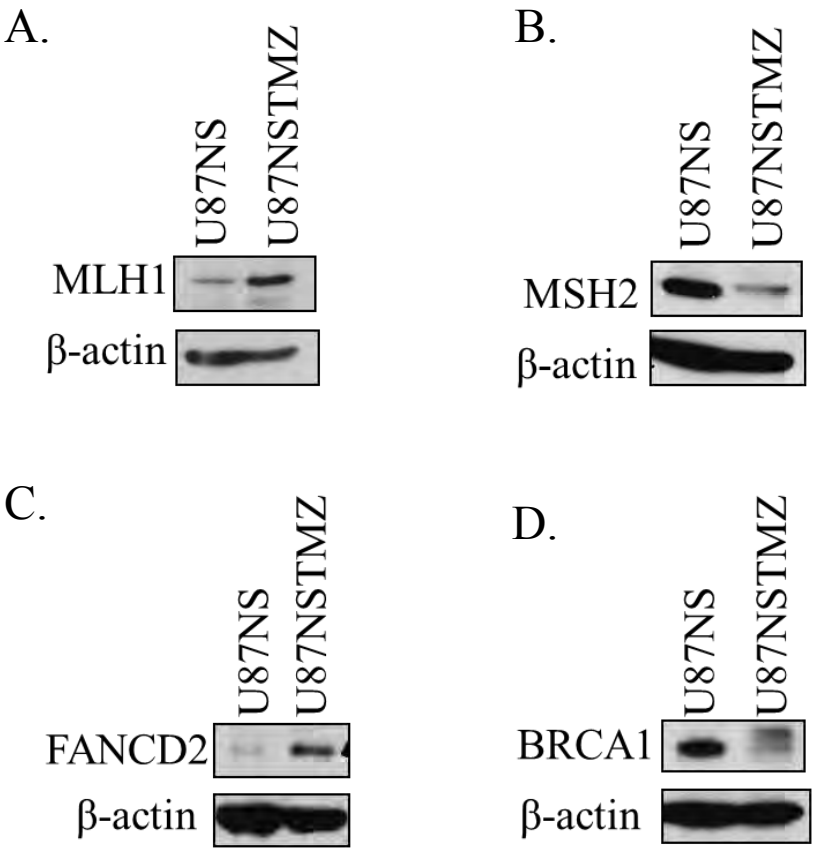

Figure 2.20 Characterization of U87NSTMZ line.
Western analysis on whole cell lysates showing difference in expression of MLH1 (A), MSH2 (B), FANCD2 (C) and BRCA1 (D) between parental U87NS and TMZ-resistant, U87NSTMZ.

CHAPTER III

TARGETING MICRORNAS TO ENHANCE A NOVEL THERAPY FOR GLIOBLASTOMA MULTIFORME

CHAPTER III

Preface

The contents of this chapter stem from a side-project carried out during my time in the Ross lab. We were interested in expanding the work done by a previous graduate student, which focused on the effects of TMZ in combination with GSIs in GBMs. In particular, we wanted to explore how miRNAs contribute to the efficacy of the therapy. While this work has been presented at the 24th EORTC-NCI-ACCR (2012) conference, it remains unpublished.

In this chapter, I was responsible for the majority of experimental set-up, data acquisition, and analysis. The UMASS flow cytometry core performed the cell sorting and flow cytometry and the UMASS tumor bank supplied us with tumor #5075.

Abstract

Our lab has previously shown that combination therapy, consisting of TMZ and a GSI, decreases recovery of GBM neurosphere cultures and propagation of secondary spheres, when compared to TMZ-only or GSI-only treatment. *In vivo* administration of TMZ + GSI in animals with pre-existing tumors inhibited tumor growth, blocked progression, and resulted in complete tumor regression in 50% of the mice. Our most recent data suggests the induction of senescence as a potential mechanism for the high efficacy of the TMZ + GSI treatment. In order to design a more targeted therapy, the signaling and regulatory mechanisms which are unique to senescence need to be elucidated. We sought to identify a miRNA signature that is differentially expressed in TMZ + GSI-treated GBM neurosphere cultures, since modulating miRNA transcript levels has therapeutic applications. We found microRNA-34a (miR-34a) expression was highly upregulated in response to TMZ or TMZ and the GSI inhibitor, DAPT. The upregulation was greatest at day 21, coinciding with senescence and suggesting a role for miR-34a in inducing senescence. Exogenous expression of miR-34a in our glioma lines reduced cell proliferation and lead to an induction of senescence, as demonstrated by senescence-associated β –galactosidase (SA-β-gal) staining. MiR-34a overexpression modified cell cycle profiles by inducing a G1 arrest, but apoptosis was not detected. Notch family members were investigated as potential targets of miR-34a through which these effects might be mediated. Overexpression of miR-34a reduced Notch-1, Notch-2, and Notch-3 levels in glioma cultures.

Introduction

TMZ and radiotherapy became the standard of care following the 2005 study by Stupp et al. which showed that addition of concurrent and adjuvant TMZ to radiotherapy significantly increased GBM patient survival (Stupp, Mason et al. 2005). However, therapy with TMZ in GBMs gives a short-lived response as cells with intrinsic or acquired resistance ultimately re-grow, causing tumor recurrence. One approach to overcome resistance has been to develop novel combination therapies. Notch is a promising candidate for combination therapy as it regulates proliferation, cell death, differentiation, and cancer stem cell maintenance (Lino, Merlo et al. 2010). Increased expression of Hey1, a Notch downstream target, in GBM patients is a poor prognosis factor associated with a 2-fold decrease in survival (Hulleman, Quarto et al. 2009). Notch inhibition in combination with other agents is promising as inhibition of Notch sensitizes cells to radiation (Wang, Chadalavada et al. 2010) and chemotherapy agents such as oxaliplatin (Meng, Shelton et al. 2009).

We have previously analyzed the combination of TMZ + GSI and shown it enhances GBM therapy (Gilbert, Daou et al. 2010). The effects of TMZ + GSI were evaluated in a secondary neurosphere formation assay (**Figure 3.1 A**), which allows us to evaluate initial response (Treatment), re-growth following a recovery period (Recovery), and the ability to give rise to secondary spheres following dissociation (Secondary). Secondary sphere counts serve as a measure of self-renewal. Drug treatment schedule consisted of a single dose of TMZ and GSI on day 0 with subsequent doses of GSI on

days two, four, and seven (**Figure 3.1. A**, green and red arrows). Two GSIs were chosen for analysis: DAPT and LY411,575. TMZ-treated cultures show an initial decrease in the number of neurospheres but eventually recover and form secondary spheres (**Figure 3.1 B**). The combination of GSI and TMZ enhanced treatment as neurospheres were not capable of self-renewal. Assessment of tumor formation in immunocompromised mice showed that TMZ + GSI treated cells had decreased tumorigenicity. Furthermore, *in vivo* TMZ + GSI treatment of pre-existing subcutaneous tumors showed no tumor progression in 50% of the mice. TMZ + GSI combination therapy is promising for overcoming resistance as cells capable of recovery are targeted and self-renewal is inhibited. Examination into the biological mechanism of TMZ + GSI treatment showed that a permanent growth arrest was induced, which in turn prevented regrowth of GBM cultures (Gilbert 2011). Induction of apoptosis did not occur, and interestingly, TMZ + GSI treated cells were more likely to undergo phagocytosis by macrophages. This is of interest as treatments that induce cytostasis, the inhibition of proliferation without induction of cell death, are being evaluated as novel therapies. Therapy-induced senescence (TIS) is one way to achieve cytostasis. Currently there is a phase 1 clinical trial to evaluate side effects and optimal dose of GSI RO4929097 in combination with TMZ and radiotherapy in patients with newly diagnosed GBM (Clinical Trial # NCT01119599) (Institute 2015).

We were interested in targeting miRNAs in order to enhance this novel combination therapy. MiRNAs are non-coding double stranded RNA molecules that

regulate gene expression. Some miRNAs serve as oncogenes or tumor suppressors (Chen 2005; Kent and Mendell 2006), and dysregulation of miRNA expression is a critical component of cancer (Dalmay and Edwards 2006). Studies have shown that aberrant expression of microRNAs is present in many human cancers, including GBMs (Lu, Getz et al. 2005). Oncogenic miR-21 is highly upregulated in GBMs and its inhibition sensitizes cells to chemotherapeutic agents and radiation (Chan, Krichevsky et al. 2005; Zhang, Wan et al. 2012; Chao, Xiong et al. 2013; Costa, Cardoso et al. 2013; Giunti, da Ros et al. 2015), expression of miR-196a is associated with poor survival (Yang, Han et al. 2014) , while upregulation of miR-195, miR-10a, and miR-455-3p occurs in TMZ-resistant GBM lines (Ujifuku, Mitsutake et al. 2010).

In this study, we show that TMZ and TMZ + GSI drug treatments upregulate the expression of miR-34a in GBM cells, which acts as a tumor suppressor in this context. Following miR-34a overexpression proliferation is inhibited, cells arrest at G1, SA-β-gal staining is present, and the invasiveness of GBM cells decreases. Our data also provides evidence for the involvement of miR-34a in the regulation of the Notch pathway. Thus, we demonstrate that miR-34a alone has therapeutic implications in GBMs.

Results

TMZ + DAPT treatment leads to altered expression of miR-34a

To identify a miRNA signature that is differentially expressed in TMZ + DAPT treated cultures, we began by examining the expression levels of a selected group of

miRNAs: miR-34a, miR-7, miR-29 family, and miR-519 following drug treatment. MiRNAs were selected based on published reports implicating their role in senescence or on a predicted target's role in senescence (Tazawa, Tsuchiya et al. 2007; Marasa, Srikantan et al. 2010; Zhao, Li et al. 2010; Martinez, Cazalla et al. 2011). U87NS and U373NS cells were treated with DMSO control, DAPT, TMZ or a combination of TMZ + DAPT according to the regimen previously described (**Figure 3.1 A**). RNA isolation from treated cultures at day 2, 8, 14, and 21 allowed us to evaluate miRNA expression at each stage of the secondary sphere assay. MiR-519 showed no detectable transcript in these glioma lines and was not further pursued. Changes in miR-7 and miR-29 expression levels are addressed in Appendix II. Expression of miR-34a was reproducibly upregulated ≥2-fold following treatment with TMZ and TMZ + DAPT in U87NS and U373NS (**Figure 3.2 A-B**). We have previously shown that U87NS and U373NS treated with TMZ (U87NS= 36.3 %; U373NS =33 % on day 7) or TMZ + DAPT (U87NS= 64 %; U373NS= 56.3 %) have a large induction of SA-β-gal expression, a marker for senescence (Gilbert 2011). For day 21 cultures, SA-β-gal positive cells remained higher in the TMZ (U87NS= 11.6 %; U373NS= 18.5 %) and TMZ + DAPT (U87NS= 79.2 %; U373NS= 82.1 %) treated neurospheres than the DMSO (U87NS=2.3 %; U373NS= 2.3 %) or DAPT only (U87NS= 2.6 %; U373NS= 2.4 %) controls. Consistent with a potential role in induction of senescence, miR-34a expression is 2-6 folds greater in TMZ and TMZ + DAPT treated cultures. For this reason, we focused on analyzing how miR-34a affects GBM cultures.

MiR-34a expression in glioma cultures

We assessed miR-34a expression levels in a panel of glioma cultures by qRT-PCR analysis of mature miR-34a (**Figure 3.3**). All of the cell lines had detectable levels of miR-34a, but U87MG had the highest levels. MiR-34a transcript levels appear to correlate with the p53 status of the lines, with p53 mutant lines having low miR-34a expressions and p53 wild-type have higher expression. It has been previously shown that p53 regulates miR-34a levels (Bommer, Gerin et al. 2007; Chang, Wentzel et al. 2007; He, He et al. 2007) and expression of miR-34a in our glioma cultures is in line with this observation. A 1.7 fold decrease in expression of miR-34a can be seen following conversion of U87MG to the neurosphere culture, U87NS.

MiR-34a exerts anti-proliferative effects on GBM cell lines

We evaluated effects of miR-34a on GBM cell line proliferation following transfection with miR-34a or negative control. In the adherent U87MG line, the neurosphere U87NS line, and our patient-derived 5075MG line, cell proliferation was significantly suppressed by miR-34a (**Figure 3.4**). In U87NS cultures, transfection with 5, 10, 20, and 30 nM miR-34a mimic led to changes in neurosphere morphology (**Figure 3.5**). Control cultures gave rise to tight, densely packed neurospheres characteristic of the U87NS cell line. MiR-34a transfected cultures formed neurospheres with large cells in loose aggregates. A simple explorative evaluation into miR-34a effects on neurosphere self-renewal was carried out by pH dissociating spheres seven days post-transfection,

replating, and observing sphere formation seven days later (**Figure 3.6**). Interestingly, secondary neurospheres failed to form in the miR-34a transfected U87NS.

MiR-34a does not promote apoptotic cell death but does arrest cells at G1

To examine whether miR-34a inhibition of proliferation was associated with induction of apoptotic cell death, we assessed the percent of Annexin-V and 7-AAD positive cells (**Figure 3.7 A**) in control versus miR-34a cells. U87NS cells harboring the miR-34a mimic showed no difference in the early apoptotic (Annexin-V $^{+}$, 7-AAD $^{-}$) or late apoptotic (Annexin-V $^{+}$, 7-AAD $^{+)}$ populations both 48 h and 72 h post-transfection. Furthermore, cleavage of PARP was not detected in cell lysates up to 96 h post-transfection (**Figure 3.7 B**). Interestingly, PARP levels appear to go down in response to miR-34a overexpression (**Figure 3.7 C**). Thapsigargin, a known inducer of apoptosis (Andersen, Lopez et al. 2015), was included as a positive control for PARP cleavage. Overexpression of miR-34a did induce a slight, but statistically significant, G1 arrest in cells (**Figure 3.8**). These results suggest that miR-34a overexpression fails to induce apoptosis but does alter cell cycle progression in glioma cells.

MiR-34a induces SA-β-gal expression

TMZ + DAPT treatment induces senescence, thereby inhibiting secondary sphere recovery and the progression of tumors *in vivo* (Gilbert 2011). Senescence is largely evident by day 7 and peaks at day 21 post-treatment. We have shown that miR-34a expression is significantly elevated at these time points in the TMZ and TMZ + DAPT

treatment groups. Because of this we examined whether dysregulation of miR-34a drives cells into senescence. Senescence was assessed via SA-β-gal staining of U87NS cells following transfection with miR-34a or negative control (**Figure 3.9 A**). SA-β-gal was evident as early as three days post-transfection (Figure 3.9B). DharmaFect 1(transfection reagent only) treated cells and negative control transfected cells had a minimal percent of cells expressing SA-β-gal, 8.1 ± 0.9 % and 10.1 ± 1.5 %, respectively. Cells overexpressing miR-34a showed a 5-fold (53 ± 1.8 %) increase of SA-β-gal staining.

Invasiveness of GBM cells was reduced in vitro by miR-34a

GBMs, by nature, are highly invasive (Wen and Kesari 2008). We wanted to determine if miR-34a regulates this process. To address this, we measured the *in vitro* ability of GBM control versus miR-34a cells to invade through Matrigel®-coated transwell chambers (**Figure 3. 10 A-B**). In just 12 h, U87MG negative control cells invaded through the Matrigel®. MiR-34a cells led to a 56 % reduction in invasive U87MG cells (p-value< 0.01). These data suggest that miR-34a regulates the invasiveness of GBM cells.

Notch family members are negatively regulated by miR-34a

In silico analysis using TargetScan (Lewis, Burge et al. 2005) and PicTar (Krek, Grun et al. 2005) predicts that miR-34a targets Notch-1 and Notch-2, which play roles in proliferation, senescence, and invasion (Lino, Merlo et al. 2010). We examined changes in expression of Notch receptors following miR-34a overexpression. Western analysis

shows that expression of miR-34a inversely correlates with the expression of Notch receptors (**Figure 3.11 A-B**). Decrease in full length (FL) and intracellular domain (ICD) of Notch-1, Notch-2, and Notch-3 occurs with as little as 5 nM miR-34a mimic in U87NS cells. Expression of Notch-1, Notch-2, and Notch-3 decreased significantly (Notch-1 ICD= 13.8-fold; Notch-2 ICD= 10.6-fold; Notch-3 ICD= 89-fold) following transfection of 20 nM mimic. This is the concentration the majority of our assays were carried out at. Similar decreases in Notch-1, Notch-2, and Notch-3 were also seen in the adherent U87MG cells (**Figure 3.11 C**). Activation of the Notch pathway occurs following the interaction of ligand on one cell with a receptor on a neighboring cell (Bray 2006). In line with this, we observed that downregulation of Notch receptors was affected by density at which assays were plated (**Figure 3.12**).

Conclusions and Discussion

We have previously shown that the combination of cytotoxic TMZ with a GSI enhances GBM therapy in both *in vitro* and *in vivo* models (Gilbert, Daou et al. 2010). Further examination revealed that efficacy of TMZ + GSI treatment is partially due to cells entering a permanent senescent state that is more susceptible to macrophage phagocytosis (Gilbert 2011). However, applications of GSI in the clinic can cause gastrointestinal toxicity so we sought to identify miRNAs that mimic the effects of TMZ + GSI as an alternative approach to enhance GBM therapy. In this study we find that miR-34a is upregulated in TMZ and TMZ + DAPT treated cells. Exogenous expression of miR-34a revealed that it functions as a tumor suppressor by: inhibiting proliferation, inducing a G1 arrest, increasing SA-β-gal staining, and decreasing the invasion potential of GBM cells. Anti-tumor effects of miR-34a were not mediated by apoptosis. Instead, these results mimic the *in vitro* effects previously demonstrated in GBM cells following TMZ + DAPT (Gilbert, Daou et al. 2010). The down-regulation of Notch family receptors (Notch-1, -2, and -3) by miR-34a might be one mechanism by which miR-34a exerts its tumor suppressive effects.Therefore, miR-34a's contribution to senescence may provide a valuable tool for the future treatment of GBMs.

Our data shows that GBM neurospheres treated with TMZ and the combination TMZ + DAPT distinctly modulate the expression of miR-34a. Upregulation of miR-34a was observed at all time points tested for the U87NS and U373NS lines. While no other studies have analyzed changes in miRNA following TMZ or GSI treatments in cancer

models, induction of miR-34a has been shown in other cancers in response to DNA damaging agents. MiR-34a was upregulated in colon cancer cell lines following Adriamycin (Tazawa, Tsuchiya et al. 2007), in the livers of mice following ENU (*N*-ethyl-*N*-nitrosourea) treatment (Li, Branham et al. 2010), in osteosarcoma lines following etoposide (Novello, Pazzaglia et al. 2014), and in muscle-invasive bladder cancer lines following cisplatin treatment (Li, Yu et al. 2014). Similarly, miR-34a was upregulated in U87MG and LNZ308 lines after TMZ-resistance was generated (Hiddingh, Raktoe et al. 2014). While the upregulation we measured is in agreement with these studies, many of those studies showed that upregulation occurred in a p53-dependent manner. In contrast in our studies, miR-34a was upregulated in both p53 wild type U87NS and p53 mutant U373NS lines, indicating that miR-34a upregulation in U373NS occurs in a p53-independent manner. However, basal levels of miR-34a in our panel of GBM cell lines did correlate with p53 status.

Initially we sought to determine if the combination of TMZ and miR-34a mimic would have therapeutic benefits in GBMs, but we were met challenges. We have previously shown that the response to TMZ + DAPT treatment is sequence-dependent, (Gilbert, Daou et al. 2010) as secondary sphere formation is inhibited only when DAPT treatment is administered 24 h following TMZ. This was difficult to model *in vitro* as cells cannot be transfected following TMZ treatment without large amounts of cell death.

Induction of cellular senescence is one mechanism by which TMZ + DAPT exerts its anti-tumor properties. Following TMZ + DAPT treatment, cells enter permanent growth arrest which in turn inhibits the recovery of cells from TMZ treatment. We found that modulating miR-34a expression recapitulates these effects *in vitro*. Inhibition of proliferation, increase in cell size, G1 arrest, and enhanced SA-β-gal expression were evident following overexpression of miR-34a. Three days following the introduction of miR-34a, 53.3 ± 1.8% of the cells were positive for SA-β-gal. This mimics the induction of senescence seen in day 7 post TMZ + DAPT treatment, in which 64.0 ± 9.5% of the cells are positive (Gilbert 2011). MiR-34a has been reported to exert an apoptotic effect in many different cancer models including: GBM (Li, Guessous et al. 2009; Guessous, Zhang et al. 2010; Luan, Sun et al. 2010; Yin, Ogawa et al. 2013; Rathod, Rani et al. 2014) neuroblastoma (Cole, Attiyeh et al. 2008), medulloblastoma (de Antonellis, Medaglia et al. 2011) and prostate (Wei-Yu Chen 2014). Interestingly, induction of apoptosis was not detected in our model. Analysis of Annexin V and 7-AAD showed no double positive (Annexin-V^+, 7-ADD^+) population when compared to control. This was further validated by the lack of PARP cleavage in miR-34a overexpressing samples up to 96 h post-transfection. However, this is in line with our lab's previous observations of TMZ + DAPT treated cultures and further confirms that cells have entered a senescent state.

GBMs are highly invasive in nature (Wen and Kesari 2008). In this study, overexpression of miR-34a reduced invasion of U87MG by 56 %, showing that miR-34a

contributes to glioma invasion. Previous examination of TMZ +DAPT therapy did not assess the contribution of Notch inhibition on invasion. Due to the large number of miR-34a targets, invasion could be regulated through many pathways. In our system, miR-34a downregulates members of the Notch family and Notch has been shown to promote invasion mediated by cross-talk with Wnt pathway proteins (Hurlbut, Kankel et al. 2007; Zhang, Chen et al. 2012). Similarly, miR-34a has sites in the 3'UTR of Wnt pathway members such as WNT1 and Dickkopf (DKK1) (Krek, Grun et al. 2005; Lewis, Burge et al. 2005) and could potentially regulated these protein directly. In human hepatocellular carcinoma cells, miR-34a has been shown to inhibit invasion by directly targeting c-Met leading to decreased phosphorylation of ERK1/2 and resulting in decreased invasion of HepG2 cells (Li, Fu et al. 2009). C-Met has also been shown to be directly regulated by miR-34a in a GBM model (Li, Guessous et al. 2009) and could regulate invasion through this pathway as well. Lastly, miR-34a might regulate invasion through another of its targets, EGFR (Yin, Ogawa et al. 2013). Notch, c- Met, Wnt, and EGFR signaling can all affect invasion as downregulation of these pathways leads to decrease in matrix metalloproteases (MMPs) (Pang, Leung et al. 2010; Paul, Bhattacharya et al. 2013). MiR-34a overexpression would lead to a downregulation of EGFR, c-Met, Wnt, or Notch signaling, which in turn would decrease MMP expression and decrease invasion of GBM cells.

Inhibition of Notch by the GSI, DAPT, enhances TMZ therapy. Of the four Notch receptors, Notch-1 and Notch-2 are predicted targets of miR-34a based on seed sequence homology to their 3'UTR. In this study we showed Notch-1, Notch-2, and Notch-3 receptors expression is downregulated by miR-34a overexpression. However, in the time since this data was generated others have published studies demonstrating that miR-34a binds directly to the 3'UTR of Notch-1(Li, Walling et al. 2009; Li, Guessous et al. 2009; Du, Sun et al. 2012; Bu, Chen et al. 2013) and Notch-2 (Li, Walling et al. 2009; Li, Guessous et al. 2009; Kang, Kim et al. 2013; Sun, Wan et al. 2014). Additionally, miR-34a has been shown to directly bind to the 3'UTR of Notch-4 and negatively regulate its expression in MCF-7 and SK-3rd mammospheres (Yu, Jiao et al. 2012). However, there are no published reports of miR-34a regulating Notch-3 directly or indirectly therefore validating this target would be of interest. Notch pathway regulation by other miRNAs shows similar anti-tumor effects. MiR-306 targets Notch-1 and Notch-2 in GBM cells decreasing viability, proliferation, G1 arrest, and invasion. (Kefas, Comeau et al. 2009). Similarly, Notch-3 regulation by miR-206 leads to apoptosis and decrease in migration (Song, Zhang et al. 2009).

Our studies demonstrate that mirR-34a functions as a tumor suppressor in GBM cells stimulating a permanent growth arrest. Targets of miR-34a include the Notch receptor family. Its anti-tumor response mimics that of cells treated with novel TMZ + DAPT combination therapy indicating that miR-34a alone has therapeutic implications in GBMs.

Materials and Methods

Cell Lines and Reagents

U87MG cells were purchased from the ATTC in 2011 and authenticated by short tandem repeat analysis in 2013 (IDEXX RADIL). U87MG cells were converted to neurosphere cultures, U87NS, by lifting cells from plates with 0.05% Trypsin-EDTA (Gibco), washing cells three times with PBS to remove traces of FBS, and plating $5x10^5$ cells per 75-cm^2 flask. Neurospheres were dissociated every seven days via acid-base dissociation (Sen, Kallos et al. 2004). Spheres were used under 10 passages following conversion. Patient-derived culture, 5075T, was established from a GBM tumor obtained from the UMASS tumor bank following debulking surgery as previously described (Gilbert, Daou et al. 2010). Briefly, the tumor sample was minced and dissociated in Trypsin solution: DMEM/F12 mix (1:1) for an hour, at 37°C, with mechanical dissociation every ten minutes. Cells are then pelleted, washed in PBS, and replated in growth media. For these studies 5075MG was propagated as an adherent line. Adherent glioma lines were cultured in DMEM (Gibco) supplemented with 1% Na pyruvate and 10% FBS. Neurospheres were maintained in DMEM:F12 (1:1) with B27 supplement (Gibco), 15 mM HEPES (Gibco) supplemented with 20 ng/mL EGF (Invitrogen) and 20 ng/mL bFGF (Invitrogen). All cells were maintained at 37 °C in 5% CO_2 and regularly tested for mycoplasma via a PCR Mycoplasma Detection Kit (MDB Bioproducts).

TMZ and N-[N-(3,5-Difluorophenacetyl)-L-alanyl]-S-phenylglycine t-butyl ester (DAPT) were purchased from Sigma Aldrich. TMZ and DAPT were resuspended at 10 mg/mL (51.5 mM) and 10 mM stocks, respectively, in 100 % DMSO (Fisher).

Antibodies against Notch-1 (D6F11, #4380), Notch-2 (D67C8, #4530), Notch-3 (D11B8, #5276), PARP (46D11, #9532), and β-actin (8H10D10, #3700) were purchased from Cell Signaling. Ki-67 (NCL-Ki67p) was purchased from Novacastra. Secondary Anti-rabbit IgG, peroxidase-linked (from donkey) and Anti-mouse IgG, peroxidase-linked (from sheep) were purchased from GE Healthcare.

Recovery and secondary sphere assay

To quantify neurospheres in a recovery and secondary sphere assay (Gilbert, Daou et al. 2010), cells are plated at clonal density (3cells/μL; 2 mL total) in 6-well plates (BD Falcon). However, in order to isolate RNA from cells at different time points in the sphere assay, the experiment was scaled up. Neurospheres were plated at $5x10^5$ cells/ 10 mL (50 cells/ μL) in 75-cm^2 flasks (BD Falcon). Because clonal density has been previously defined as ≤ 10cells/ μL (Chaddah, Arntfield et al. 2012) one set of experiments were plated at $2x10^5$ cells/ 20 mL (10 cells/ μL), allowing us to verify that cell density did not affect outcome of the assay. Cells were treated with either 200 μM TMZ, 1 μM DAPT, combination of 200 μM TMZ + 1 μM DAPT, or vehicle control, DMSO. DAPT only and TMZ + DAPT treatment groups received subsequent 1 μM DAPT treatments on days two, four, and seven of the assay (**Figure 3.1 A**). TMZ only

and DMSO control wells were treated with DMSO on these days. All treatment groups were fed with neurosphere medium (2 mL) on day seven eeeeee. On day 14 of the assay, spheres were dissociated using a basic pH dissociation method (Sen, Kallos et al. 2004), and a dilution of the culture was re-plated. Cells from each treatment group were collected at days 2, 8, 14, and 21 of the assay for subsequent RNA isolation. Cells were collected from a total of four assays.

RNA Isolation and Detection

RNA isolation and small RNA enrichment (>200 bp) were carried out using the miRVANA miRNA isolation kit (Applied Biosystems) according to manufacturer's protocol. Reverse transcription was performed using the TaqMan miRNA Reverse Transcription Kit. Expression levels of mature miR-34a (hsa-miR-34a-5p) were measured by TaqMan MicroRNA Assays (Applied Biosystems). U6 (RNU6B) small nuclear RNA was used as a normalization control. Expression levels were quantified on ABI Prism 7900HT sequence detection system (Applied Biosystems) using TaqMan Universal Master Mix II with UNG. Relative gene expression was calculated using the ΔΔCt method. RNA was isolated and analyzed in three independent experiments.

siRNA

U87MG and U87NS were plated at $5x10^4$ cells per well in a 6-well plate and transfected with hsa-miR-34a-5p (MC11030) miRVana miRNA mimic (Applied Biosystems) using DharmaFect 1 Transfection Reagent (Dharmacon) according to

manufacturer's protocol. A non-targeting Negative Control #1 (Applied Biosystems) was used as a negative control. Initial transfection efficiencies were examined using Cy3™ Dye-Labeled Pre-miR Negative Control #1 (Ambion) (**Figure 3.14**). To test optimal transfection conditions, concentrations, and cell density we utilized Cy3 labeled negative control siRNA. Monitoring Cy3 fluorescence signal allowed us to analyze transfection efficiencies.

Western Blotting

Cells were lysed in RIPA lysis buffer (Boston Bioproducts) supplemented with a protease inhibitor cocktail (complete mini tab, Roche Applied Science, IN). Bradford assay (Protein Assay Dye Reagent Concentrate, 1:4 dilution, Bio-Rad) was used to measure protein concentrations. Lysates were analyzed by SDS-PAGE, and proteins were electro-transferred onto 0.45 μM PVDF membranes. Membranes were blocked in Tris-buffered saline (TBS) containing 5 % milk and 0.1 % Tween-20 at room temperature for one h. All primary antibodies were incubated overnight at 4 ºC followed by room temperature incubation with a secondary antibody conjugated with horseradish peroxidase for 1 h. Detection was performed with lab made chemiluminescent reagent consisting of 30 mL 1.25 mM Luminol in 0.1 M Tris pH 8.5 (solution B), 30 μLof 68 mM p-coumaric acid in DMSO (solution A) and 30 μL of 3 % hydrogen peroxide (Matthews, Batki et al. 1985). Membranes were soaked in chemiluminescent reagent for 10 min at RT and exposed to film. Quantification of band intensity was carried out using Image J.

Proliferation Assays

U87MG, U87NS, and 5075MG were plated in duplicate and transfected with miR-34a mimic or negative control as described above. On selected days, cells were collected and proliferation was assessed via trypan blue exclusion. Changes in proliferation of each line were analyzed from at least three independent experiments.

Immunocytochemistry

Cells were transfected with mimics or controls and were collected 72 h post-transfection. Neurospheres were spun down on to slides using Shandon double cytofunnels (Thermo Fisher Scientific). Cells were fixed in 4 % paraformaldehyde for 15 mins at RT and permeabilized in TBS containing 0.25 % Triton X-100 (TBS-T). Blocking was carried out by incubating cells in 10 % goat serum with 1 % BSA and 0.3 M Glycine in TBS-T for one h at RT. Cells were incubated in primary antibody overnight at 4 °C followed by RT incubation with a fluorophore-conjugated secondary for one h at RT. Vectashield Hardset mounting media containing DAPI was added (Vector Laboratories) and cells were visualized under a microscope. Ki-67 positive cells were quantified and measured as a percent of positive over total cells.

Flow Cytometry and Cell Cycle

Cell cycle distribution was analyzed by flow cytometry. Cells were harvested 72 h post-transfection, washed with PBS, and fixed with ice-cold 70 % ethanol/30 % PBS.

Cells were re-suspended in PBS containing PI (40 μg/ml), RNase A (100 μg/ml) and Triton X-100 (0.05 %), and incubated at 37 ºC for 30 min. Samples were run by UMASS Flow Cytometry facility. DNA content was determined using a FACScan flow cytometer system (Becton Dickinson), and results were analyzed with FlowJo. Experiments were performed in duplicate.

Cell Death

Apoptosis was evaluated via flow cytometry for Annexin-V-FITC (BD Bioscience) and 7-Aminoactinomycin D (7-AAD) (Molecular Probes, Life Technologies). Cells were transfected with miR-34a mimic or negative control, at 48 h and 72 h cells were harvested, and stained with Annexin-V-FITC and 7-AAD. Samples were run by UMASS Flow Cytometry Core and results were analyzed with FlowJo.

Senescence Assays

Senescence was analyzed by quantifying senescence-associated β-galactosidase (SA-β-gal) using Senescence Detection Kit (Calbiochem) according to manufacturer's protocols. Cells were transfected with mimics or controls and analyzed five days post-transfection. Neurospheres were collected and spun down on to slides using Shandon double cytofunnels (Thermo Fisher Scientific) before staining. To quantify SA-β-gal positive cells, at least 2,500 cells were counted in random fields from each of the three independent replicates.

Invasion Assay

Upper surface of 8 μM pore transwells (Costar) were coated with Matrigel® Basement Membrane Matrix, LDEV-free (10 μg/well) (Corning) and dried overnight. U87MG were plated at $5x10^4$ cells per well in a 6-well plate and transfected with miR-34a mimic and negative control. At 72 h post-transfection, cells were released by trypsinization, stopping the reaction by addition of 1 % BSA in DMEM . Cells were resuspended at $5x10^5$ cells/mL in 0.1 % BSA/DMEM and 100 μL of this cell/media mixture was added to the top of the transwell. Each condition was plated in duplicate. Cells were serum-starved 24 h prior to the assay and DMEM, and 20 % FBS was used as a chemoattractant in the lower chamber. Assays proceeded for 12 h at 37 °C. Then the upper surface of the transwell was swabbed with a Q-tip twice to remove residual cells. Cells that had invaded through the Matrigel® were fixed with methanol for 10 mins and mounted on a slide using Vectashield Hardset Mounting media containing DAPI (Vector Laboratories). Cells in 14 random fields were quantified.

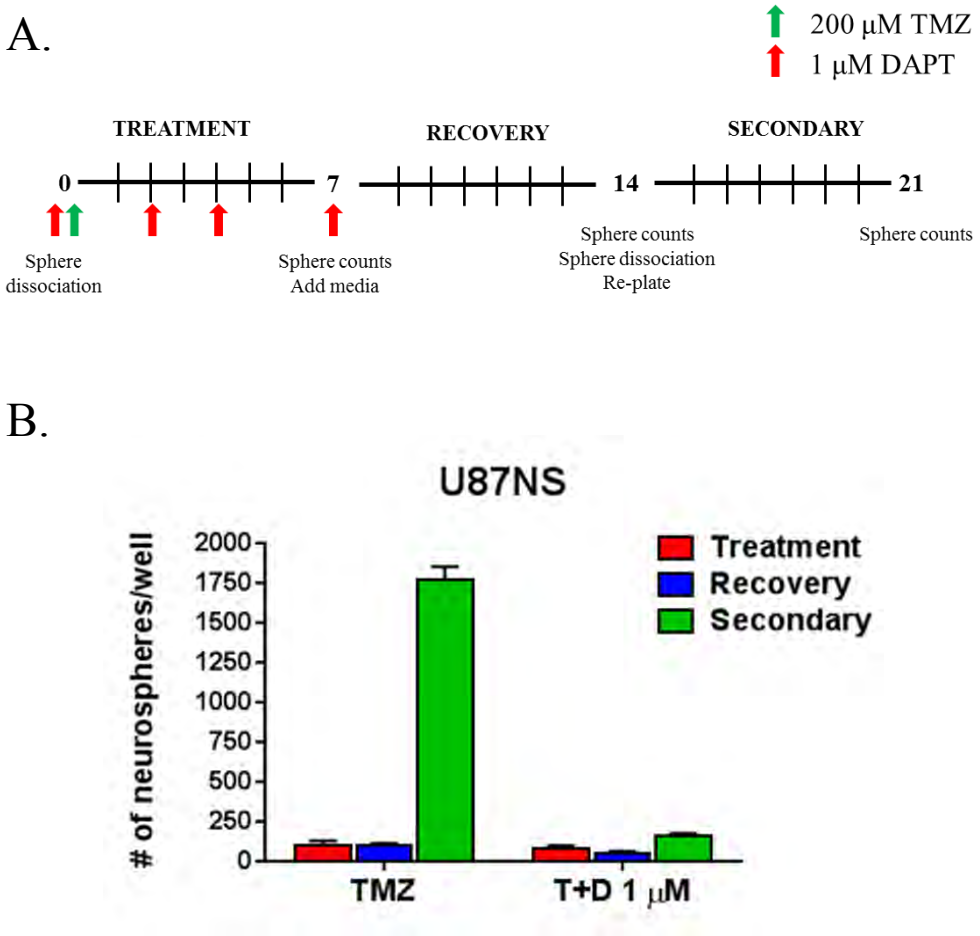

Figure 3.1 TMZ + GSI treatment decreased secondary sphere formation of glioma cultures.
Schematic of drug treatment schedule and neurosphere assay carried out to assess response, recovery, and secondary sphere formation following treatments (A). U87NS cells were plated in duplicate and treated with DMSO, DAPT (red arrows), TMZ (green arrows), or a combination of TMZ + DAPT (T+D) and spheres were counted on day 7, 14, and 21 (B). Cells treated with TMZ show an initial response (red) but eventually repopulate the culture (green). TMZ + DAPT cultures fail to recover as demonstrated by a significant decrease in secondary sphere formation compared to TMZ-only treated cultures. Mean ± SEM of a representative result from at least three independent experiments.

A.

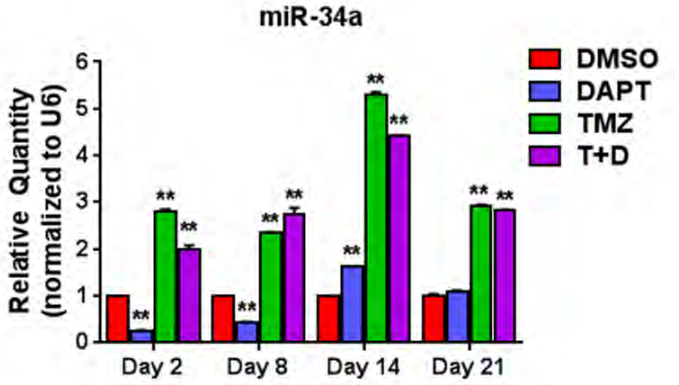

B.

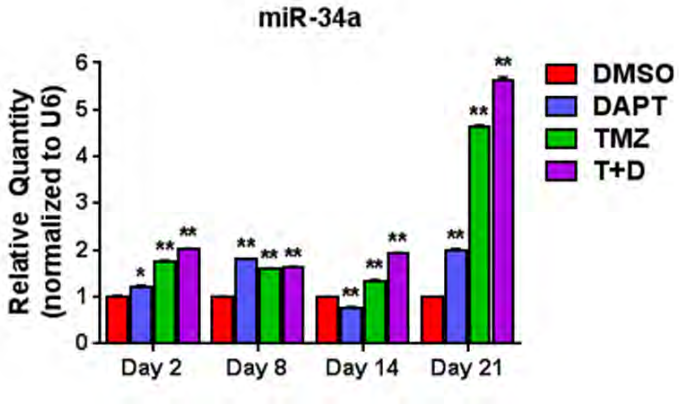

Figure 3.2 MiR-34a transcript increases in response to TMZ and the combination of TMZ + DAPT.
RNA lysates were collected from each of the treatment groups at several time points during a neurosphere assay and levels of miR-34a transcript were quantified by qRT-PCR. Induction of miR-34a expression occurred in response to TMZ and TMZ +DAPT in both U87NS (A) and U373NS (B) cells. This appears to be independent of p53 as the response is similar in both the p53 wild type U87NS and p53 mutant U373NS line. A representative figure from at least three independent replicates is shown. * p-value <0.05, ** p-value <0.01

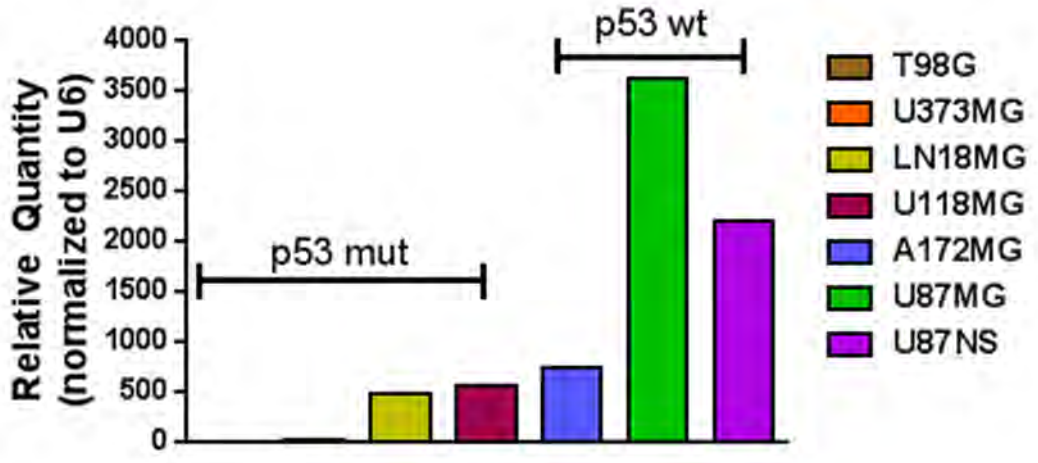

Figure 3.3 Glioma cultures express varying levels of miR-34a transcript.
RNA was isolated from seven GBM lines and mature miR-34a was quantified via qRT-PCR. Raw data was normalized to U6. Expression of miR-34a shows an apparent correlation with p53 status.

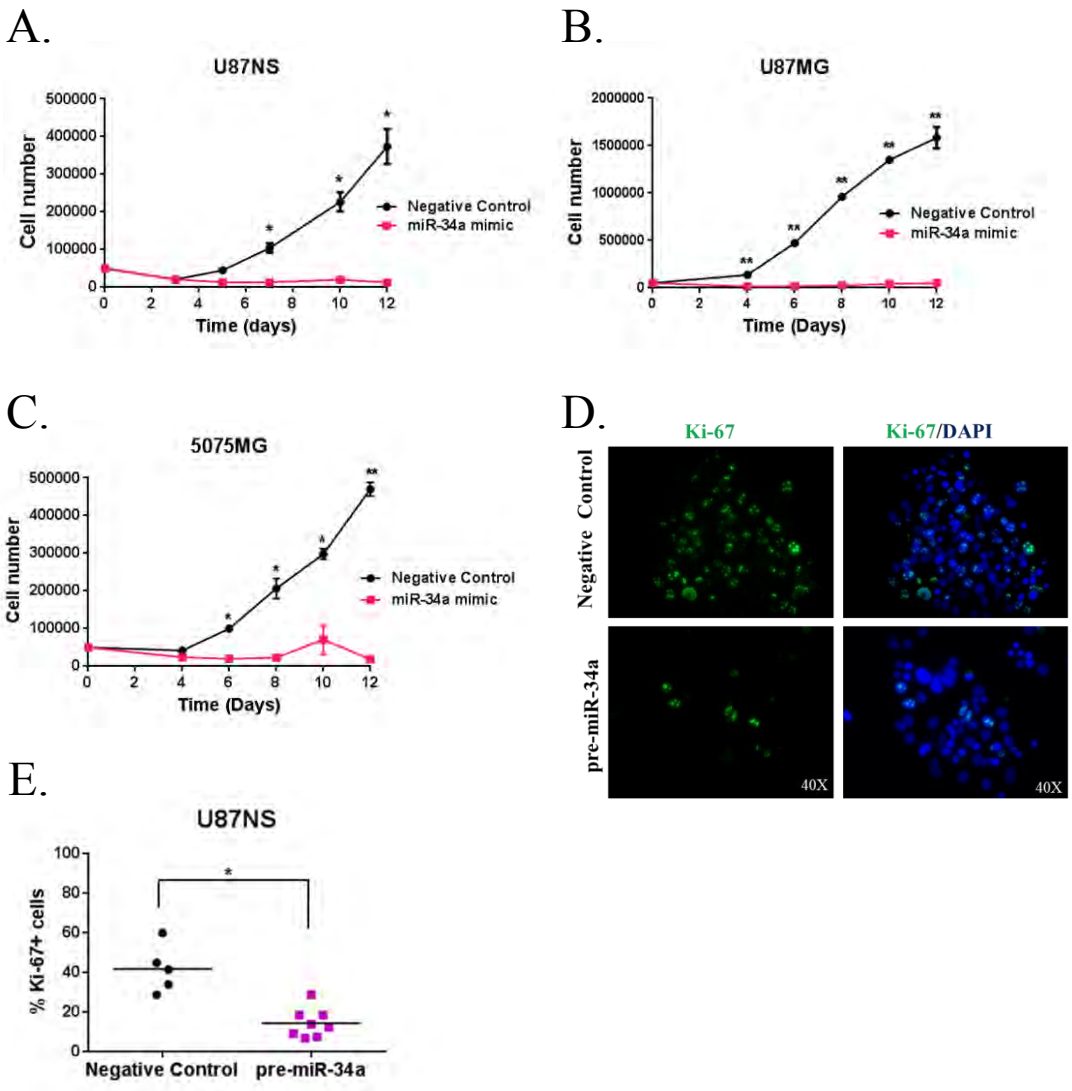

Figure 3.4 Exogenous miR-34a expression suppresses GBM growth.
U87NS (A), U87MG (B), and 5075MG (C) were transfected with either miR-34a mimic or scrambled negative control. Changes in cell numbers were quantified via trypan blue exclusion (A-C). Three days post-transfection U87NS spheres were stained for proliferation marker Ki-67 (D) and Ki-67+ cells were quantified (E). miR-34a overexpression decreased the proliferation of GBM cell lines. Data are reported as mean ± SEM. Representative from at three independent experiments shown. * p-value <0.05, ** p-value <0.01

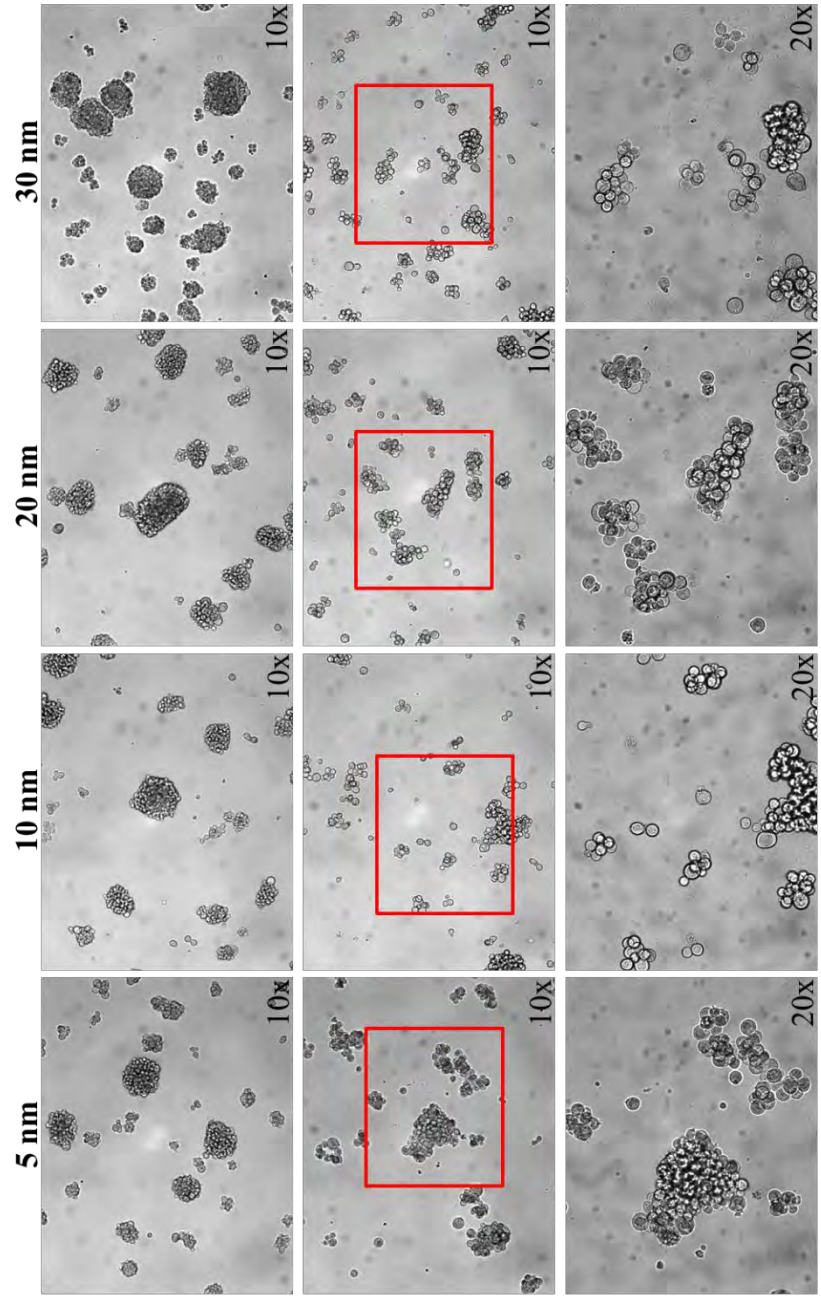

Figure 3.5 Neurosphere morphology is affected by increased miR-34a. Representative micrographs of U87NS neurospheres transfected with 5, 10, 20, or 30 nM miR-34a mimic or negative control. Area within the red box is magnified and displayed below. Exogenous miR-34a gives rise to cells, which are enlarged and do not form dense neurospheres as seen in control transfected cultures.

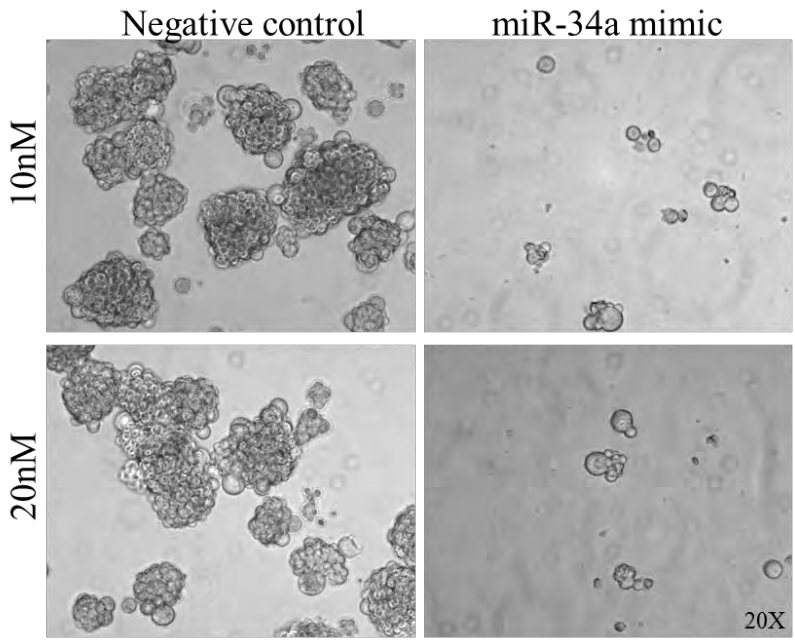

Figure 3.6 Mir-34a disrupts neurosphere renewal.
U87NS cells were plated at $5x10^4$ cells/well and transfected with miR-34a or negative control at 10 nM and 20 nM. Seven days post-transfection cells were pH dissociated and replated to evaluate secondary sphere growth. Neurospheres failed to give rise to secondary spheres.

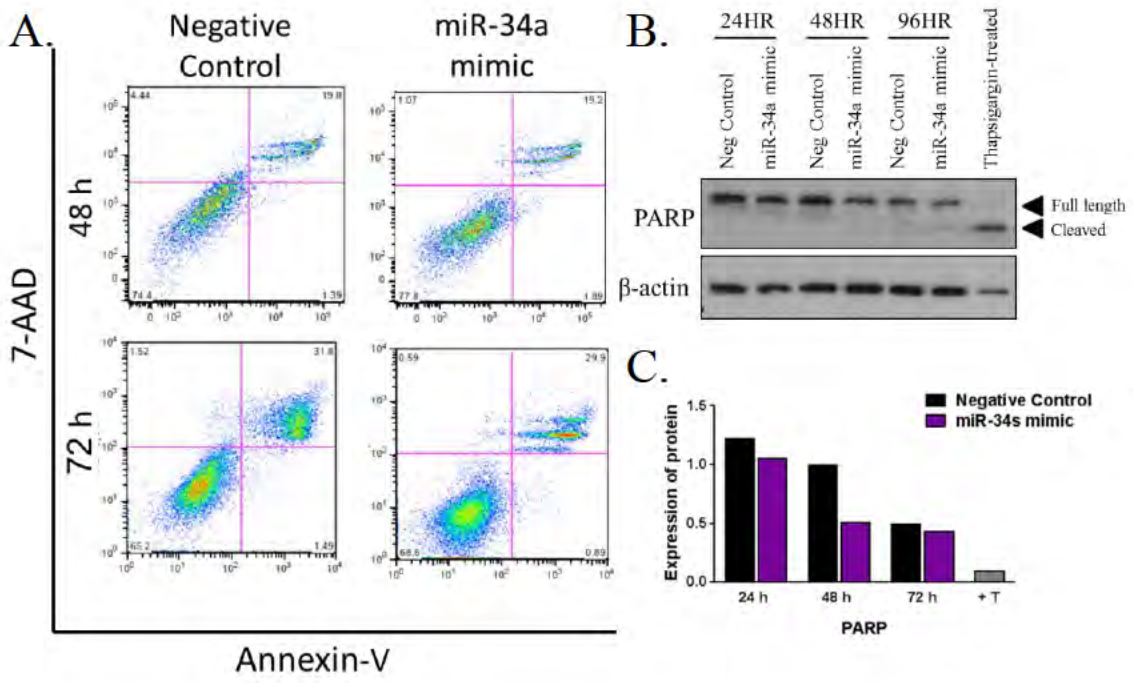

Figure 3.7 Apoptosis was not induced in U87NS cultures overexpressing miR-34a. Flow analysis for Annexin-V-FITC and 7-AAD staining was carried out 48 h and 72 h post-transfection of U87NS cells (A). Representative from three independent experiments. Western blot analysis for PARP and PARP cleavage (B). Cells were transfected with 20 nM pre-34a or negative control and whole cell lysates were collected at 24, 48, and 96 h post-transfection. Thapsigargin-treated cells were included as a positive control for PARP cleavage. A histogram shows the average band density normalized to β-actin (C). + T= Thapsigargin-treated. Annexin-V and 7-AAD showed no difference in apoptosis between miR-34a mimic and control. PARP cleavage was not detected following miR-34a overexpression. This indicates that the inhibitory effect of miR-34a on cell proliferation cannot be attributed to an apoptotic response.

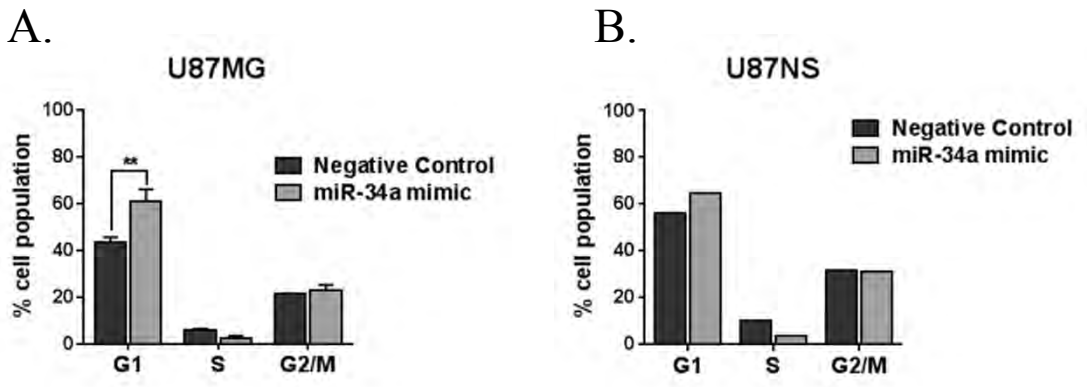

Figure 3.8 Cells arrest in G1 following overexpression of miR-34a.
U87MG and U87NS were transfected with miR-34a mimic or negative control. Flow analysis for PI was done 72 h post-transfection (A-B) and indicated a slight G1 arrest within the U87MG (A) cultures and U87NS (B). Mean ± SEM. U87NS and U87MG data is a representative of two replicates. G2/M phase is unaltered between control and miR-34a overexpression cultures. ** p-value <0.01

A.

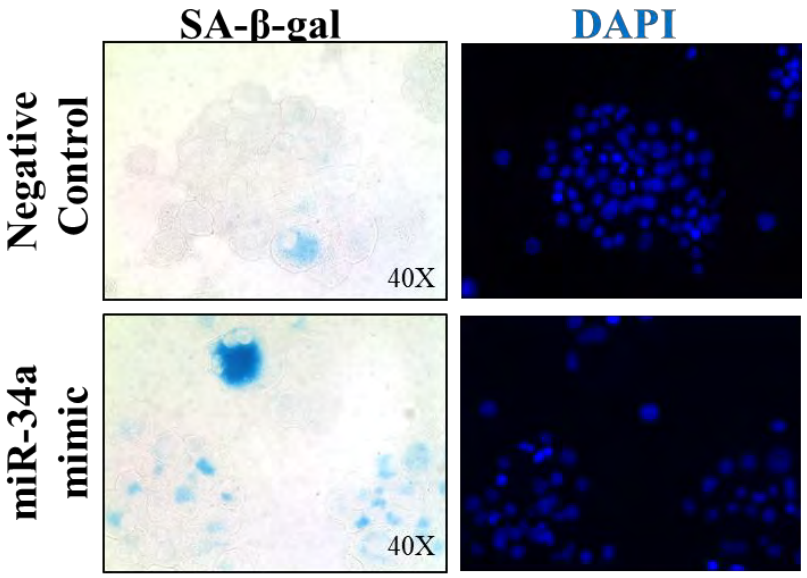

B.

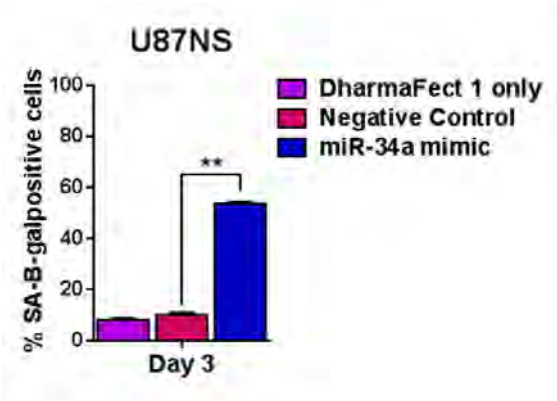

Figure 3.9 SA-β-gal induction occurs in response to miR-34a overexpression. Representative micrographs of SA-β-gal staining in U87NS cells transfected with 20nM miR-34a mimic or negative control. Neurospheres were spun down unto slides and stained for SA-β-gal and DAPI (A). SA-β-gal positive cells were counted (B). U87NS overexpressing miR-34a had a 5-fold increase in SA-β-gal positive cells than negative control. Data plotted as mean ± SEM from three independent experiments. ** p-value <0.01.

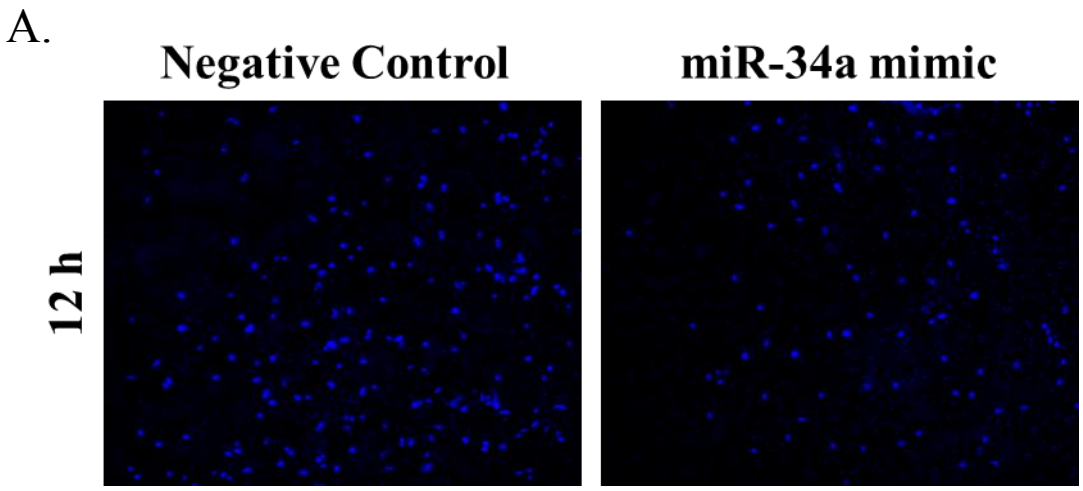

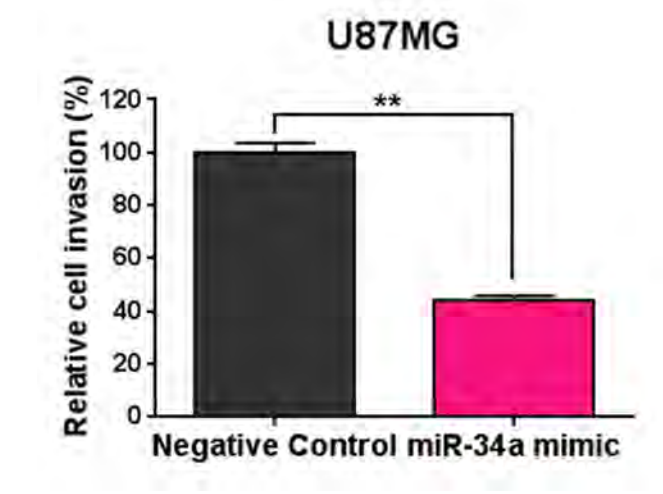

Figure 3.10 MiR-34a reduces invasiveness of glioma cells.
Representative micrographs of DAPI stained cells which have invaded through Matrigel® coated transwell chambers (A) GBM U87MG cells were transfected with miR-34a mimic or negative control and assessed for invasion via a transwell invasion assay. Cells were allowed to invade for 12 h, at which time cells that had invaded were fixed, stained with DAPI and counted. (B) Forced expression of miR-34a inhibits transwell glioma cell invasion. Mean ± SEM of two independent replicates. ** p-value <0.01.

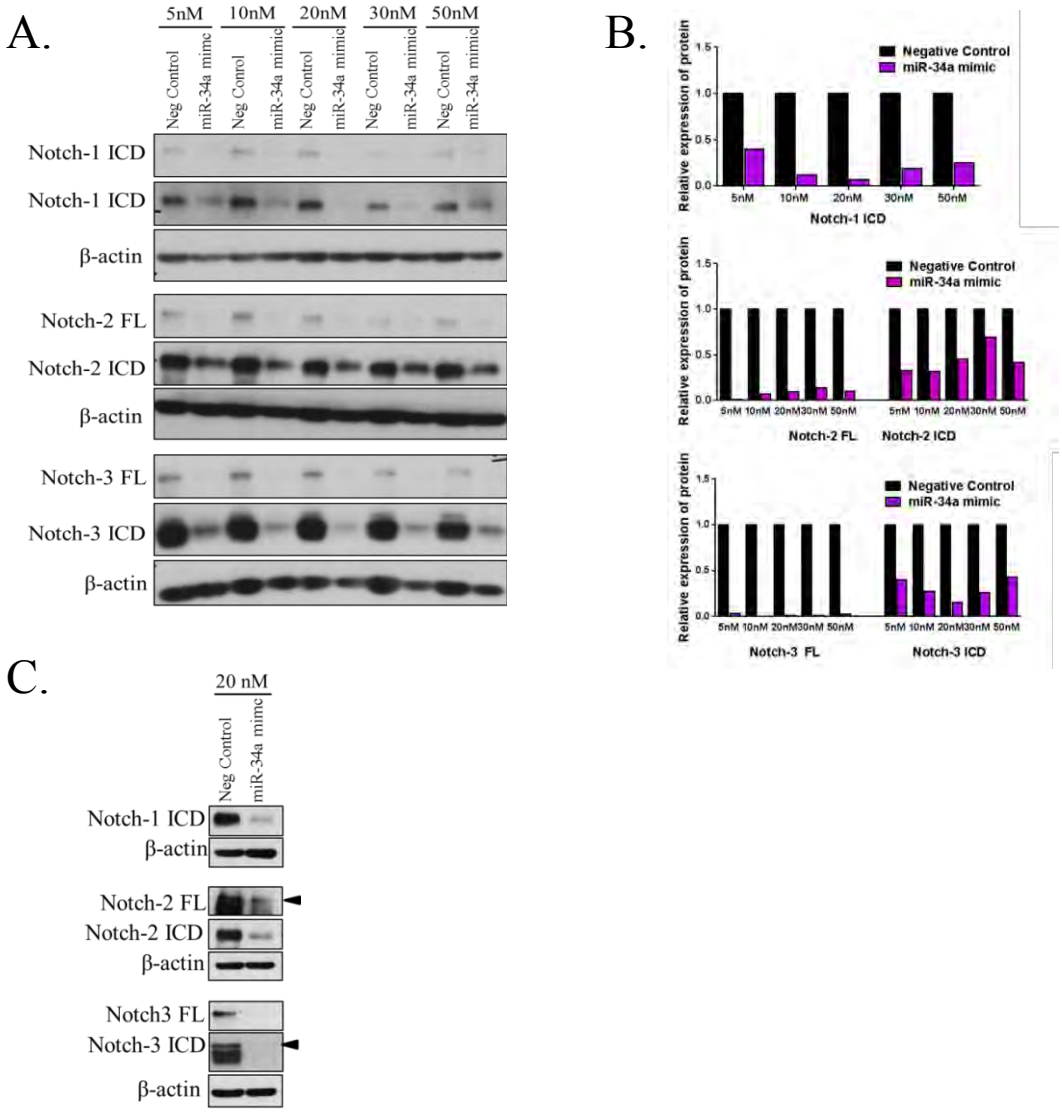

Figure 3.11 MiR-34a suppresses expression of Notch family members.
Notch-1, Notch-2, and Notch-3 expression in U87NS (A-B) and U87MG (C) transfected with miR-34a mimic or negative control was determined by Western blot analysis. Whole cells lysates were collected and probed for the expression of each Notch receptor. A histogram shows the average band density normalized to β-actin (B). MiR-34a suppresses the expression of full length (FL) and ICD of Notch family members.

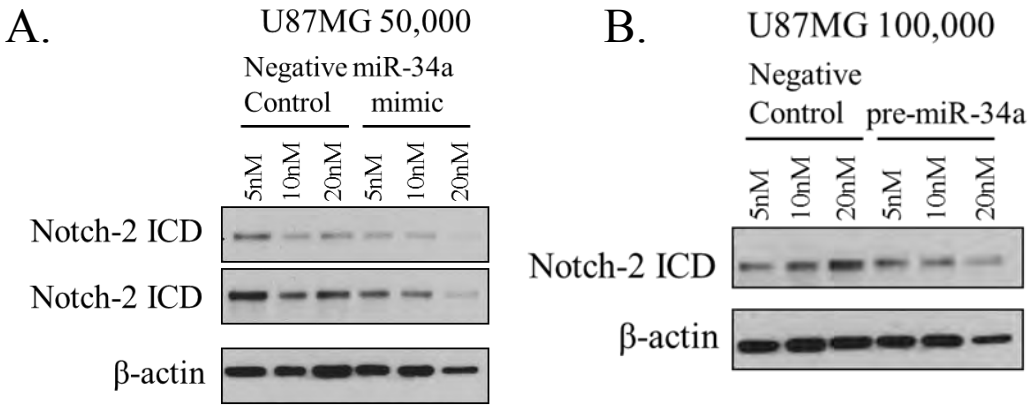

Figure 3.12 Suppression of Notch family members is affected by cell density.
U87MG were plated at $5x10^4$ cells (A) and $1x10^5$ cells (B) per well, transfected with varying doses of miR-34a mimic or negative control, and analyzed for expression of Notch-2 via Western blot. Cell density plays a role in the suppression of Notch-2 expression by miR-34 with lower concentrations leading to Notch suppression in less dense cultures.

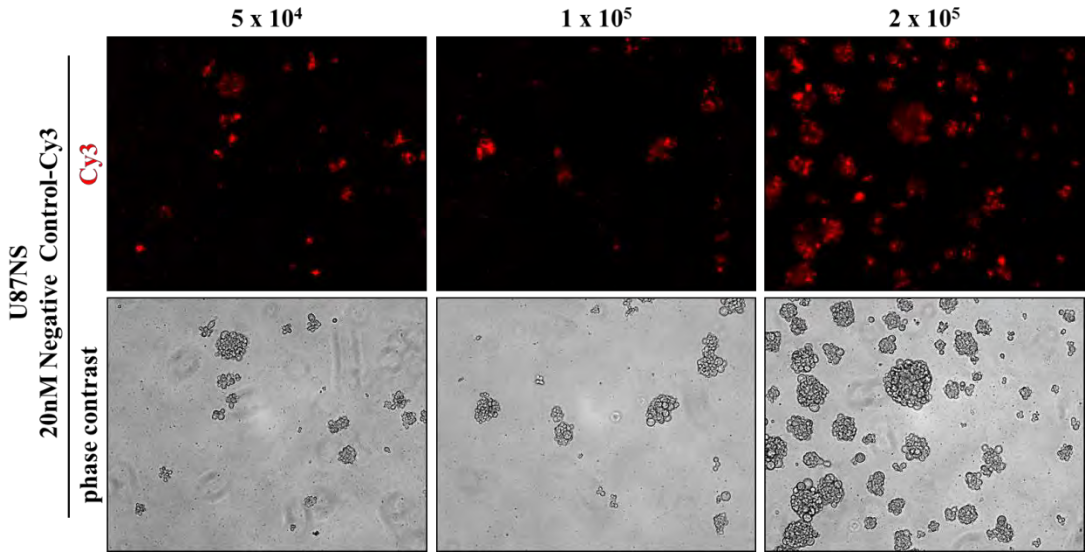

Figure 3.13 Optimization of miRNA transfections.
A Cy3-labeled scrambled oligo was used to optimize transfection efficiencies in GBM neurospheres. U87NS were plated at $5x10^4$, $1x10^5$, or $2x10^5$, transfected with 20 nM Negative control-Cy3, and Cy3 signal was monitored.

CHAPTER IV

FINAL CONCLUSIONS AND FUTURE DIRECTIONS

GBMs are malignant brain tumors with limited treatment options. The current standard of care consisting of surgery, radiation, and TMZ gives a median survival of 12-14 months but does not cure, as only a dismal 9.8% of patients survive 5-yrs or longer (Stupp, Hegi et al. 2009). This poor survival is attributed to the high incidence of recurrence in patients with 80-90% of recurrences occurring within seven months of diagnosis at the site of the original tumor (Wen and Kesari 2008; Milano, Okunieff et al. 2010). The work contained within this thesis sought to explore novel strategies to overcome resistance in GBMs. Two approaches were taken: 1) evaluation of novel imidazotetrazine analogues designed to overcome resistance and 2) modulating miR-34a expression to mimic effects of novel TMZ + GSI therapy. Together they contribute to the understanding of the mechanisms underlying resistance and provide us with insight into ways to develop more effective chemotherapies.

Bypassing DNA repair with Novel Imidazotetrazines

In my first study we evaluated two novel imidazotetrazine analogues designed to overcome resistance in GBMs (**Figure 2.1**). The key to this approach is to bypass DNA repair pathways with chemotherapeutic agents which form adducts that cannot be processed. We demonstrated that both the monofunctional, DP86, and bifunctional, DP68, had significant higher efficacy in GBM cells lines than TMZ (**Table 2.1**).

Established lines, neurosphere cultures, patient-derived cell lines, and models of TMZ resistance were all sensitive to both DP86 and DP68 independent of their expression of MGMT expression (**Figure 2.3, Figure 2.5**). This is exciting because, in contrast to DP68 and DP86, the efficacy of TMZ is dependent on repressed MGMT expression. *In vitro* inhibition of MGMT in cells enhanced TMZ efficacy in MGMT positive GBM cells while DP86 and DP68 sensitivity was unchanged (**Figure 2.7**). Similarly, both TMZ analogues were independent of the MMR DNA repair pathway as knockdown of MLH1 did not alter efficacy (**Figure 2.8**). Evaluation of DP86 and DP68 in a secondary sphere assay showed inhibition of recovery and secondary sphere formation demonstrating that the self-renewing population is effectively killed (**Figure 2.10**). DP68 is an effective cross-linker (**Figure 2.11**) and exhibited cell cycle profile distinct from TMZ marked by an S-phase accumulation before G2/M arrest (**Figure 2.12**). Recovery of DP68 induced damage was found to be dependent on ATR and FANCD2, but not ATM (**Figure 2.14-15**). Unfortunately, we were unable to exert any anti-tumor response with either DP68 or DP86 in *in vivo* drug treatments of immunocompromised mice (**Figure 2.16-18, Table 2.2**). Phamacokinetics studies demonstrated that both drugs had relatively short half-life and limited absorption (**Figure 2.19**).

While cytotoxicity of TMZ is attributed to *O*6-meG lesions, methylation of *N*7-G and *N*3-A is much more common (Denny, Wheelhouse et al. 1994; Zhang, Stevens et al. 2012). *N*7-G and *N*3-A TMZ lesions are processed by the base excision repair pathway (BER), which is responsible for removing damaged bases (Fu, Calvo et al. 2012; Svilar,

Dyavaiah et al. 2012). DP68 and DP86 were designed to generate anticancer activity from *N*7-G adducts (Garelnabi, Pletsas et al. 2012); however, we did not evaluate the contribution of *N*3-A and *N*7-G lesions to DP68 and DP86 toxicity. This can be examined by inhibiting the BER pathway via shRNAs targeting PARP-1. The BER deficient cells (shPARP-1) would then be treated with DP68 or DP86 and evaluated via a CyQUANT assay. If N3-A and N7-G do contribute to DP68 and DP86's toxicity, we would see an increase in sensitivity to drug treatments. Because another member of the PARP family, PARP-2, may be able to compensate for loss of PARP-1, this protein can also be knockdown should one fail to see a response in the initial PARP-1 knockdown.(Ménissier de Murcia, Ricoul et al. 2003). Contribution of *N*3-A and *N*7-G can also be studied by targeting DNA glycosylases which work in BER to recognize and excise the damage. One of these glycosylases, alkylpurine-DNA-N-glycosylase (APNG), is an attractive target because it has been shown to confer TMZ resistance in *in vitro* and *in vivo* models of GBM (Agnihotri, Gajadhar et al. 2012). Patients with tumors positive for APNG staining had poor OS. Furthermore, when patients with methylated MGMT promoters, meaning TMZ sensitivity, were stratified into good OS and poor OS groups, a greater number of APNG positive tumors were found in the poor OS group. Established lines as well as the primary GBM6 line used in our analysis of DP68 and DP86 are APNG positive (Agnihotri, Gajadhar et al. 2012). Future studies that examine *N*7-G and *N*3-A contribution to DP68 and DP86 toxicity would be informative.

The most detrimental factor affecting the survival of GBM patients is the emergence of TMZ resistance, which leads to re-growth of tumors. Despite extensive research, many of the molecular mechanisms that regulate resistance remain undefined. In our study, U87NSTMZ, U251TMZ, and GBM12TMZ cells lines were generated as models of acquired TMZ resistance. Resistance of GBM12TMZ results from expression of MGMT, which could not be attributed to changes in promoter methylation (Kitange, Mladek et al. 2012). Instead GBM12TMZ showed greater acetylation of histone H3K9 (H3K9-ac). In contrast, U251TMZ and U87NSTMZ do not express MGMT (**Figure 2.3 D**). In our examination of the U87NSTMZ lines we found MLH1 and FANCD2 upregulated and MSH2 and BRCA1 downregulated compared to parental U87NS cells (**Figure 2.20 A-D**). Our studies are in line with Chen et al in which FA-proficient cells are resistant to BCNU and TMZ treatments. Loss of BRCA1 is associated with chemo sensitivity and not resistance as was observed in our U87NSTMZ line. However, simultaneous loss of p53 binding protein (53BP1) in BRCA1 null cells has been shown to rescue chemo resistance in breast cancer cells; our GBM cells might utilize the same mechanism to drive resistance (Bouwman, Aly et al. 2010). Expression of 53BP1 in our resistant lines was not analyzed but would be interesting. Contribution of FANCD2 and BRCA1 to TMZ resistance is not well documented and would benefit from further study.

The MMR pathway is important for detection and subsequent repair of base pair mismatch that occurs due to uncorrected *O*6-meG lesions. The changes that we observed for MSH2, a key player in MMR, are similar to those already reported in the literature.

For instance, TMZ-resistant lines generated by McFaline-Figueroa et al showed decreased MSH2 levels. Interestingly, although the decrease was modest (30%), it was sufficient to elicit resistance. Increased MLH1 expression in our U87NSTMZ line contrasts with our earlier experiments where MLH1 was knocked down in U87MG and T98G lines. Loss of MLH1 in U87MG and T98G mediated resistance to TMZ treatment (**Figure 2.8 C-D**). U87MG shMLH1 lines were as much as 5.2-fold less sensitive to TMZ than U87MG cells, with TMZ IC_{50}s as high as 795 μM, a concentration that could not be achieved in the clinic without toxicity. Our MLH1 knockdown experiments are in line with previous studies. Loss of MLH1 expression has been associated with TMZ resistance in GBM cell lines (Happold, Roth et al. 2012; Shinsato, Furukawa et al. 2013). Interestingly, a study by Samimi et al examined ovarian carcinomas pre and post platinum treatment and unexpectedly found that patients who showed a complete response to therapy had the lowest percent of MLH1 positive cells in post-treatment samples (Samimi, Fink et al. 2000). Similar results were seen in Stark et al analysis of initial versus recurrent GBM tumors. Patients with positive MLH1 expression in initial samples had increased survival. The MLH1 staining is hypothesized to be due to an accumulation of a non-functional protein (Stark, Doukas et al. 2010). This observation could explain the increase in MHL1 that we observe in our U87NSTMZ line. We did not examine other members of the MMR pathway, including Mutα component, MSH6, and MutL component, PMS2. The *in vitro* and clinical data on PMS2 indicates that it is reduced in TMZ-resistant lines and recurrent tumors (Felsberg, Thon et al. 2011; Happold, Roth et al. 2012). MSH6 has been associated with GBM tumor progression, and

mutations in MSH6 arise during TMZ therapy and contribute to resistance (Yip, Miao et al. 2009) (Cahill, Levine et al. 2007). Expression of PMS2 or MSH6 in our U87NSTMZ cell line was not analyzed. These data are a perfect example of the complexity of resistance in cancer and demonstrate that our novel compounds overcome resistance mediated by multiple different DNA repair pathways.

While TMZ-resistance was evaluated in our study, we did not examine if repeated DP86 or DP68 exposure would give rise to resistance. This can be pursued in the future, as it would allow us to study which pathways GBM cells use to circumvent the damage caused by DP86 and DP68. Our data (**Figure 2.14-2.15**) shows that inhibition of FANCD2 or ATR sensitizes cells to DP68 but it also highlights a mechanism by which resistance can be acquired; overexpression of members of the FA-pathway and the ATR kinase could enhance repair of DP68-induced ICLs. On such member, FANCD2, and ATR interact with proteins involved in mediating ICL repair, such as BRCA1 and RAD51. In multiple myeloma cells resistance to the cross-linker Melphalan has been attributed to the overexpression of FANCF and RAD51C (Chen, Van der Sluis et al. 2005). A study of 131 FFPE GBM tumors showed FANCD2 staining in 93% of samples while normal brain tissue had little to no FANCD2 staining (Patil, Sayal et al. 2014). Primary GBM cultures established in that study, showed FANCD2 was not only expressed but the pathway was active in the cells. It would be of interest to generate a DP68 resistant line through repeated exposure to DP68, similar to how our TMZ-resistant lines were established. We would then be able to measure protein levels of FA-pathway

members, starting with FANCD2, ATR, BRCA1, and Rad51 in our DP68-resistant lines. The hypothesis is that these proteins would be overexpressed in DP68-resistant cultures. We could subsequently knock down the above-mentioned proteins and carry out dose-response experiments to see if they regain DP68 sensitivity. Simultaneously, comet assays would allow us to evaluate the increase in ICL formation if the cells are no longer resistant. It is possible, and more than likely, that a single gene knockdown will not completely account for the resistance at which point double knockdowns can be pursued.

We did not evaluate the effects of DP68 on normal cells; however, examining potential toxicity to normal human astrocytes (NHA) is important and should be evaluated in the future. *In vitro* TMZ studies have shown that NHAs treated with 100 μM TMZ arrest at G1 and a small population at G2/M but show no induction of γH_2AX or apoptosis and expression of cell cycle proteins such as p53, p21, and Chk2 remain unchanged (Sato, Kurose et al. 2009). We would predict our TMZ-analogues to have similar effects on NHAs. However, there is one caveat: cultured astrocytes are more proliferative than normal brain such that they are poor model to determine "normal damage". Effects of DP68 on normal cells would best be analyzed in an *in vivo* intracranial model following treatment with DP68, unfortunately, without an efficient delivery system we are unable to do this.

Experience treating patients with TMZ or the crosslinker, BCNU, establishes that the most common, but manageable, side effect is damage to the bone marrow (Zielske

and Gerson 2002). I would predict that our novel TMZ compounds will have the same side effects, but without an effective delivery, we cannot really make a definitive statement. However, low levels of MGMT in hematopoietic precursors are thought to be responsible for the myelosuppression that arises following TMZ and BCNU treatment (Zielske and Gerson 2002). This is of concern as DP68 deposits adducts onto the O6-G which cannot be repaired by MGMT thus potentially could give rise to greater bone marrow toxicity than TMZ. This could be studied using primary hematopoietic stem cells in colony forming assays following treatment with compound of interest, in our case DP68 (Clarke, Pereira et al. 2007). A decrease in the number of colonies formed would indicate potential toxicity. Similarly, a mouse model containing humanized bone-marrow can be utilized to study toxicity *in vivo* (Cai, Wang et al. 2011). If we had an effective delivery system, these would be great parameters to test.

We demonstrated that DP68 activates the DDR with as little as 3 μM (**Figure 2.13 B)** and inhibits self-renewal of U118NS spheres with a single 10 μM dose (**Figure 2.10 B**). It is promising that DP68 can exert such strong anti-tumor effects at such a low dose as it could limit toxicity to normal cells. Additionally, we showed that FANCD2 or ATR inhibition sensitizes GBM cells to DP68 treatment (**Figure 2.14-2.15**). Therefore, ATR or FANCD2 deficient cells would likely be hypersensitive to DP68, which could be exploited to treat ATR or FANCD2 deficient tumors at concentrations that minimize toxicity to normal cells. However, all this work was carried out *in vitro,* which is not an adequate model for the analysis of the therapeutic window.

Unfortunately DP86 and DP68 failed to demonstrate an effect *in vivo* despite varying treatment regimens and delivery methods (**Figure 2.16-18, Table 2.2**). Both TMZ analogues were rapidly eliminated from plasma, and their half-life is much shorter compared to TMZ (DP86 $t_{1/2}$ = 14.4 min; DP68 $t_{1/2}$ = 14.3 min; TMZ $t_{1/2}$ = 53 min). Based on these data changes to DP86 and DP68's chemical properties are needed to enhance drug delivery.

In vivo efficacy of DP68 is limited by its poor aqueous solubility. One approach to enhance the efficacy of this compound would be inclusion of DP68 in cyclodextrin, a process that enhances solubility of compounds and their bioavailability (Del Valle 2004). In our own pharmacokinetic analysis (**Figure 2.19**) DP68 and DP86 were formulated in 0.9% NaCl, 10% (w/v) HP-β-cyclodextrin demonstrating that this could be an effective approach to overcome solubility issues seen with DP68. Another technique to increase solubility would be the conversion of DP68 into a salt form (Savjani, Gajjar et al. 2012). Thirdly, encapsulation of cytotoxic drugs by nanocarriers is a great option to try to overcome limiting factors such as poor solubility and pharmacokinetics (Yu, Tai et al. 2010). The nanocarriers can be designed to target the tumor cell by coupling a moiety to the nanocarrier such as antibody molecules or synthetic ligands (Pastorino, Brignole et al. 2013). Tsutsui et al created a bionanocapsules that targeted EGFR*vIII* by conjugating it to an anti-EFGR antibody that recognized the deletion variant (Tsutsui, Tomizawa et al. 2007). Conjugated EGFR antibody-bionanocapsules were effectively delivered to GBM

cells *in vitro* and to brain tumor tissue in a mouse intracranial model. These are three promising approaches which could be tested.

DP68's and D86's poor pharmacokinetic properties limit their efficacy. This is evident as DP86 displayed no solubility issues and yet failed to be effective in our *in vivo* GBM xenograft model (**Figures 2.16-2.17**). DP68 and DP86's half-lifes of 14 mins is significantly shorter than TMZ's half-life of 55 mins. In order to circumvent this, delivery methods can be modified. Two approaches to test are impregnation of the drug into biodegradable polymer wafers and the use of osmotic pumps for infusion of the drugs; two methods which would provide the tumor with continuous DP68 and DP86 delivery. BCNU is an example of a chemotherapy compound with a short half-life which was reformulated as a polymer wafer (GLIADEL®). This method has been shown to provide constant drug levels within the tumor for 5 days (Fleming and Saltzman 2002). Osmotic pumps can be implanted subcutaneously to be used in subcutaneous xenograft models or used with a catheter to infuse into the brain in intracranial models (DURECT 2015). Future experiments utilizing osmotic pumps implanted subcutaneously to deliver DP68 and DP86 *in vivo* to a subcutaneous xenograft models would be a good place to start before moving into the more invasive intracranial models. If this proves effective it would allow us to define the *in vivo* efficacy of our novel TMZ analogues, toxicity profile, and therapeutic window for these agents.

Ideally we would want to develop a drug that retains the good chemical properties of TMZ but avoids TMZ-induced resistance. Properties of this drug would include: modest stability at neutral pH to pass through the BBB, solubility in both aqueous and organics as this would facilitate passage to the tumor and through the BBB, and good pharmacokinetics. The poor aqueous solubility of DP68 is a major reason why this otherwise promising drug might never be tested in the clinic. A drug with good acid stability would be nice, but not essential, as it allows oral administration. The drug-induced DNA damage would be poorly reversed by MGMT and other DNA repair proteins as was seen with DP68 and DP86.

DNA interstrand crosslinking is difficult to repair and, hence, desirable. As a result, we would be happy to test crosslinkers but consider it too restrictive to only test crosslinkers, as such we would continue to test monofunctional compounds. For example, TMZ is a great monovalent drug, and I would not want to miss a more effective TMZ-like drug. Also, the larger size of crosslinkers may reduce solubility (MW DP68= 534 g/mol, MW DP86= 331 g/mol, MW TMZ= 194 g/mol).

We want to learn from our experiences with DP68 and DP86 and eliminate inappropriate compounds as early as possible. Our scheme involves three steps: characterization by the medical chemists, initial characterization by our lab, and finishing with detailed studies of any promising compounds. To begin we would seek out medicinal chemists to examine solubility of pure drug candidates in water and organic

solvents. Simultaneously, they would examine the rates of hydrolysis at acidic and neutral pHs. This can be done via a spectrophotometric assay, taking advantage of differences in absorbance values between the parent compound and the hydrolysis product. Following this, we would begin the initial characterization of compounds by acquiring dose-response curves with a MGMT+ and MGMT- GBM line via MTT assay. Once efficacy *in vitro* is established we would move to IP administration of nude mice bearing subcutaneous GBM xenografts. While intracranial GBM models are the best, for initial experiments I prefer subcutaneous tumors as one does not have to worry about penetrance of the BBB. The final step would involve more details studies of promising compounds. Here we would examine efficacy of the compounds in intracranial tumors generated from injection of luciferase-labeled GBM cells, including testing of additional models of TMZ-resistant cells that we and our collaborators have derived as some of these models are resistant by mechanisms other than MGMT. Finally, we would carry out pharmacokinetic studies. HPLC assays can be done to assess drug levels in serum, brain and other organs. If we discover an effective anti-cancer drug that does not pass through the BBB, its efficacy in other cancer models can be tested.

Overall, this study serves as a proof-of-concept for these novel imidazotetrazine analogues that create DNA lesions insensitive to DNA repair by MGMT or the MMR pathway. Importantly, the cross-linking activity of DP68 was efficacious in all models of TMZ resistance tested and prevented regrowth of cultures following treatment. Unfortunately, GBM patients succumb to disease due to recurrence. DP86 and DP68

could be the therapy that fills this unmet clinical need by overcoming mechanisms of TMZ resistance.

Targeting miR-34a as Therapy in GBMs

In my second study, we examined the role of miRNAs in our novel TMZ + GSI therapy. MiR-34a was found to be upregulated following TMZ and TMZ + GSI treatment in both, p53 wild type, U87NS cells and, p53 mutant, U373NS cells (**Figure 3.2**). In a panel of GBM cell lines, levels of miR-34a transcript were associated with p53 status of the lines (**Figure 3.3**). *In vitro* examination of miR-34a in GBM cultures shows it functions as a tumor suppressor. MiR-34a overexpression significantly inhibits proliferation of cells (**Figure 3.4)** and gives rise to loosely bound neurosphere made up of large cells (**Figure 3.5**). These neurospheres do not form secondary spheres following dissociation (**Figure 3.6**). This decrease in cell number is not due to an induction of apoptosis (**Figure 3.7**) but rather a permanent growth arrest as miR-34a mediates G1 arrest (**Figure 3.8**) and a large induction of SA-β-gal staining (**Figure 3.9**). These phenotypes mimic the effects of our TMZ + GSI treatment. Additionally, miR-34a decreases invasion of our GBM cells (**Figure 3.10**) In our GBM models, miR-34a overexpression downregulares Notch family members, suggesting that these effects could partially be due to suppression of Notch receptors by miR-34a (**Figure 3.11**).

We showed that miR-34a is upregulated in both TMZ and TMZ + GSI treated U87NS and U373NS cells. While previous studies have noted upregulation of miR-34a

following radiation and/or cytotoxic therapy (Tazawa, Tsuchiya et al. 2007; Li, Branham et al. 2010; Li, Yu et al. 2014; Novello, Pazzaglia et al. 2014), few have studied miRNA expression changes following TMZ or DAPT treatment, and even less in the context of GBMs. A single study analyzed the expression of miRNAs following TMZ treatment in T98G cells. They found that five miRNAs were downregulated and nine miRNAs, upregulated; none of which were miR-34a (Tunca, Tezcan et al. 2012). While this is in contrast to what we found, it is not surprising as T98G expresses very low basal levels of miR-34a compared to other GBM cells lines (**Figure 3.2**), and it has mutant p53. MiR-34a is transcriptionally activated by p53 (Bommer, Gerin et al. 2007; Chang, Wentzel et al. 2007; He, He et al. 2007) and in return regulates p53 indirectly by inhibiting expression of p53 regulators such as Sirtuin 1 (SIRT1), Ying-Yang 1 (YY1), and, MAGE-A (Yamakuchi, Ferlito et al. 2008; Chen, Yu et al. 2011; Weeraratne, Amani et al. 2011). Surprisingly, in our study miR-34a transcript levels are upregulated in both, p53 wild type, U87NS and, p53 mutant, U373NS cells. Additional p53 mutant cell lines can be analyzed to evaluate if this is a cell-specific response. Alternatively, in U373NS, miR-34a upregulation could occur through a p53-independent mechanism. The molecular determinants of p53-independent regulation of miR-34a are being explored. In primary human fibroblasts, BRAF-induced senescence caused a p53-independent upregulation of miR-34a mediated by an ETS transcription factor, ELK1 (Christoffersen, Shalgi et al. 2010). In another study, miR-34a was shown to target histone deacetylase 1 (HDAC1), leading to the induction of p21, independent of p53 (Zhao, Lammers et al. 2013).

Elucidating other potential p53-independent pathways at work is of interest as p53 signaling is altered in 87% of GBMs (Cancer Genome Atlas Research 2008).

The miR-34 family consists of miR-34a, miR-34b, and miR-34c. MiR-34b and miR-34c are located at chromosome 11q23.1 and are expressed from a polycistronic transcript while miR-34a maps to chromosome 1p36.23 a region deleted in 34% of GBM patients (Cole, Attiyeh et al. 2008; Ichimura, Vogazianou et al. 2008). While our focus was miR-34a, it would be of interest to also quantify changes in miR-34b and miR-34c expression following TMZ and TMZ + DAPT expression to see if they are differentially expressed following drug treatment.

In vitro studies evaluating the efficacy of the combination of miR-34a and other conventional chemotherapeutic agents has been conducted in models of breast, lung, colon, bladder, medulloblastoma, liver, prostate, and head and neck cancers. (Weeraratne, Amani et al. 2011; Bader 2012; Misso, Di Martino et al. 2014). Interestingly, miR-34a and TMZ combination treatment has yet to be evaluated. While this was one of our original aims of the study, we were unable to examine the combination of miR-34a and TMZ as we could not mimic the TMZ + GSI treatment schedule. We had previously shown that TMZ + GSI response is schedule dependent. Inhibition of secondary sphere formation and induction of SA-β-gal staining are dependent on DAPT being administered 24 h after TMZ. DAPT pre-treatment or co-treatment with TMZ fails to inhibit secondary spheres and does not lead to a permanent senescent arrest (Gilbert 2011) (Gilbert, Daou

et al. 2010). However, we were unable to treat cells with TMZ and subsequently transfect cells with miR-34a mimic without causing large amounts of cell death. The use of a different delivery method, as discussed above, is appealing for future experiments. One study showed efficient uptake of miR-21 inhibitor within polymer-nanoparticles which allowed evaluation of miR-21 and TMZ combination therapy in GBM cell lines (Qian, Ren et al. 2012). MiR-34a encapsulation within a nanoparticle is appealing. We could then evaluate the efficacy, if any, of combining miR-34a and TMZ treatment. Although, miR-34a elicits a strong anti-glioma response on its own, coupled with TMZ it might act synergistically thus allowing for sub-optimal doses to be administered without sacrificing efficacy. The mode of action of TMZ is distinct enough from miR-34s that the combination of miR-34a and TMZ might show added benefits.

MiRNAs are known to regulate many cellular processes including: proliferation, apoptosis, senescence, differentiation, and invasion (Di Leva, Garofalo et al. 2014). Furthermore, they may regulate multiple genes within a pathway and several pathways at once, making them attractive candidates for therapy (Lal, Thomas et al. 2011). MiR-34a with its strong tumor suppressor phenotype and mis-expression in a number of cancers (Lodygin, Tarasov et al. 2014) makes it ideal for miRNA replacement therapy. Several approaches can be taken to overexpress miR-34a *in vivo* (Costa and Pedroso de Lima 2013; Li, Ren et al. 2014). One approach is to express pri-miR or pre-miR sequences from a viral vector. The pri-miR or pre-miR messages subsequently undergo processing within the cell. However, expression of miRNAs from viral vectors can be challenging

due to limited infectivity and failure of proper transcription and processing of gene product. This is in part due to the misexpression of miRNA processing machinery in many cancers (Kumar, Lu et al. 2007; Melo, Ropero et al. 2009). Another approach is the use of miRNA mimics, synthetic double strand RNA molecules, which mimic the miRNA:miRNA* duplex generated following Dicer cleavage of pre-miR message. It is made up of a guide strand identical to the mature miRNA sequence and a passenger strand. The guide strand is incorporated into the RISC which then binds complementary sequences in the 3'UTR of target genes. Methyl (2'-O-Me), methoxyethyl (2'-MOE), or fluorine (2'-F) can be added to enhance the stability. Packaging of miRNA mimics within different lipid or polymer based-nanoparticles are being evaluated to insure effective delivery *in vivo* (Ben-Shushan, Markovsky et al. 2014). Of interest is Mirna Therapeutics NOV340 technology (SMARTICLES®) that allows encapsulation of miRNA within an ionizable lipid-based carrier. In areas of low pH, such as within tumors, the particles are cationic and can adhere to the cells within the tumor. In contrast, at physiological pH 7-7.5 the particles are slightly anionic (Bader 2012). A phase I clinical trial of a Mirna Therapeutic MRX34 (miR-34a mimic encapsulated in NOV340) is underway to evaluate safety and tolerability in liver and hematological malignancies (Clinical Trial #NCT01829971) (Mirna Therapeutics 2015). Following our *in vitro* analysis of miR-34a in GBM, efficacy of miR-34a needs to be evaluated in an *in vivo* intracranial model. In collaboration with a gene therapy lab, we have begun to clone lentiviral vectors from which the pre-miR-34a sequence can be expressed. Similarly, lentiviral vectors with miRNA tough decoys (Xie, Ameres et al. 2012) were generated to inhibit miR-34a. These

will allow us to study miR-34a function within an *in vivo* GBM model as a single agent or in combination with TMZ.

One well known side effect of GSIs is the gastrointestinal (GI) toxicity that arises as a response to Notch inhibition in the crypts of the intestine. Inhibition of Notch drives cells to differentiate into mucin secreting goblet cells (van Es, van Gijn et al. 2005). In this study we demonstrated that miR-34a inhibits Notch-1, Notch-2 and Notch-3 (**Figure 3.11**). We can then hypothesize that systemic delivery of a miR-34a mimic could elicit similar GI toxicity. It has been found that addition of dexamethasone to GSI therapy alleviates GSI-induced GI toxicity (Real, Tosello et al. 2009). However, as of yet, *in vivo* treatment of miR-34a mimics has shown minor to no systemic toxicity (Misso, Di Martino et al. 2014).

Future experiments to determine if miR-34a requires inhibition of Notch signaling to have therapeutic value are needed. In order to answer this question we can utilize a U87MG line retrovirally infected to express constitutively-active NICD-1. MiR-34a mimic or negative control can be transfected in the NICD-1 line and effects on proliferation, cell cycle, senescence, and invasion assessed. If the NICD does not rescue from miR-34a's anti-GBM effects it would lead us to examine another one of its targets, such as EGFR. Similarly, lines expressing constitutively active forms of NICD-2 and NICD-3 can be generated and tested.

Our findings indicate that novel TMZ + GSI treatment upregulates miR-34a. This is in line with what we know about p53, Notch, and miR-34a. P53 regulates expression of miR-34a and Notch downregulates p53 (Purow, Sundaresan et al. 2008). Therefore, the induction of p53 by TMZ and the inhibition of Notch by GSI, would contribute to upregulate miR-34a. We showed that miR-34a decrease expression of Notch-1, Notch-2, and Notch-3.MiR-34a replacement therapy, mediated by Notch downregulation, may provide growth inhibition of tumors by forcing cells into a permanent senescence state.

Ultimate goal: Prevent Recurrence of Tumor

Despite an aggressive treatment schedule, the prognosis for patients remains bleak, as GBM patients undergo tumor recurrence and few live past 5 years post-diagnosis (Stupp, Hegi et al. 2009). Patients are left with limited options consisting of a combination of: further surgical resection, rechallenging with TMZ, or treatment with other agents such as the anti-VEGF antibody, bevacizumab. However, these measures are not curative and patients ultimately succumb to the disease. These approaches fail to target the radiation and chemotherapy resistant population of cells that can self-renew and repopulate the tumor; the CSC hypothesis states that CSCs are that resistant population. This necessitates drug regimens that bypass DNA repair mechanism and eliminate all cells within the initial tumor, including those with self-renewal capability, in an attempt to overcome recurrence.

Both our strategies, treating cells with novel TMZ analogues or overexpressing miR-34a, are effective in our GBM cultures grown as neurospheres (**Figure AI.1 B**). These heterogeneous spheroid cultures are thought to be a model of CSCs as they can self-renew, express stem cell markers, differentiate down multiple lineages, and give rise to GBM tumors following injection into the brain (Singh, Clarke et al. 2003; Varghese, Olstorn et al. 2008; Chen, Nishimura et al. 2010). We did not characterize our cells for stem cells markers or capability to differentiate so we do not claim we are working with a stem cell population but rather a stem-like population. Our established, primary, and TMZ-resistant neurospheres were sensitive to treatment by DP68, and to a less extent DP86 (**Table 2.1**). Similarly, overexpression of miR-34a significantly decreased proliferation of GBM neurospheres (**Figure 3.4 A**). These data are promising as they indicate that both strategies are effective in targeting a stem-like population. Additionally, the cultures did not form secondary spheres and indication that the cells capable of self-renewal have been targeted. DP68 inhibited secondary spheres independent of MGMT expression (**Figure 2.10**). This is significant as primary GBM stem-like cultures ($CD133^{+}$) positive for MGMT have been shown to require 100-fold more TMZ (Beier, Rohrl et al. 2008). Similarly, miR-34a overexpressing neurospheres failed to give rise to secondary spheres after being dissociated and re-plated as single cells (**Figure 3.6**). Together these two approaches provide more durable effects on GBM cultures *in vitro* and these data suggest that both strategies effectively target stem-like cells. *In vivo* applications of both of these strategies are needed to see if the efficacy can be translated into an intracranial tumor model.

Conclusions

The work presented within this dissertation contributes to our understanding of the complexity of resistance in GBMs and explores two novel approaches to generate more effective therapies. Our evaluation of two novel imidazotetrazines, DP86 and DP68, shows that these compounds are highly efficacious in GBMs, independent of MGMT and MMR. The applications of such a drug in the clinic would have a vast impact. While inefficient in their current form, the current study of DP86 and DP68 serves as a proof-of-concept for this novel class of compounds. In our second study, we identified a tumor suppressor miRNA, miR-34a, which mimics the response elicited by our novel TMZ + GSI therapy. Forced expression of miR-34a had a strong anti-tumor effect as several processes were affected: decrease in proliferation, G1 cell cycle arrest, induction of SA-β-gal, and decrease in invasion. While Notch family members were downregulated with increased miR-34a, these strong changes in phenotype are likely to be the result of downregulation of multiple oncogenes at once. MiRNAs ability to regulate multiple genes within a pathway and several pathways at once makes them attractive candidates for therapy in contrast to a targeted therapy approach. These target therapies are usually limited by the emergence of primary or secondary resistance from acquired mutations; miRNA therapy could overcome this obstacle. Together these two strategies provide us with insight into ways to develop more effective chemotherapies with the ultimate goal, preventing recurrences of patients' tumors.

APPENDIX

APPENDIX I

Generation of established line-derived neurospheres and patient-derived cell lines

For our studies, three different GBM culture models were utilized: established monolayer cultures, neurospheres generated from these monolayer cultures, and patient-derived GBM cell lines (**Table AI.1**, **Figure AI.1A**). From a panel of GBM monolayer lines (**Table A.1**, blue), four of the seven established lines gave rise to neurospheres upon serum removal and addition of growth factors. T98G, A172MG, and LN-229 lines did not give rise to spheres under these conditions. This is consistent with results from others (Broadley, Hunn et al. 2011). In contrast, one lab reported the successful growth of T98G and LN-229 as neurospheres by seeding cells in 2% poly (2-hydroxyethyl methacrylate)-coated flasks, which was not attempted here (Hong, Chedid et al. 2012). Also, A172MG have been shown to give rise to spheres but only following lentiviral introduction of Oct-4 and Sox-2 (Dr. John Laterra presentation given at UMASS Medical School, 2012). Neurosphere cultures can be propagated for many passages (>30 passages for U87NS). However, for our studies, we used neurosphere cultures for at most 10 passages post-conversion to minimize changes that result from long-term passaging *in vitro* (Vukicevic, Jauch et al. 2010).

Isolation of GBM cell lines from primary and recurrent patient specimens was also carried out (**Table AI.1**, purple and grey). GBM tumors were obtained following surgical debulking according to IRB protocols. The tumor samples were minced and

subject to enzymatic digestion using Trypsin-EDTA in Hanks Buffered Saline solution:DMEM/F12 mix (1:1). Samples were incubated in a 37° C water bath for 1-3 h. During the incubation period, samples were mechanically dissociated every 10 mins via repeated pipetting. and included mechanical dissociation (via repeated pipetting) every ten minutes. Red blood cells in the samples were then lysed with ammonium chloride solution (Stem Cell Technologies) according to manufacturer's protocol. Finally, cells were pelleted, washed in PBS, and replated in neurosphere growth media.

One patient-derived tumor, 5276T, was isolated by another procedure (Panchision, Chen et al. 2007). Briefly, cells were minced and enzymatically digested with 200 mg/mL Liberase DH (Roche) in 1X Hanks Buffered Saline Solution containing 1 mM $MgCl_2$ and 200 units/mL DNase. Minced tumor in Liberase solution was incubated for 15-30 mins in a rotator oven set to 37° C. Recovery of viable cells from Liberase digested samples was low at incubation times longer than 30 mins. Limiting the digestions to 30 min allowed for better and more consistent results. Red blood cells were lysed before cells were centrifuged at 200 x g for 5 min, and the pellet was re-suspended in 1X HBSS + 1 mM $MgCl_2$ + 200 U/mL DNAse. Cells were triturated with a P1000 pipette tip, pelleted, and replated in neurosphere growth media.

Morphological differences were observed between the various glioma cultures (**Figure AI.1B**). Among the converted neurosphere lines, two grew as free-floating spheres (U87NS and U138NS), one displayed a semi-adherent morphology with small

processes extending from the edges of the spheres (U118NS), and one was predominantly adherent (LN-18NS). The patient-derived lines described in **Table AI.1** were predominantly free-floating spheres with the exception of 4304T. This line did not give rise to neurospheres and instead grew as a monolayer in serum-free conditions.

Many of the tumors efficiently formed xenograft tumors upon engraftment in immunodeficient male Nu/Nu mice (Charles River Labs). U87NS formed tumors following pH dissociation and subcutaneous injection ($1x10^6$/100 uL PBS) into the right flank of mice. Similarly, U87NS gave rise to tumors in an intracranial model. Mice were anesthetized with an IP injection of Ketamine (10 mg/mL)-Xylazine (1.2 mg/mL) at a dose of 0.1 mL/10 g of mouse. U87NS were pH dissociating cells and $5x10^5$/5 μL PBS) cells were injected (rate of 1 μL/min) into the subventricular zone via stereotaxic surgery, using these coordinates from the bregma: lateral +2.3 mm, anterior +0.7 mm, and distal 3.0 mm. Subcutaneous injection of the analgesic Buprenex (0.1 mg/kg) was given immediately after surgery and 4-6 h following. Primary lines 4268T, 4304T, 5075T, and 5276T all engrafted subcutaneously in the flanks of Nu/Nu mice and were further passaged *in vivo*. Cells were allowed to rest for 24 h following enzymatic digest before being centrifuged and resuspended in growth media and Matrigel® Basement Membrane Matrix High Concentration (HC), LDEV-free (1:1) (Corning) subcutaneous injection ($1x10^6$/ 200 μL) into the right flank of mice.

Converted neurospheres had the same MGMT (**Figure AI.2A**) expression patterns as their monolayer counterparts. Growth differences were observed between monolayer and sphere cultures (**Figure AI.2B**) when cell numbers were tracked for several passages. $5x10^5$ cells were plated and split once a week and live cell numbers were quantified via trypan blue exclusion assays. U118NS cultures gave rise to 2.4-fold fewer cells than U118MG while U87NS had the opposite effect, generating 1.4-fold more cells than U87MG. Growth of GBM lines as neurospheres is thought to enrich for a cancer stem cell-like phenotype (A and H 2011) so a slower proliferative state is not surprising. However, U87NS do not follow this prediction. While we did not test for stem cell markers such as Sox2, Oct 4, and Nanog, others found an increase of stem cell markers for U87NS (Broadley, Hunn et al. 2011)(Ledur, Villodre et al. 2012) and LN-18NS (Broadley, Hunn et al. 2011). Cell cycle analysis of U87MG and U87NS was carried out via flow analysis of PI-stained cells (**Figure AI. 2C**) and revealed decreased G1 and S populations for the U87NS line and a marked increase in the G2/M population. This work was further validated by co-staining for Click iT® EdU-Alexa Fluor-488 (Invitrogen) and PI (**Figure AI. 2D**) and analysis via flow cytometry. EdU (5-ethynyl-2'-deoxyuridine) is a modified thymidine analog, just like BrdU, that is incorporated during DNA synthesis. The decrease of G1/S and increase of G2/M increase as U87NS neurospheres are passaged. G1 lengthening is associated with differentiation while NSC exhibit higher G2/M (Roccio, Schmitter et al. 2013). Our findings therefore align with published observations. Further examination of differences in expression of cell cycle

regulators between sphere cultures and their monolayer counterpart would help to elucidate which players are responsible for the differences in cell cycle populations.

Table AI. 1 GBM cell lines: monolayers, neurospheres, and patient-derived cultures.

CELL LINE	Neurosphere formation	MGMT	p53	PTEN	IDH1	EGFR Amplified
Monolayer cultures and derived neurospheres						
U87MG	Yes, U87NS	Negative protein	wild type	-	T.B.D.	-
U118MG	Yes, U118NS	Positive protein	p53 mut	-	T.B.D.	-
U138MG	Yes, U138NS	Positive protein	p53 mut	T.B.D.	T.B.D.	-
LN-18	Yes, LN-18NS	T.B.D.	p53 mut	+	T.B.D.	-
T98G	No	Positive protein	p53 mut	+	T.B.D.	-
A172MG	No	Negative protein	wild type	-	T.B.D.	-
LN-229	No	T.B.D.	p53 mut	+	T.B.D.	-
Patient-derived cultures						
4268T	Yes	Promoter Me -	T.B.D.	T.B.D.	-	-
4304T	No	T.B.D.	T.B.D.	T.B.D.	-	T.B.D.
5075T	Yes	Promoter Me +	T.B.D.	T.B.D.	-	-
5276T	Yes	T.B.D.	T.B.D.	T.B.D.	-	Amplified
2927T2 (recurrent)	Yes	T.B.D.	T.B.D.	T.B.D.	-	T.B.D.

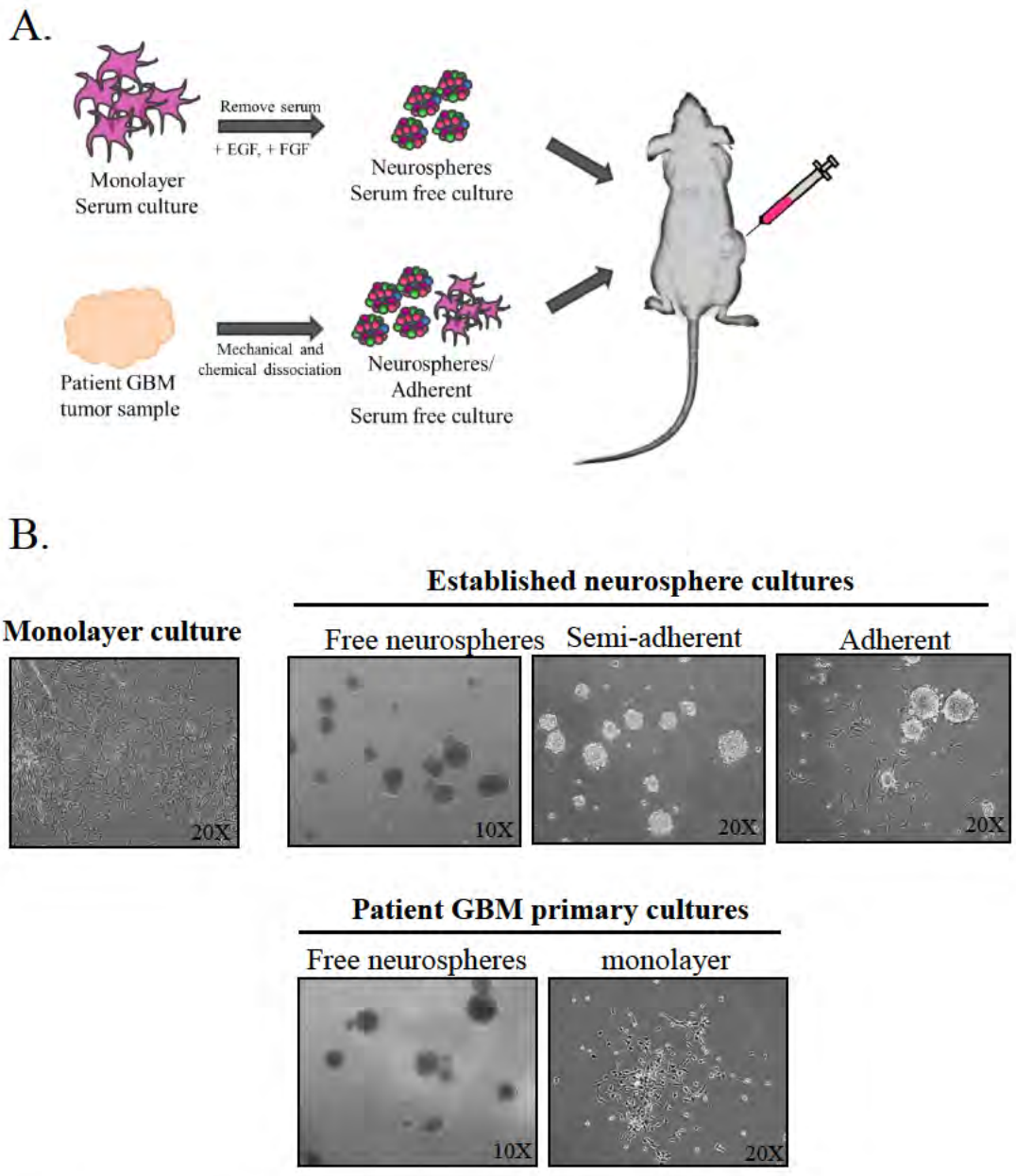

Figure AI.1 GBM cell lines propagated as neurospheres.
Schematic (A) depicting how neurosphere lines were generated, either by growth of established GBM lines in serum-free media or dissociation of primary tumors. Lines were then tested for their ability to propagate *in vivo*. Phase-contrast microscopy (B) of GBM cultures: monolayer, established neurospheres, and primary GBM tumor cultures. Morphological differences can be seen among the cell lines.

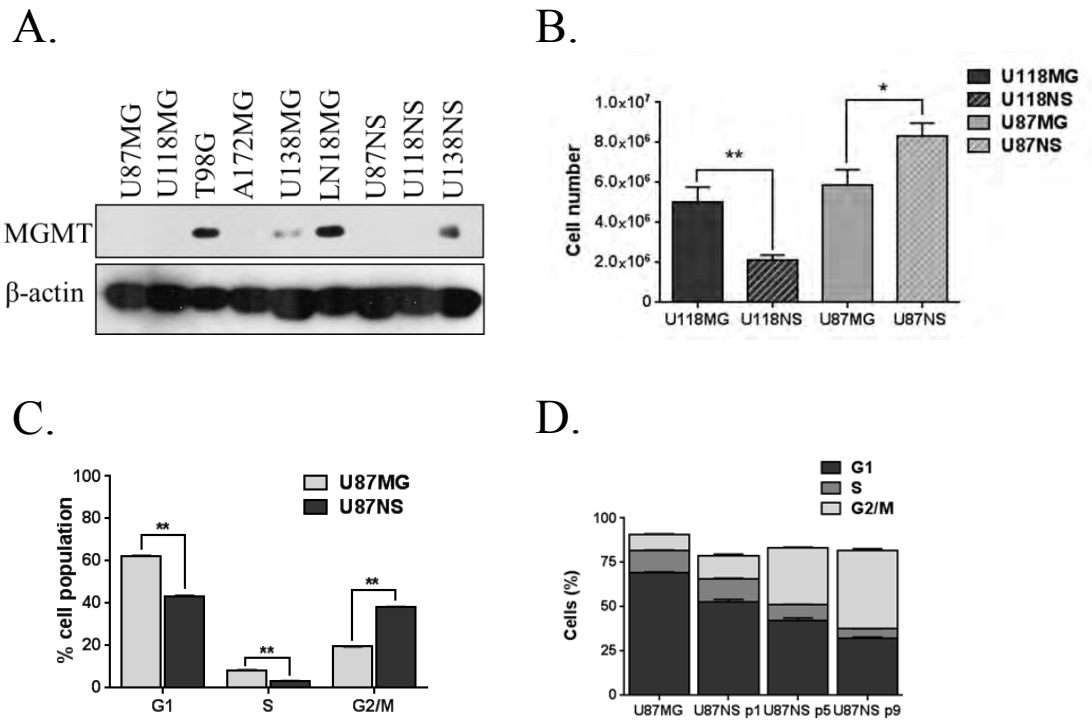

Figure AI.2 Characterization of established GBM neurospheres.
MGMT expression (A) of established and that of neurosphere lines generated show MGMT expression patterns are maintained after conversion to neurospheres in these three cell lines. Cell numbers (B) of monolayer and respective neurosphere cultures were tracked for more than eight passages via trypan blue exclusion assays. U118NS spheres showed reduction in cell numbers while U87NS showed an increase in cell number when compared to their monolayer counterparts. Flow analysis of PI (C) or EdU/PI stained (D) U87NS and U87MG cultures shows that conversion of U87MG to neurospheres leads to reductions of G1- and S-phases while increasing G2/M phase. Data are mean ± SEM of triplicate samples but from one independent experiment *$p<0.05$, **$p<0.001$

APPENDIX II

TMZ + DAPT treatment leads to miR-7 downregulation while miR-29 family expression is slightly upregulated

As part of our goal to identify a miRNA signature that is differentially expressed in TMZ + DAPT treated cultures, we examined miR-7, miR-29a and miR-34a in our initial analysis. MiR-7 is of interest as it is downregulated in senescent WI38 cultures and targets EGFR as well as components of the mTOR and PI3K pathways (Fang, Xue et al. 2012) MiR-29 family members function as tumor suppressors in GBM and, like miR-34a, target Notch family members.

To determine whether miR-7 or miR-29 family members are differentially expressed in TMZ + DAPT treated GBM neurosphere cultures, we carried out qRT-PCR analysis. U87NS and U373NS cells were treated with DMSO, DAPT alone, TMZ alone, or TMZ + DAPT and analyzed by a 21-day neurosphere assay. For these preliminary experiments, cells were plated and treated with drug. RNA was isolated from cells on days 2, 8, 14, and 21 of the assay using the miRVANA miRNA isolation kit (Applied Biosystems). Due to our interest in quantifying microRNAs, small RNA enrichment (<200bp) was carried out according to the manufacturer's protocol. Reverse transcription was performed using TaqMan miRNA Reverse Transcription Kit. Expression levels of mature miR-7a (hsa-miR-7), miR-29a (hsa-miR-29a), miR-29b (hsa-miR-29b), and miR-29c (hsa-miR-29c) were measured by TaqMan MicroRNA Assays (Applied Biosystems),

and U6 small nuclear RNA was used to normalize all samples. Expression levels were quantified on an ABI Prism 7900HT sequence detection system (Applied Biosystems) using TaqMan Universal Master Mix II with Uracil N-glycosylase (UNG). UNG within the master mix is activated prior to starting PCR cycling and works to prevent amplification of contaminants from previous PCR reactions.

MiR-7 expression decreased following treatment with TMZ and TMZ + DAPT with its lowest level on day 8 (**Figure AII.1 A and B**). By day 14, there was a significant rebound for miR-7 levels in both the TMZ and TMZ + DAPT samples; however, cell death was evident in all day 14 neurosphere cultures , introducing variability and limiting the reproducibility of this time point. By day 21, transcript levels of miR-7 increased in the TMZ and TMZ + DAPT treated groups for both U87NS (**Figure AII.1 A**) and U373NS (**Figure AII.1 B**). However, despite this increase, the miR-7 transcript levels were less than those of the DMSO control. It has previously been shown that U87NS and U373NS treated with TMZ (U87NS= 36%; U373NS =33%) or TMZ + DAPT (U87NS= 64%; U373NS= 56%) by day seven have a large induction of SA-β-gal (Gilbert 2011), which is a marker for senescence. For day 21 cultures, SA-β-gal positive cells remained higher for TMZ (U87NS= 11.6%; U373NS= 18.5%) and TMZ + DAPT (U87NS= 79.2%; U373NS= 82.1%) treated neurospheres than the DMSO (U87NS=2.3%; U373NS= 2.3%) or DAPT only (U87NS= 2.6%; U373NS= 2.4%) controls. MicroRNA profiling of senescent human fibroblasts, WI-38, showed that miR-7 is downregulated (Marasa, Srikantan et al. 2010), and inhibition of miR-7 in lung carcinoma cells, A549,

decreased cell growth (Cheng, Byrom et al. 2005) . The decreased levels of miR-7 transcript at day 8 and day 21 could contribute to the induction of senescence in these samples, potentially through a predicted target, Retinoblastoma (Rb). Whether the decrease in miR-7 transcripts contributes to the induction of senescence or senescence leads to its downregulation remains to be tested.

The miR-29 family consists of three mature miRNAs: miR-29a, miR-29b, and miR-29c, and expression levels of all three were analyzed in treated U87NS cells at days 2, 8, and 21 (**Figure AII.2**). MiR-29a, b, and c showed increased transcript levels in TMZ + DAPT treated cultures by day 8, and this elevation was maintained up to day 21, with the exception of the miR-29a transcript, which decreased to control levels. Mir-34a levels were quantified within these same samples, and similar expression patterns were observed. Since both families are predicted to target Notch family members, it is possible that they function within the same network.

Exogenous miR-29a expression decreases proliferation

We analyzed the effects of miR-29a overexpression in U87MG. Cells were plated at 50,000 cells/well (6-well plate) and transfected with a 20 nM miR-29a mimic or a 20 nM negative control with DharmaFect Transfection Reagent 1 (Dharmacon) according to the manufacturer's protocol. At various time-points, cells were collected and counted via trypan blue exclusion. This particular data set is based on a single biological experiment with duplicate wells.

Trypan blue exclusion counts showed that overexpression of miR-29a reduced the proliferation of U87MG cells compared to control transfected cells (**Figure AII.3 A and B**). This preliminary data suggests that miR-29a acts as a tumor suppressor by decreasing growth of GBM cultures.

MiR-29a alters expression of members of Notch and Wnt signaling pathways

In silico analysis using TargetScan, miRanda, and PicTar predicts that miR-29a targets the 3'UTR of Notch-2 and several members of Wnt signaling: Frizzled family receptor 5 (FZD5), low density lipoprotein receptor-related protein 6 (LRP6), catenin beta interacting protein 1 (CTNNBIP1, β-catenin), and glycogen synthase kinase 3-beta (GSK-3β). Following transfection with pre-miR-29a or negative control, we assessed changes in protein levels of some of these genes. U87NS cells were plated and transfected with 5, 10, 20, 30, or 50 nM of pre-miR29a or negative control, as previously described. Cell lysates were collected, separated by SDS-PAGE, and electro-transferred onto 0.45 μM PVDF membranes. Membranes were blocked in TBS + 5% milk and 0.1% Tween-20 at RT for one hour. All primary antibodies were incubated overnight at 4 º C followed by RT incubation with a secondary antibody conjugated with horseradish peroxidase for 1 h. Detection was performed with lab-made chemoluminescent reagent as previously described in Chapter 2. Antibodies against Notch-1 (D6F11, #4380), Notch-2 (D67C8, #4530), LRP6 (C47E12, #3395), and β-actin (8H10D10, #3700) were purchased from Cell Signaling. Anti β-catenin (clone 8E7, #05-665) was from Upstate. Secondary

Anti-rabbit IgG, peroxidase-linked (from donkey) and Anti-mouse IgG peroxidase-linked (from sheep) were purchased from GE Healthcare.

Overexpression of miR-29a in U87NS cells leads to a concentration-dependent decrease in Notch-2 protein (**Figure AII.4 A**). Western blots showed that miR concentrations as low as 10 nM decrease both the full length and intracellular domains of Notch-2. Simultaneously, we tested the effects on another member of the Notch receptor family, Notch-1, which *in silico* analysis does not predict to be a target for miR-29a (**Figure AII.4 B**). While transfection with either 30 nM or 50 nM of pre-miR-29a mimic appears to decrease by 50% expression of Notch-1 in U87NS cells, follow up westerns are needed to validate this observation. Further experiments utilizing a luciferase reporter with the 3'UTR of Notch-1 or Notch-2 cloned are needed to determine whether Notch-2 and Notch-1 are direct or indirect targets.

Changes in Wnt pathway proteins following miR-29a expression were also analyzed for U87NS cultures (**Figure AII.5**). We focused on the co-receptor for Wnt, LRP6, as well as the transcriptional co-activator, β-catenin. Surprisingly, as little as 10 nM of exogenous miR-29a leads to a minor increase of LRP6 and a much greater induction of β-catenin. Studies to examine whether the 3'UTR's of LRP6 and β-catenin respond to miR-29a are needed. The current data provides insight into the potential regulation of Notch-2, LRP6, and β-catenin by miR-29a.

Since these data were generated, a report was published demonstrating that exogenous miR-29a leads to decreased proliferation in esophageal squamous cell carcinoma (Liu, Duan et al. 2015). Changes in Notch1 mRNA and protein levels were not observed following overexpression of miR-29a, validating the lack of Notch1 repression that we observed when overexpressing miR-29a at lower concentrations (**Figure AII. 4B**). The Notch1 downstream target, Hes 1, was upregulated in response to increased miR-29a. Follow-up experiments showed that miR-29a regulates Hes1 through an indirect mechanism, and it is indeed a player in the regulation of Notch signaling.

A.

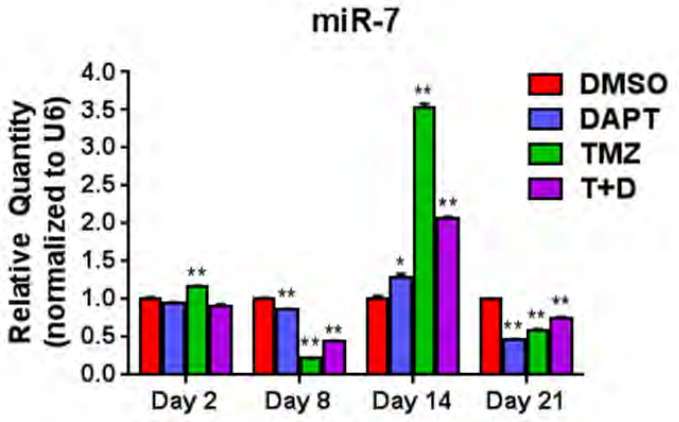

B.

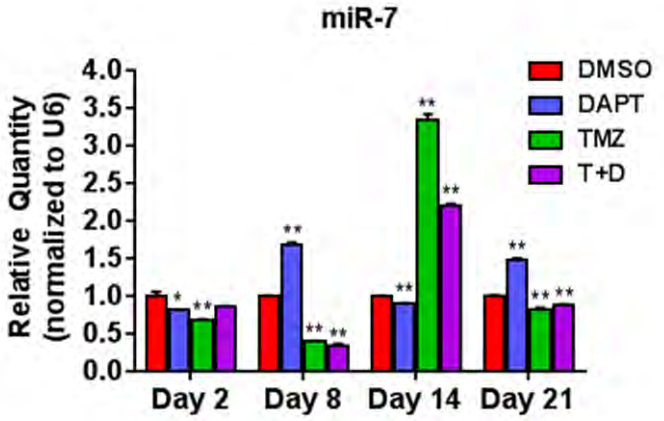

Figure AII.1 Expression of miR-7 transcript is reduced by day 8 in GBM neurospheres in response to TMZ and TMZ + DAPT.
U87NS (A) and U373NS (B) cultures were treated with DMSO, 1 μM DAPT, 200 μM TMZ, or combination of 200 μM TMZ + 1 μM DAPT. RNA was isolated from cells collected at day 2, 8, 14, and 21 and miR-7 transcript levels were quantified by qRT-PCR. Expression levels were normalized to U6, and each sample is plotted relative to the DMSO control. TMZ-only and TMZ + DAPT treatment groups had a decrease in miR-7 expression which correlated with SA-β-gal staining at day 8 and day 21. Representative data, mean ± SEM, from three independent experiments are shown. * $p<0.05$, ** $p<0.001$

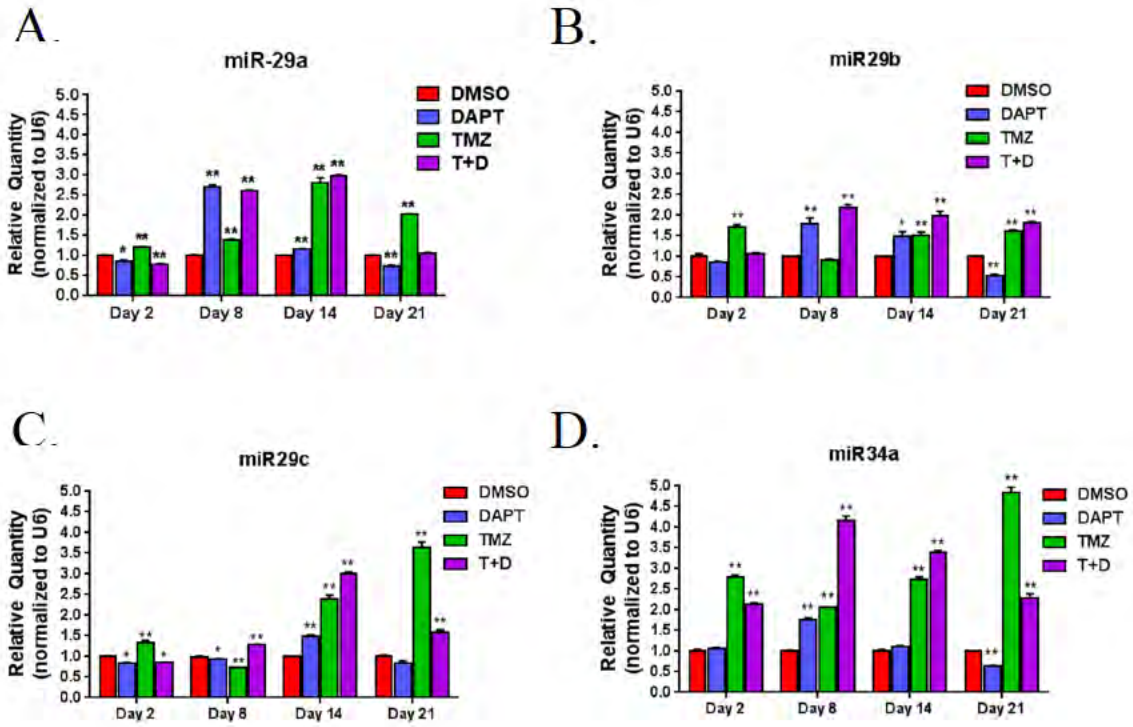

Figure AII.2 TMZ + DAPT leads to an early induction of miR-29 family members. U87NS cultures were treated with DMSO, DAPT, TMZ, or combination of TMZ + DAPT as previously described. RNA was isolated from cells at day 2, 8, and 21, and mature miR-29a (A), miR-29b (B), and miR-29c (C) transcript levels were quantified by qRT-PCR. Expression levels were normalized to U6, and each sample is plotted relative to the DMSO control. MiR-29 family members showed a slight increase in transcript levels following TMZ + DAPT treatment. Changes in expression of miR-29a, miR-29b, and miR-29c showed analogous, but smaller, changes than miR-34a (D) based on the same set of samples. Data are mean ± SEM from one experiment with each sample quantified in triplicate. *$p<0.05$, **$p<0.001$

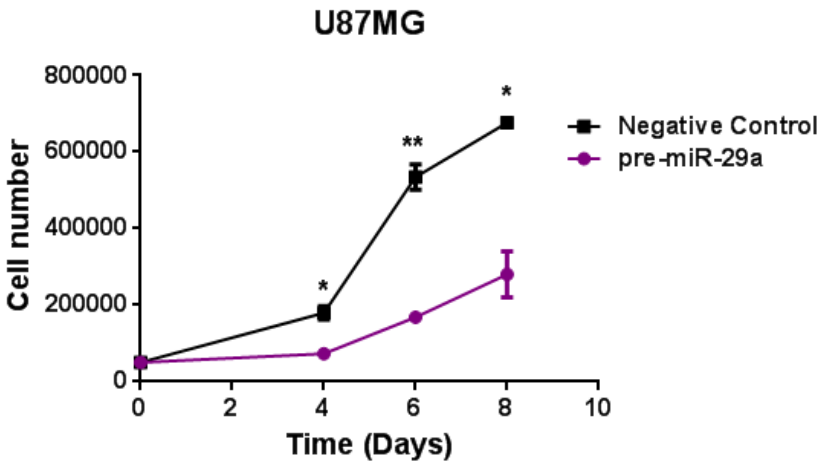

Figure AII.3 Effects of exogenous miR-29a on proliferation of GBM cell lines. Proliferation of U87MG (A) was measured following transfection with 20 nM miR-29a mimic or negative control via trypan blue exclusion assays. Cells overexpressing miR-29a had a significantly decrease in proliferation than control transfected cells. Data are mean ± SEM of one experiment perfomed in duplicate. *$p<0.05$, **$p<0.01$

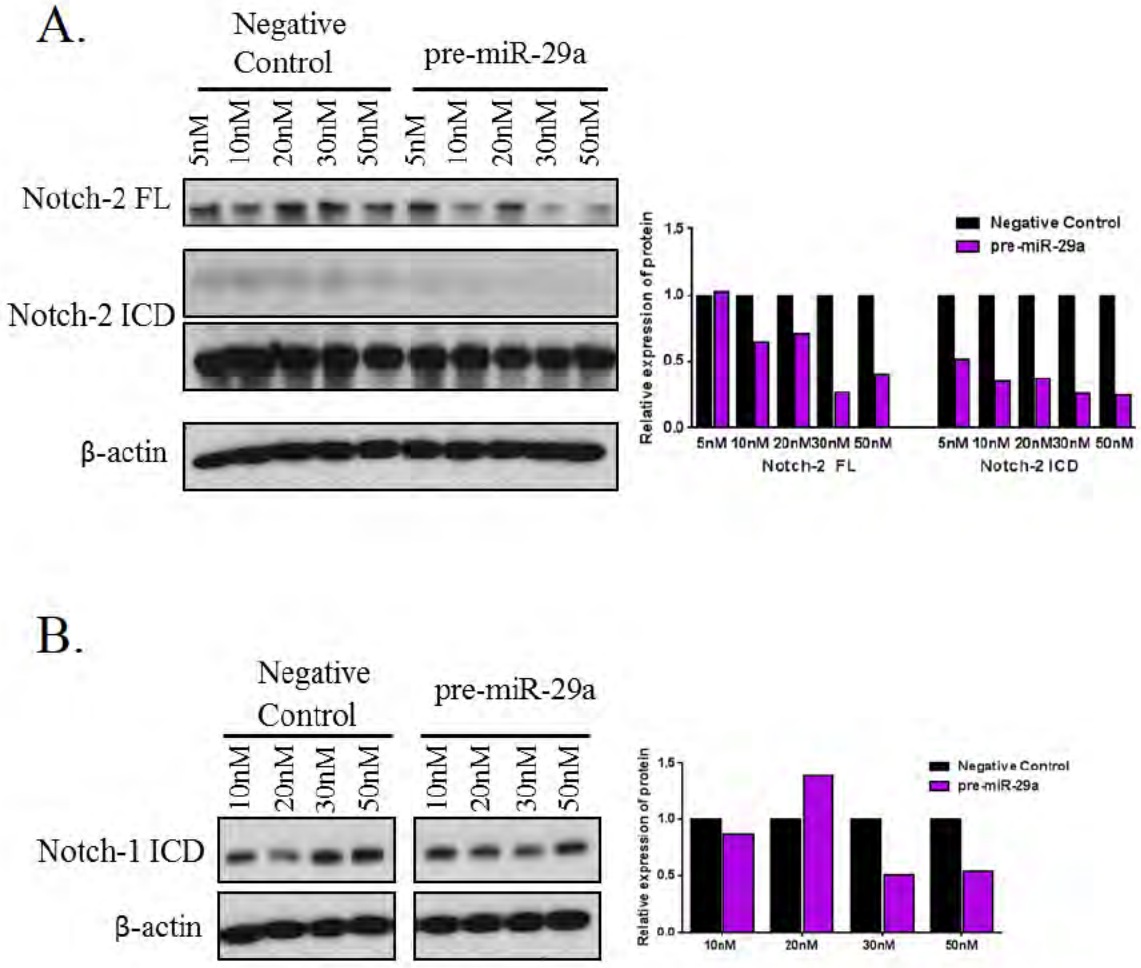

Figure AII.4 Endogenous Notch-2 is repressed by miR-29a.
U87NS cultures were transfected with a various concentrations of pre-miR-29a and matching negative control. Whole cell lysates were were used for western blots to detect Notch-2 (A) or Notch-1 (B). β-actin was used as a loading control in both immunoblots. A histogram shows the average band density normalized to β-actin. MiR-29a overexpression leads to a decrease of both the FL and ICD of Notch-2. Notch-1 levels decrease only with high concentrations of miR-29a.

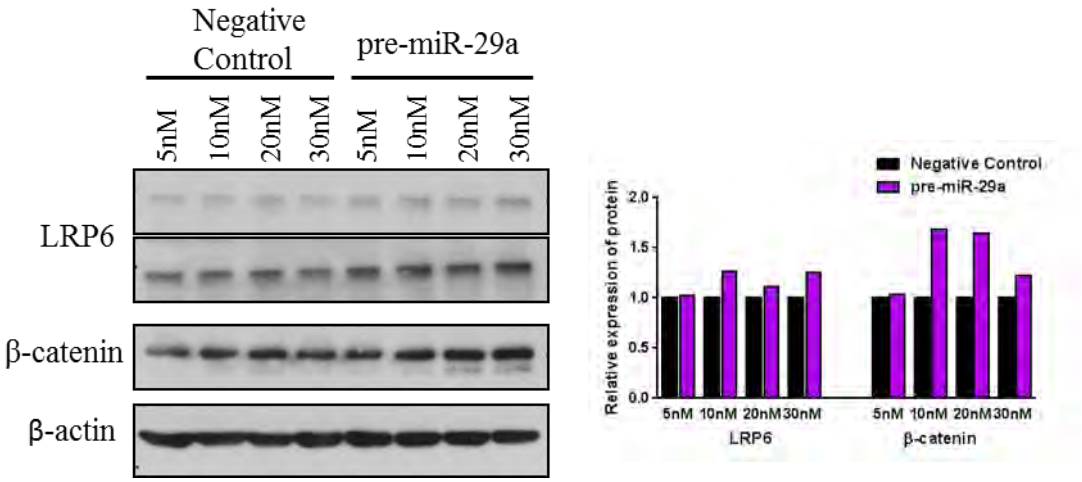

Figure AII.5 MiR-29a overexpression leads to increased Wnt-pathway signaling. U87NS cells were transfected with 5, 10, 20, or 30 nM pre-miR-29a or negative control. Whole cell lysates were collected and analyzed by western blot for expression of Wnt-signaling pathway components, LRP6 and β-catenin. β-actin was used as a loading control. Overexpression of miR-29a lead to the induction β-catenin while causing minimal increase in LRP6 protein expression.

REFERENCES

A, C. and A. H (2011). "Glioma Stem Cells: Cell Culture, Markers and Targets for New Combination Therapies."

Agnihotri, S., A. S. Gajadhar, et al. (2012). "Alkylpurine-DNA-N-glycosylase confers resistance to temozolomide in xenograft models of glioblastoma multiforme and is associated with poor survival in patients." J Clin Invest **122**(1): 253-66.

Ahmad, I., R. Patel, et al. (2011). "HER2 overcomes PTEN (loss)-induced senescence to cause aggressive prostate cancer." Proceedings of the National Academy of Sciences of the United States of America **108**(39): 16392-7.

Ahmed, R., M. J. Oborski, et al. (2014). "Malignant gliomas: current perspectives in diagnosis, treatment, and early response assessment using advanced quantitative imaging methods." Cancer Manag Res **6**: 149-70.

Altaner, C. (2008). "Glioblastoma and stem cells." Neoplasma **55**(5).

Alvarez-Garcia, I. and E. A. Miska (2005). "MicroRNA functions in animal development and human disease." Development **132**(21): 4653-62.

Andersen, T. B., C. Q. Lopez, et al. (2015). "Thapsigargin--from Thapsia L. to mipsagargin." Molecules **20**(4): 6113-27.

Andreassen, P. R., A. D. D'Andrea, et al. (2004). "ATR couples FANCD2 monoubiquitination to the DNA-damage response." Genes Dev **18**(16): 1958-63.

Antoniou, A., A. Hebrant, et al. (2013). "Cancer stem cells, a fuzzy evolving concept: a cell population or a cell property?" Cell Cycle **12**(24): 3743-8.

Bader, A. G. (2012). "miR-34 - a microRNA replacement therapy is headed to the clinic." Front Genet **3**: 120.

Bao, S., Q. Wu, et al. (2006). "Glioma stem cells promote radioresistance by preferential activation of the DNA damage response." Nature **444**(7120): 756-60.

Bartel, D. P. (2004). "MicroRNAs: genomics, biogenesis, mechanism, and function." Cell **116**(2): 281-97.

Barvaux, V. A., M. Ranson, et al. (2004). "Dual repair modulation reverses Temozolomide resistance in vitro." Mol Cancer Ther **3**(2): 123-7.

Beier, D., S. Rohrl, et al. (2008). "Temozolomide preferentially depletes cancer stem cells in glioblastoma." Cancer Res **68**(14): 5706-15.

Ben-Shushan, D., E. Markovsky, et al. (2014). "Overcoming obstacles in microRNA delivery towards improved cancer therapy." Drug Deliv Transl Res **4**(1): 38-49.

Bidlingmaier, S., X. Zhu, et al. (2008). "The utility and limitations of glycosylated human CD133 epitopes in defining cancer stem cells." J Mol Med **86**(9): 1025-32.

Bleasdale, C., B. T. Golding, et al. (1991). "The mechanism of decomposition of *N*-methyl-*N*-nitrosourea in aqueous solution according to ^{13}C and ^{15}N NMR studies: quantitative fragmentaion to cyanate." J. Chem. Soc., Chem. Commun.: 1726-1728.

Blower, P. E., J. H. Chung, et al. (2008). "MicroRNAs modulate the chemosensitivity of tumor cells." Mol Cancer Ther **7**(1): 1-9.

Bommer, G. T., I. Gerin, et al. (2007). "p53-mediated activation of miRNA34 candidate tumor-suppressor genes." Curr Biol **17**(15): 1298-307.

Bouwman, P., A. Aly, et al. (2010). "53BP1 loss rescues BRCA1 deficiency and is associated with triple-negative and BRCA-mutated breast cancers." Nat Struct Mol Biol **17**(6): 688-95.

Bray, S. J. (2006). "Notch signalling: a simple pathway becomes complex." Nat Rev Mol Cell Biol **7**(9): 678-89.

Brennan, C. W., R. G. Verhaak, et al. (2013). "The somatic genomic landscape of glioblastoma." Cell **155**(2): 462-77.

Broadley, K. W., M. K. Hunn, et al. (2011). "Side Population is Not Necessary or Sufficient for a Cancer Stem Cell Phenotype in Glioblastoma Multiforme." Stem Cells **29**(3): 452-61.

Bu, P., K. Y. Chen, et al. (2013). "A microRNA miR-34a-regulated bimodal switch targets Notch in colon cancer stem cells." Cell Stem Cell **12**(5): 602-15.

Cahill, D. P., K. K. Levine, et al. (2007). "Loss of the mismatch repair protein MSH6 in human glioblastomas is associated with tumor progression during temozolomide treatment." Clin Cancer Res **13**(7): 2038-45.

Cai, S., H. Wang, et al. (2011). "Humanized bone marrow mouse model as a preclinical tool to assess therapy-mediated hematotoxicity." Clin Cancer Res **17**(8): 2195-206.

Cancer Genome Atlas Research, N. (2008). "Comprehensive genomic characterization defines human glioblastoma genes and core pathways." Nature **455**(7216): 1061-8.

Chaddah, R., M. Arntfield, et al. (2012). "Clonal neural stem cells from human embryonic stem cell colonies." J Neurosci **32**(23): 7771-81.

Chan, J. A., A. M. Krichevsky, et al. (2005). "MicroRNA-21 is an antiapoptotic factor in human glioblastoma cells." Cancer Res **65**(14): 6029-33.

Chandramohan, V., X. Bao, et al. (2013). "Construction of an immunotoxin, D2C7-(scdsFv)-PE38KDEL, targeting EGFRwt and EGFRvIII for brain tumor therapy." Clin Cancer Res **19**(17): 4717-27.

Chang, T. C., E. A. Wentzel, et al. (2007). "Transactivation of miR-34a by p53 broadly influences gene expression and promotes apoptosis." Mol Cell **26**(5): 745-52.

Chao, T. F., H. H. Xiong, et al. (2013). "MiR-21 mediates the radiation resistance of glioblastoma cells by regulating PDCD4 and hMSH2." J Huazhong Univ Sci Technolog Med Sci **33**(4): 525-9.

Chen, C. C., T. Taniguchi, et al. (2007). "The Fanconi anemia (FA) pathway confers glioma resistance to DNA alkylating agents." J Mol Med (Berl) **85**(5): 497-509.

Chen, C. Z. (2005). "MicroRNAs as oncogenes and tumor suppressors." N Engl J Med **353**(17): 1768-71.

Chen, J., Y. Li, et al. (2012). "A restricted cell population propagates glioblastoma growth after chemotherapy." Nature **488**(7412): 522-6.

Chen, J., R. M. McKay, et al. (2012). "Malignant glioma: lessons from genomics, mouse models, and stem cells." Cell **149**(1): 36-47.

Chen, Q., P. C. Van der Sluis, et al. (2005). "The FA/BRCA pathway is involved in melphalan-induced DNA interstrand cross-link repair and accounts for melphalan resistance in multiple myeloma cells." Blood **106**(2): 698-705.

Chen, Q. R., L. R. Yu, et al. (2011). "Systematic proteome analysis identifies transcription factor YY1 as a direct target of miR-34a." J Proteome Res **10**(2): 479-87.

Chen, R., M. C. Nishimura, et al. (2010). "A hierarchy of self-renewing tumor-initiating cell types in glioblastoma." Cancer Cell **17**(4): 362-75.

Cheng, A. M., M. W. Byrom, et al. (2005). "Antisense inhibition of human miRNAs and indications for an involvement of miRNA in cell growth and apoptosis." Nucleic Acids Res **33**(4): 1290-7.

Christensen, K., H. D. Schroder, et al. (2008). "CD133 identifies perivascular niches in grade II-IV astrocytomas." J Neurooncol **90**(2): 157-70.

Christoffersen, N. R., R. Shalgi, et al. (2010). "p53-independent upregulation of miR-34a during oncogene-induced senescence represses MYC." Cell Death Differ **17**(2): 236-45.

Clarke, E., C. Pereira, et al. (2007). "Toxicity testing using hematopoietic stem cell assays." Regen Med **2**(6): 947-56.

Clemons, M., J. Kelly, et al. (2005). "O6-(4-bromothenyl)guanine reverses temozolomide resistance in human breast tumour MCF-7 cells and xenografts." Br J Cancer **93**(10): 1152-6.

Cole, K. A., E. F. Attiyeh, et al. (2008). "A functional screen identifies miR-34a as a candidate neuroblastoma tumor suppressor gene." Mol Cancer Res **6**(5): 735-42.

Collins, A. R., A. A. Oscoz, et al. (2008). "The comet assay: topical issues." Mutagenesis **23**(3): 143-51.

Costa, P. M., A. L. Cardoso, et al. (2013). "MicroRNA-21 silencing enhances the cytotoxic effect of the antiangiogenic drug sunitinib in glioblastoma." Hum Mol Genet **22**(5): 904-18.

Costa, P. M. and M. C. Pedroso de Lima (2013). "MicroRNAs as Molecular Targets for Cancer Therapy: On the Modulation of MicroRNA Expression." Pharmaceuticals (Basel) **6**(10): 1195-220.

Dalmay, T. and D. R. Edwards (2006). "MicroRNAs and the hallmarks of cancer." Oncogene **25**(46): 6170-5.

Dang, L., D. W. White, et al. (2009). "Cancer-associated IDH1 mutations produce 2-hydroxyglutarate." Nature **462**(7274): 739-44.

Daniels, D. S., C. D. Mol, et al. (2000). "Active and alkylated human AGT structures: a novel zinc site, inhibitor and extrahelical base binding." The EMBO journal **19**(7): 1719-30.

de Antonellis, P., C. Medaglia, et al. (2011). "MiR-34a targeting of Notch ligand delta-like 1 impairs CD15+/CD133+ tumor-propagating cells and supports neural differentiation in medulloblastoma." PLoS One **6**(9): e24584.

Deans, A. J. and S. C. West (2011). "DNA interstrand crosslink repair and cancer." Nat Rev Cancer **11**(7): 467-80.

Del Valle, E. M. M. (2004). "Cyclodextrins and their uses: a review." Process Biochemistry **39**(9): 1033-1046.

Denny, B. J., R. T. Wheelhouse, et al. (1994). "NMR and molecular modeling investigation of the mechanism of activation of the antitumor drug temozolomide and its interaction with DNA." Biochemistry **33**(31): 9045-51.

Di Leva, G., M. Garofalo, et al. (2014). "MicroRNAs in cancer." Annu Rev Pathol **9**: 287-314.

Du, R., W. Sun, et al. (2012). "Hypoxia-induced down-regulation of microRNA-34a promotes EMT by targeting the Notch signaling pathway in tubular epithelial cells." PLoS One **7**(2): e30771.

DURECT. (2015). "Alzet Osmotic Pumps." from www.alzet.com.

Dy, G. K., J. P. Thomas, et al. (2005). "A phase I and pharmacologic trial of two schedules of the proteasome inhibitor, PS-341 (bortezomib, velcade), in patients with advanced cancer." Clin Cancer Res **11**(9): 3410-6.

Eckert, A., M. Kloor, et al. (2007). "Microsatellite instability in pediatric and adult high-grade gliomas." Brain Pathol **17**(2): 146-50.

Fan TY, W. H., Xiang P, Liu YW, Li HZ, Lei BX, Yu M, Qi ST. (2014). "Inhibition of EZH2 reverses chemotherapeutic drug TMZ chemosensitivity in GBM." Int J Clin Exp Pathol **7**(10): 6662-70.

Fang, Y., J. L. Xue, et al. (2012). "MicroRNA-7 inhibits tumor growth and metastasis by targeting the phosphoinositide 3-kinase/Akt pathway in hepatocellular carcinoma." Hepatology **55**(6): 1852-62.

Felsberg, J., N. Thon, et al. (2011). "Promoter methylation and expression of MGMT and the DNA mismatch repair genes MLH1, MSH2, MSH6 and PMS2 in paired primary and recurrent glioblastomas." Int J Cancer **129**(3): 659-70.

Fink, D., S. Aebi, et al. (1998). "The role of DNA mismatch repair in drug resistance." Clin Cancer Res **4**(1): 1-6.

Fleming, A. B. and W. M. Saltzman (2002). "Pharmacokinetics of the carmustine implant." Clin Pharmacokinet **41**(6): 403-19.

Friedman, R. C., K. K. Farh, et al. (2009). "Most mammalian mRNAs are conserved targets of microRNAs." Genome Res **19**(1): 92-105.

Fu, D., J. A. Calvo, et al. (2012). "Balancing repair and tolerance of DNA damage caused by alkylating agents." Nat Rev Cancer **12**(2): 104-20.

Fung, L. K., M. G. Ewend, et al. (1998). "Pharmacokinetics of interstitial delivery of carmustine, 4-hydroperoxycyclophosphamide, and paclitaxel from a biodegradable polymer implant in the monkey brain." Cancer Res **58**(4): 672-84.

Gan, H. K., A. H. Kaye, et al. (2009). "The EGFRvIII variant in glioblastoma multiforme." J Clin Neurosci **16**(6): 748-54.

Garelnabi, E. A., D. Pletsas, et al. (2012). "Strategy for Imidazotetrazine Prodrugs with Anticancer Activity Independent of MGMT and MMR." ACS Med Chem Lett **3**(12): 965-8.

Garelnabi, E. A. E., D. Pletsas, et al. (2012). "Strategy for imidazotetrazine prodrugs with anticancer activity independent of MGMT and MMR." ACS Med. Chem. Lett. **3**(12): 965-968.

Gerson, S. L. (2002). "Clinical relevance of MGMT in the treatment of cancer." J Clin Oncol **20**(9): 2388-99.

Ghosal, G. and J. Chen (2013). "DNA damage tolerance: a double-edged sword guarding the genome." Transl Cancer Res **2**: 107-129.

Giannini, C., J. N. Sarkaria, et al. (2005). "Patient tumor EGFR and PDGFRA gene amplifications retained in an invasive intracranial xenograft model of glioblastoma multiforme." Neuro Oncol **7**(2): 164-76.

Gilbert, C. A. (2011). Blocking the Notch Pathway with Gamma-Secretase Inhibitors Enhances Temozolomide Treatment of Gliomas through Therapy-Induced Senescence: A Dissertation. Graduate School of Biomedical Sciences. GSBS Dissertations and Theses, University of Massachusetts Medical School.

Gilbert, C. A., M. C. Daou, et al. (2010). "Gamma-secretase inhibitors enhance temozolomide treatment of human gliomas by inhibiting neurosphere repopulation and xenograft recurrence." Cancer Res **70**(17): 6870-9.

Giunti, L., M. da Ros, et al. (2015). "Anti-miR21 oligonucleotide enhances chemosensitivity of T98G cell line to doxorubicin by inducing apoptosis." Am J Cancer Res **5**(1): 231-42.

Gong, X., P. H. Schwartz, et al. (2011). "Neural stem/progenitors and glioma stem-like cells have differential sensitivity to chemotherapy." Neurology **76**(13): 1126-34.

Griffiths-Jones, S. (2014). miRBase: the microRNA database. **21**.

Grossman, S. A., C. Reinhard, et al. (1992). "The intracerebral distribution of BCNU delivered by surgically implanted biodegradable polymers." J Neurosurg **76**(4): 640-7.

Grossman, S. A., X. Ye, et al. (2011). "Immunosuppression in patients with high-grade gliomas treated with radiation and temozolomide." Clinical cancer research : an official journal of the American Association for Cancer Research **17**(16): 5473-80.

Guessous, F., Y. Zhang, et al. (2010). "microRNA-34a is tumor suppressive in brain tumors and glioma stem cells." Cell Cycle.

Gynther, M., K. Laine, et al. (2008). "Large neutral amino acid transporter enables brain drug delivery via prodrugs." J Med Chem **51**(4): 932-6.

Happold, C., P. Roth, et al. (2012). "Distinct molecular mechanisms of acquired resistance to temozolomide in glioblastoma cells." J Neurochem **122**(2): 444-55.

He, L., X. He, et al. (2007). "A microRNA component of the p53 tumour suppressor network." Nature **447**(7148): 1130-4.

Hegi, M. E., A. C. Diserens, et al. (2004). "Clinical trial substantiates the predictive value of O-6-methylguanine-DNA methyltransferase promoter methylation in glioblastoma patients treated with temozolomide." Clin Cancer Res **10**(6): 1871-4.

Hermisson, M., A. Klumpp, et al. (2006). "O^6-methylguanine DNA methyltransferase and p53 status predict temozolomide sensitivity in human malignant glioma cells." J Neurochem **96**(3): 766-76.

Hiddingh, L., R. S. Raktoe, et al. (2014). "Identification of temozolomide resistance factors in glioblastoma via integrative miRNA/mRNA regulatory network analysis." Sci Rep **4**: 5260.

Higgins, D. M., R. Wang, et al. (2013). "Brain tumor stem cell multipotency correlates with nanog expression and extent of passaging in human glioblastoma xenografts." Oncotarget **4**(5): 792-801.

Hong, X., K. Chedid, et al. (2012). "Glioblastoma cell line-derived spheres in serumcontaining medium versus serum-free medium: a comparison of cancer stem cell properties." Int J Oncol **41**(5): 1693-700.

Hu, H., L. Du, et al. (2010). "ATM is down-regulated by N-Myc-regulated microRNA-421." Proc Natl Acad Sci U S A **107**(4): 1506-11.

Hulleman, E., M. Quarto, et al. (2009). "A role for the transcription factor HEY1 in glioblastoma." J Cell Mol Med **13**(1): 136-46.

Hurlbut, G. D., M. W. Kankel, et al. (2007). "Crossing paths with Notch in the hyper-network." Curr Opin Cell Biol **19**(2): 166-75.

Iacopino, F., C. Angelucci, et al. (2014). "Isolation of cancer stem cells from three human glioblastoma cell lines: characterization of two selected clones." PLoS One **9**(8): e105166.

Ichimura, K., A. P. Vogazianou, et al. (2008). "1p36 is a preferential target of chromosome 1 deletions in astrocytic tumours and homozygously deleted in a subset of glioblastomas." Oncogene **27**(14): 2097-108.

Institute, N. C. (2015). "RO4929097, Temozolomide, and Radiation Therapy in Treating Patients With Newly Diagnosed Malignant Glioma." NCT01119599 https://www.clinicaltrials.gov/ct2/show/NCT01119599?term=Clinical+trial+%23+NCT01119599&rank=1.

Institute, N. C. (2015). "SEER Stat Fact Sheets: Brain and Other Nervous System Cancer." from http://seer.cancer.gov/statfacts/html/brain.html.

Ivanovska, I., A. S. Ball, et al. (2008). "MicroRNAs in the miR-106b family regulate p21/CDKN1A and promote cell cycle progression." Mol Cell Biol **28**(7): 2167-74.

Jaksch, M., J. Munera, et al. (2008). "Cell cycle-dependent variation of a CD133 epitope in human embryonic stem cell, colon cancer, and melanoma cell lines." Cancer Res **68**(19): 7882-6.

Johnson, B. E., T. Mazor, et al. (2014). "Mutational analysis reveals the origin and therapy-driven evolution of recurrent glioma." Science **343**(6167): 189-93.

Kang, J., E. Kim, et al. (2013). "Rhamnetin and cirsiliol induce radiosensitization and inhibition of epithelial-mesenchymal transition (EMT) by miR-34a-mediated suppression of Notch-1 expression in non-small cell lung cancer cell lines." J Biol Chem **288**(38): 27343-57.

Kanzawa, T., J. Bedwell, et al. (2003). "Inhibition of DNA repair for sensitizing resistant glioma cells to temozolomide." J Neurosurg **99**(6): 1047-52.

Kao, W. H., A. I. Riker, et al. (2011). "Upregulation of Fanconi anemia DNA repair genes in melanoma compared with non-melanoma skin cancer." J Invest Dermatol **131**(10): 2139-42.

Kato, T., A. Natsume, et al. (2010). "Efficient delivery of liposome-mediated MGMT-siRNA reinforces the cytotoxity of temozolomide in GBM-initiating cells." Gene Therapy **17**(11): 1363-71.

Kee, Y. and A. D. D'Andrea (2010). "Expanded roles of the Fanconi anemia pathway in preserving genomic stability." Genes Dev **24**(16): 1680-94.

Kefas, B., L. Comeau, et al. (2009). "The neuronal microRNA miR-326 acts in a feedback loop with notch and has therapeutic potential against brain tumors." J Neurosci **29**(48): 15161-8.

Kent, O. A. and J. T. Mendell (2006). "A small piece in the cancer puzzle: microRNAs as tumor suppressors and oncogenes." Oncogene **25**(46): 6188-96.

Kim, S. H., K. Joshi, et al. (2015). "EZH2 protects glioma stem cells from radiation-induced cell death in a MELK/FOXM1-dependent manner." Stem Cell Reports **4**(2): 226-38.

Kimelberg, H. K. and M. Nedergaard (2010). "Functions of astrocytes and their potential as therapeutic targets." Neurotherapeutics **7**(4): 338-53.

Kitange, G. J., B. L. Carlson, et al. (2009). "Evaluation of MGMT promoter methylation status and correlation with temozolomide response in orthotopic glioblastoma xenograft model." J Neurooncol **92**(1): 23-31.

Kitange, G. J., A. C. Mladek, et al. (2012). "Inhibition of histone deacetylation potentiates the evolution of acquired temozolomide resistance linked to MGMT upregulation in glioblastoma xenografts." Clin Cancer Res **18**(15): 4070-9.

Kleinberg, L. R., J. Weingart, et al. (2004). "Clinical course and pathologic findings after Gliadel and radiotherapy for newly diagnosed malignant glioma: implications for patient management." Cancer Invest **22**(1): 1-9.

Kondo, N., A. Takahashi, et al. (2011). "FANCD1/BRCA2 plays predominant role in the repair of DNA damage induced by ACNU or TMZ." PLoS One **6**(5): e19659.

Kondo, N., A. Takahashi, et al. (2010). "DNA damage induced by alkylating agents and repair pathways." J Nucleic Acids **2010**: 543531.

Krek, A., D. Grun, et al. (2005). "Combinatorial microRNA target predictions." Nat Genet **37**(5): 495-500.

Kreso, A., C. A. O'Brien, et al. (2013). "Variable clonal repopulation dynamics influence chemotherapy response in colorectal cancer." Science **339**(6119): 543-8.

Kreth, S., J. Heyn, et al. (2010). "Identification of valid endogenous control genes for determining gene expression in human glioma." Neuro Oncol **12**(6): 570-9.

Kumar, M. S., J. Lu, et al. (2007). "Impaired microRNA processing enhances cellular transformation and tumorigenesis." Nat Genet **39**(5): 673-7.

Lagos-Quintana, M., R. Rauhut, et al. (2001). "Identification of novel genes coding for small expressed RNAs." Science **294**(5543): 853-8.

Lal, A., M. P. Thomas, et al. (2011). "Capture of microRNA-bound mRNAs identifies the tumor suppressor miR-34a as a regulator of growth factor signaling." PLoS Genet **7**(11): e1002363.

Lalezari, S., A. P. Chou, et al. (2013). "Combined analysis of O6-methylguanine-DNA methyltransferase protein expression and promoter methylation provides optimized prognostication of glioblastoma outcome." Neuro Oncol **15**(3): 370-81.

Lau, N. C., L. P. Lim, et al. (2001). "An abundant class of tiny RNAs with probable regulatory roles in *Caenorhabditis elegans*." Science **294**(5543): 858-62.

Ledur, P. F., E. S. Villodre, et al. (2012). "Extracellular ATP reduces tumor sphere growth and cancer stem cell population in glioblastoma cells." Purinergic Signal **8**(1): 39-48.

Lee, R., P. Kermani, et al. (2001). "Regulation of cell survival by secreted proneurotrophins." Science **294**(5548): 1945-8.

Lee, R. C., R. L. Feinbaum, et al. (1993). "The C. elegans heterochronic gene lin-4 encodes small RNAs with antisense complementarity to lin-14." Cell **75**(5): 843-54.

Lewis, B. P., C. B. Burge, et al. (2005). "Conserved seed pairing, often flanked by adenosines, indicates that thousands of human genes are microRNA targets." Cell **120**(1): 15-20.

Li, A., J. Walling, et al. (2009). "Unsupervised analysis of transcriptomic profiles reveals six glioma subtypes." Cancer Res **69**(5): 2091-9.

Li, H., G. Yu, et al. (2014). "Cisplatin-induced epigenetic activation of miR-34a sensitizes bladder cancer cells to chemotherapy." Mol Cancer **13**: 8.

Li, N., H. Fu, et al. (2009). "miR-34a inhibits migration and invasion by down-regulation of c-Met expression in human hepatocellular carcinoma cells." Cancer Lett **275**(1): 44-53.

Li, X. J., Z. J. Ren, et al. (2014). "MicroRNA-34a: a potential therapeutic target in human cancer." Cell Death Dis **5**: e1327.

Li, Y., F. Guessous, et al. (2009). "MicroRNA-34a inhibits glioblastoma growth by targeting multiple oncogenes." Cancer Res **69**(19): 7569-76.

Li, Z., W. S. Branham, et al. (2010). "Genomic analysis of microRNA time-course expression in liver of mice treated with genotoxic carcinogen N-ethyl-N-nitrosourea." BMC Genomics **11**: 609.

Lino, M. M., A. Merlo, et al. (2010). "Notch signaling in glioblastoma: a developmental drug target?" BMC Med **8**: 72.

Liu, C., P. Duan, et al. (2015). "miR-29a activates Hes1 by targeting Nfia in esophageal carcinoma cell line TE-1." Oncol Lett **9**(1): 96-102.

Liu, G., X. Yuan, et al. (2006). "Analysis of gene expression and chemoresistance of CD133+ cancer stem cells in glioblastoma." Mol Cancer **5**: 67.

Lodygin, D., V. Tarasov, et al. (2014). "Inactivation of miR-34a by aberrant CpG methylation in multiple types of cancer." Cell Cycle **7**(16): 2591-2600.

Louis, D. N., H. Ohgaki, et al. (2007). "The 2007 WHO classification of tumours of the central nervous system." Acta Neuropathol **114**(2): 97-109.

Lown, J. W. and S. M. Chauhan (1981). "Mechanism of action of (2-haloethyl)nitrosoureas on DNA. Isolation and reactions of postulated 2-(alkylimino)-3-nitrosooxazolidine intermediates in the decomposition of 1,3-bis(2-chloroethyl)-, 1-(2-chloroethyl)-3-cyclohexyl-, and 1-(2-chloroethyl)-3-(4'-trans-methylcyclohexyl)-1-nitrosourea." J Med Chem **24**(3): 270-9.

Lown, J. W. and S. M. S. Chauhan (1982). "Discrimination between alternative pathways of aqueous decomposition of anti-tumor (2-chloroethyl) nitrosoureas using specific O-18 labeling." J Org Chem **47**: 851-856.

Lu, J., G. Getz, et al. (2005). "MicroRNA expression profiles classify human cancers." Nature **435**(7043): 834-8.

Luan, S., L. Sun, et al. (2010). "MicroRNA-34a: a novel tumor suppressor in p53-mutant glioma cell line U251." Arch Med Res **41**(2): 67-74.

Lyakhovich, A. and J. Surralles (2007). "FANCD2 depletion sensitizes cancer cells repopulation ability in vitro." Cancer Lett **256**(2): 186-95.

Ma, Y., A. Creanga, et al. (2006). "Prevalence of off-target effects in Drosophila RNA interference screens." Nature **443**(7109): 359-63.

Marasa, B. S., S. Srikantan, et al. (2010). "MicroRNA profiling in human diploid fibroblasts uncovers miR-519 role in replicative senescence." Aging (Albany NY) **2**(6): 333-43.

Martinez, I., D. Cazalla, et al. (2011). "miR-29 and miR-30 regulate B-Myb expression during cellular senescence." Proc Natl Acad Sci U S A **108**(2): 522-7.

Martinez, R., H. K. Schackert, et al. (2005). "Low-level microsatellite instability phenotype in sporadic glioblastoma multiforme." J Cancer Res Clin Oncol **131**(2): 87-93.

Matthews, J. A., A. Batki, et al. (1985). "Enhanced chemiluminescent method for the detection of DNA dot-hybridization assays." Anal. Biochem. **151**: 205-209.

Maxwell, J. A., S. P. Johnson, et al. (2008). "Mismatch repair deficiency does not mediate clinical resistance to temozolomide in malignant glioma." Clin Cancer Res **14**(15): 4859-68.

Mazor, T., A. Pankov, et al. (2015). "DNA Methylation and Somatic Mutations Converge on the Cell Cycle and Define Similar Evolutionary Histories in Brain Tumors." Cancer Cell **28**(3): 307-17.

McFaline-Figueroa, J. L., C. J. Braun, et al. (2015). "Minor Changes in Expression of the Mismatch Repair Protein MSH2 Exert a Major Impact on Glioblastoma Response to Temozolomide." Cancer Res.

McGarrity, J. F. and T. Smyth (1980). "Hydrolysis of diazomethane-kinetics and mechanism." J Am Chem Soc **102**: 7303-7308.

McGirt, M. J., K. D. Than, et al. (2009). "Gliadel (BCNU) wafer plus concomitant temozolomide therapy after primary resection of glioblastoma multiforme." J Neurosurg **110**(3): 583-8.

Meetei, A. R., J. P. de Winter, et al. (2003). "A novel ubiquitin ligase is deficient in Fanconi anemia." Nat Genet **35**(2): 165-70.

Melo, S. A., S. Ropero, et al. (2009). "A TARBP2 mutation in human cancer impairs microRNA processing and DICER1 function." Nat Genet **41**(3): 365-70.

Meng, R. D., C. C. Shelton, et al. (2009). "gamma-Secretase inhibitors abrogate oxaliplatin-induced activation of the Notch-1 signaling pathway in colon cancer cells resulting in enhanced chemosensitivity." Cancer Res **69**(2): 573-82.

Ménissier de Murcia, J., M. Ricoul, et al. (2003). "Functional interaction between PARP-1 and PARP-2 in chromosome stability and embryonic development in mouse." THe EMBO Journal **22**(9): 2255-2263.

Middlemas, D. S., C. F. Stewart, et al. (2000). "Biochemical correlates of temozolomide sensitivity in pediatric solid tumor xenograft models." Clin Cancer Res **6**(3): 998-1007.

Mihaliak, A. M., C. A. Gilbert, et al. (2010). "Clinically relevant doses of chemotherapy agents reversibly block formation of glioblastoma neurospheres." Cancer Lett **296**(2): 168-77.

Milano, M. T., P. Okunieff, et al. (2010). "Patterns and timing of recurrence after temozolomide-based chemoradiation for glioblastoma." Int J Radiat Oncol Biol Phys **78**(4): 1147-55.

Mirna Therapeutics, I. (2015). "A Multicenter Phase I Study of MRX34, MicroRNA miR-RX34 Liposomal Injection." NCT01829971 https://www.clinicaltrials.gov/ct2/show/NCT01829971?term=MRX34&rank=1.

Misso, G., M. T. Di Martino, et al. (2014). "Mir-34: a new weapon against cancer?" Mol Ther Nucleic Acids **3**: e194.

Nakano, I., M. Masterman-Smith, et al. (2008). "Maternal embryonic leucine zipper kinase is a key regulator of the proliferation of malignant brain tumors, including brain tumor stem cells." J Neurosci Res **86**(1): 48-60.

Norden, A. D., G. J. Lesser, et al. (2013). "Phase 2 study of dose-intense temozolomide in recurrent glioblastoma." Neuro Oncol **15**(7): 930-5.

Novello, C., L. Pazzaglia, et al. (2014). "p53-dependent activation of microRNA-34a in response to etoposide-induced DNA damage in osteosarcoma cell lines not impaired by dominant negative p53 expression." PLoS One **9**(12): e114757.

Ohgaki, H. and P. Kleihues (2013). "The definition of primary and secondary glioblastoma." Clin Cancer Res **19**(4): 764-72.

Orom, U. A., F. C. Nielsen, et al. (2008). "MicroRNA-10a binds the 5'UTR of ribosomal protein mRNAs and enhances their translation." Mol Cell **30**(4): 460-71.

Pal, T., J. Permuth-Wey, et al. (2008). "A review of the clinical relevance of mismatch-repair deficiency in ovarian cancer." Cancer **113**(4): 733-42.

Panchision, D. M., H. L. Chen, et al. (2007). "Optimized flow cytometric analysis of central nervous system tissue reveals novel functional relationships among cells expressing CD133, CD15, and CD24." Stem Cells **25**(6): 1560-70.

Pang, R. T., C. O. Leung, et al. (2010). "MicroRNA-34a suppresses invasion through downregulation of Notch1 and Jagged1 in cervical carcinoma and choriocarcinoma cells." Carcinogenesis **31**(6): 1037-44.

Panigrahi, M., P. K. Das, et al. (2011). "Brain tumor and Gliadel wafer treatment." Indian journal of cancer **48**(1): 11-7.

Park, C. K., J. E. Kim, et al. (2012). "The Changes in MGMT Promoter Methylation Status in Initial and Recurrent Glioblastomas." Transl Oncol **5**(5): 393-7.

Park, D. M. and J. N. Rich (2009). "Biology of glioma cancer stem cells." Mol Cells **28**(1): 7-12.

Parsons, D. W., S. Jones, et al. (2008). "An integrated genomic analysis of human glioblastoma multiforme." Science **321**(5897): 1807-12.

Pasquinelli, A. E., B. J. Reinhart, et al. (2000). "Conservation of the sequence and temporal expression of let-7 heterochronic regulatory RNA." Nature **408**(6808): 86-9.

Pastorino, F., C. Brignole, et al. (2013). "Nanocarrier-mediated targeting of tumor and tumor vascular cells improves uptake and penetration of drugs into neuroblastoma." Front Oncol **3**: 190.

Pastrana, E., V. Silva-Vargas, et al. (2011). "Eyes wide open: a critical review of sphere-formation as an assay for stem cells." Cell Stem Cell **8**(5): 486-98.

Patil, A. A., P. Sayal, et al. (2014). "FANCD2 re-expression is associated with glioma grade and chemical inhibition of the Fanconi Anaemia pathway sensitises gliomas to chemotherapeutic agents." Oncotarget **5**(15): 6414-6424.

Paul, I., S. Bhattacharya, et al. (2013). "Current Understanding on EGFR and Wnt/beta-Catenin Signaling in Glioma and Their Possible Crosstalk." Genes Cancer **4**(11-12): 427-46.

Pegg, A. E. (2000). "Repair of O(6)-alkylguanine by alkyltransferases." Mutation research **462**(2-3): 83-100.

Pei, C., H. Chen, et al. (2013). "A high frequency of MSH6 G268A polymorphism and survival association in glioblastoma." The International journal of neuroscience **123**(2): 114-20.

Perry, J., A. Chambers, et al. (2007). "Gliadel wafers in the treatment of malignant glioma: a systematic review." Current oncology **14**(5): 189-94.

Perry, J., M. Okamoto, et al. (2012). "Novel therapies in glioblastoma." Neurol Res Int **2012**: 428565.

Phillips, R. M. and T. H. Ward (2001). "Influence of extracellular pH on the cytotoxicity and DNA damage of a series of indolequinone compounds." Anticancer research **21**(3B): 1795-801.

Phuphanich, S., J. G. Supko, et al. (2010). "Phase 1 clinical trial of bortezomib in adults with recurrent malignant glioma." J Neurooncol **100**(1): 95-103.

Platet, N., S. Y. Liu, et al. (2007). "Influence of oxygen tension on CD133 phenotype in human glioma cell cultures." Cancer Lett **258**(2): 286-90.

Pletsas, D., E. A. Garelnabi, et al. (2013). "Synthesis and Quantitative Structure-Activity Relationship of Imidazotetrazine Prodrugs with Activity Independent of O6-

Methylguanine-DNA-methyltransferase, DNA Mismatch Repair, and p53." J Med Chem **56**: 7120-7132.

Pletsas, D., R. T. Wheelhouse, et al. (2006). "Polar, functionalized guanine-O6 derivatives resistant to repair by O6-alkylguanine-DNA alkyltransferase: implications for the design of DNA-modifying drugs." Eur J Med Chem **41**(3): 330-9.

Pratt, W. B., R. W. Ruddon, et al. (1994). Anticancer Drugs. New York Citty, Oxford University Press.

Prensner, J. R. and A. M. Chinnaiyan (2011). "Metabolism unhinged: IDH mutations in cancer." Nature medicine **17**(3): 291-3.

Purow, B. W., T. K. Sundaresan, et al. (2008). "Notch-1 regulates transcription of the epidermal growth factor receptor through p53." Carcinogenesis **29**(5): 918-25.

Qian, X., Y. Ren, et al. (2012). "Sequence-dependent synergistic inhibition of human glioma cell lines by combined temozolomide and miR-21 inhibitor gene therapy." Mol Pharm **9**(9): 2636-45.

Quinn, J. A., A. Desjardins, et al. (2005). "Phase I trial of temozolomide plus O6-benzylguanine for patients with recurrent or progressive malignant glioma." J Clin Oncol **23**(28): 7178-87.

Quintavalle, C., D. Mangani, et al. (2013). "MiR-221/222 target the DNA methyltransferase MGMT in glioma cells." PLoS One **8**(9): e74466.

Ramirez, Y. P., J. L. Weatherbee, et al. (2013). "Glioblastoma Multiforme Therapy and Mechanisms of Resistance." Pharmaceuticals **6**(12): 1475-1506.

Rathod, S. S., S. B. Rani, et al. (2014). "Tumor suppressive miRNA-34a suppresses cell proliferation and tumor growth of glioma stem cells by targeting Akt and Wnt signaling pathways." FEBS Open Bio **4**: 485-95.

Real, P. J., V. Tosello, et al. (2009). "Gamma-secretase inhibitors reverse glucocorticoid resistance in T cell acute lymphoblastic leukemia." Nat Med **15**(1): 50-8.

Reese, J. S., X. Qin, et al. (2001). "MGMT expression in murine bone marrow is a major determinant of animal survival after alkylating agent exposure." Journal of hematotherapy & stem cell research **10**(1): 115-23.

Rellecke, P., K. Kuchelmeister, et al. (2004). "Mismatch repair protein hMSH2 in primary drug resistance in in vitro human malignant gliomas." J Neurosurg **101**(4): 653-8.

Roccio, M., D. Schmitter, et al. (2013). "Predicting stem cell fate changes by differential cell cycle progression patterns." Development **140**(2): 459-70.

Rodrigues, A., B. Gomes, et al. (2013). "DNA Repair and Resistance to Cancer Therapy."

Rohle, D., J. Popovici-Muller, et al. (2013). "An inhibitor of mutant IDH1 delays growth and promotes differentiation of glioma cells." Science **340**(6132): 626-30.

Roos, W. P., T. Nikolova, et al. (2009). "Brca2/Xrcc2 dependent HR, but not NHEJ, is required for protection against O(6)-methylguanine triggered apoptosis, DSBs and chromosomal aberrations by a process leading to SCEs." DNA Repair (Amst) **8**(1): 72-86.

Safa, A. R., M. R. Saadatzadeh, et al. (2015). "Glioblastoma stem cells (GSCs) epigenetic plasticity and interconversion between differentiated non-GSCs and GSCs." Genes Dis **2**(2): 152-163.

Saleem, A., G. D. Brown, et al. (2003). "Metabolic activation of temozolomide measured in vivo using positron emission tomography." Cancer Res **63**(10): 2409-15.

Samimi, G., D. Fink, et al. (2000). "Analysis of MLH1 and MSH2 expression in ovarian cancer before and after platinum drug-based chemotherapy." Clinical Cancer Research **6**(4): 1415-1421.

Sato, A., J. Sunayama, et al. (2011). "MEK-ERK signaling dictates DNA-repair gene MGMT expression and temozolomide resistance of stem-like glioblastoma cells via the MDM2-p53 axis." Stem Cells **29**(12): 1942-51.

Sato, Y., A. Kurose, et al. (2009). "Diversity of DNA damage response of astrocytes and glioblastoma cell lines with various p53 status to treatment with etoposide and temozolomide." Cancer Biology & Therapy **8**(5): 452-457.

Savjani, K. T., A. K. Gajjar, et al. (2012). "Drug solubility: importance and enhancement techniques." ISRN Pharm **2012**: 195727.

Sen, A., M. S. Kallos, et al. (2004). "New tissue dissociation protocol for scaled-up production of neural stem cells in suspension bioreactors." Tissue Eng **10**(5-6): 904-13.

Shealy, Y. F. and C. A. Krauth (1966). "Imidazoles. II. 5(or 4)-(Monosubstituted triazeno)imidazole-4(or 5)-carboxamides." J Med Chem **9**(1): 35-8.

Shi, L., J. Chen, et al. (2010). "MiR-21 protected human glioblastoma U87MG cells from chemotherapeutic drug temozolomide induced apoptosis by decreasing Bax/Bcl-2 ratio and caspase-3 activity." Brain Res **1352**: 255-64.

Shi, L., S. Zhang, et al. (2013). "MiR-200c increases the radiosensitivity of non-small-cell lung cancer cell line A549 by targeting VEGF-VEGFR2 pathway." PLoS One **8**(10): e78344.

Shinsato, Y., T. Furukawa, et al. (2013). "Reduction of MLH1 and PMS2 confers temozolomide resistance and is associated with recurrence of glioblastoma." Oncotarget **4**(12): 2261-70.

Simon, J. A. and C. A. Lange (2008). "Roles of the EZH2 histone methyltransferase in cancer epigenetics." Mutat Res **647**(1-2): 21-9.

Singh, S. K., I. D. Clarke, et al. (2003). "Identification of a cancer stem cell in human brain tumors." Cancer Res **63**(18): 5821-8.

Singh, S. K., C. Hawkins, et al. (2004). "Identification of human brain tumour initiating cells." Nature **432**(7015): 396-401.

Song, G., Y. Zhang, et al. (2009). "MicroRNA-206 targets notch3, activates apoptosis, and inhibits tumor cell migration and focus formation." J Biol Chem **284**(46): 31921-7.

Spiro, T. P., L. Liu, et al. (2001). "Temozolomide: the effect of once- and twice-a-day dosing on tumor tissue levels of the DNA repair protein O(6)-alkylguanine-DNA-alkyltransferase." Clin Cancer Res **7**(8): 2309-17.

Srinivasan, A. and B. Gold (2012). "Small-molecule inhibitors of DNA damage-repair pathways: an approach to overcome tumor resistance to alkylating anticancer drugs." Future medicinal chemistry **4**(9): 1093-111.

Stark, A. M., A. Doukas, et al. (2010). "The expression of mismatch repair proteins MLH1, MSH2 and MSH6 correlates with the Ki67 proliferation index and survival in patients with recurrent glioblastoma." Neurol Res **32**(8): 816-20.

Stevens, M. F., J. A. Hickman, et al. (1987). "Antitumor activity and pharmacokinetics in mice of 8-carbamoyl-3-methyl-imidazo[5,1-d]-1,2,3,5-tetrazin-4(3H)-one (CCRG 81045; M & B 39831), a novel drug with potential as an alternative to dacarbazine." Cancer Res **47**(22): 5846-52.

Stupp, R., M. E. Hegi, et al. (2009). "Effects of radiotherapy with concomitant and adjuvant temozolomide versus radiotherapy alone on survival in glioblastoma in a randomised phase III study: 5-year analysis of the EORTC-NCIC trial." Lancet Oncol **10**: 2960-2965.

Stupp, R., W. P. Mason, et al. (2005). "Radiotherapy plus concomitant and adjuvant temozolomide for glioblastoma." N Engl J Med **352**(10): 987-96.

Sun, F., M. Wan, et al. (2014). "Crosstalk between miR-34a and Notch Signaling Promotes Differentiation in Apical Papilla Stem Cells (SCAPs)." J Dent Res **93**(6): 589-595.

Suva, M. L., E. Rheinbay, et al. (2014). "Reconstructing and reprogramming the tumor-propagating potential of glioblastoma stem-like cells." Cell **157**(3): 580-94.

Suva, M. L., N. Riggi, et al. (2009). "EZH2 is essential for glioblastoma cancer stem cell maintenance." Cancer Res **69**(24): 9211-8.

Svilar, D., M. Dyavaiah, et al. (2012). "Alkylation Sensitivity Screens Reveal a Conserved Cross-species Functionome." Mol Cancer Res **10**(12): 1580-96.

Svilar, D., M. Dyavaiah, et al. (2012). "Alkylation sensitivity screens reveal a conserved cross-species functionome." Mol Cancer Res **10**(12): 1580-96.

Tazawa, H., N. Tsuchiya, et al. (2007). "Tumor-suppressive miR-34a induces senescence-like growth arrest through modulation of the E2F pathway in human colon cancer cells." Proc Natl Acad Sci U S A **104**(39): 15472-7.

Tolcher, A. W., S. L. Gerson, et al. (2003). "Marked inactivation of O6-alkylguanine-DNA alkyltransferase activity with protracted temozolomide schedules." Br J Cancer **88**(7): 1004-11.

Trojan, J., S. Zeuzem, et al. (2002). "Functional analysis of hMLH1 variants and HNPCC-related mutations using a human expression system." Gastroenterology **122**(1): 211-219.

Tsutsui, Y., K. Tomizawa, et al. (2007). "Development of bionanocapsules targeting brain tumors." J Control Release **122**(2): 159-64.

Tunca, B., G. Tezcan, et al. (2012). "Olea europaea leaf extract alters microRNA expression in human glioblastoma cells." J Cancer Res Clin Oncol **138**(11): 1831-44.

Turriziani, M., P. Caporaso, et al. (2006). "O6-(4-bromothenyl)guanine (PaTrin-2), a novel inhibitor of O6-alkylguanine DNA alkyl-transferase, increases the inhibitory activity of temozolomide against human acute leukaemia cells in vitro." Pharmacol Res **53**(4): 317-23.

Ujifuku, K., N. Mitsutake, et al. (2010). "miR-195, miR-455-3p and miR-10a(*) are implicated in acquired temozolomide resistance in glioblastoma multiforme cells." Cancer Lett **296**(2): 241-8.

van Es, J. H., M. E. van Gijn, et al. (2005). "Notch/gamma-secretase inhibition turns proliferative cells in intestinal crypts and adenomas into goblet cells." Nature **435**(7044): 959-63.

van Nifterik, K. A., J. van den Berg, et al. (2010). "Absence of the MGMT protein as well as methylation of the MGMT promoter predict the sensitivity for temozolomide." Br J Cancer **103**(1): 29-35.

Varghese, M., H. Olstorn, et al. (2008). "A comparison between stem cells from the adult human brain and from brain tumors." Neurosurgery **63**(6): 1022-33; discussion 1033-4.

Veliz, I., Y. Loo, et al. (2015). "Advances and challenges in the molecular biology and treatment of glioblastoma-is there any hope for the future?" Ann Transl Med **3**(1): 7.

Venere, M., H. A. Fine, et al. (2011). "Cancer stem cells in gliomas: Identifying and understanding the apex cell in cancer's hierarchy." Glia **59**(8): 1148-54.

Viel, T., P. Monfared, et al. (2013). "Optimizing glioblastoma temozolomide chemotherapy employing lentiviral-based anti-MGMT shRNA technology." Molecular therapy : the journal of the American Society of Gene Therapy **21**(3): 570-9.

Villalva, C., U. Cortes, et al. (2012). "O6-Methylguanine-methyltransferase (MGMT) promoter methylation status in glioma stem-like cells is correlated to Temozolomide sensitivity under differentiation-promoting conditions." International journal of molecular sciences **13**(6): 6983-94.

Vlachostergios, P. J., E. Hatzidaki, et al. (2013). "Bortezomib downregulates MGMT expression in T98G glioblastoma cells." Cell Mol Neurobiol **33**(3): 313-8.

Vukicevic, V., A. Jauch, et al. (2010). "Genetic instability and diminished differentiation capacity in long-term cultured mouse neurosphere cells." Mech Ageing Dev **131**(2): 124-32.

Wang, A. T. and A. Smogorzewska (2015). "SnapShot: Fanconi anemia and associated proteins." Cell **160**(1-2): 354-354 e1.

Wang, F., J. Travins, et al. (2013). "Targeted inhibition of mutant IDH2 in leukemia cells induces cellular differentiation." Science **340**(6132): 622-6.

Wang, J., P. O. Sakariassen, et al. (2008). "CD133 negative glioma cells form tumors in nude rats and give rise to CD133 positive cells." Int J Cancer **122**(4): 761-8.

Wang, R., K. Chadalavada, et al. (2010). "Glioblastoma stem-like cells give rise to tumour endothelium." Nature **468**(7325): 829-33.

Weeraratne, S. D., V. Amani, et al. (2011). "miR-34a confers chemosensitivity through modulation of MAGE-A and p53 in medulloblastoma." Neuro Oncol **13**(2): 165-75.

Wei-Yu Chen, S.-Y. L., Yung-Sheng Chang, Juan Juan Yin, Hsiu-lien Yeh, Tarek H. Mouhieddine, Ola Hadadeh, Wassim Abou-Kheir, Yen-Nien Liu (2014). "MicroRNA-34a regulates WNT/TCF7 signaling and inhibits bone metastasis in Ras-activated prostate cancer." Oncotarget **6**(1).

Wen, P. Y. and S. Kesari (2008). "Malignant gliomas in adults." N Engl J Med **359**(5): 492-507.

Wheelhouse, R. T. and M. F. G. Stevens (1993). "Decomposition of the antitumour drug Temozolomide in deuterated phosphate buffer: methyl group transfer is accompanied by deuterium exchange." J Chem Soc, Chem Commun: 1177.

White, D. E., D. Negorev, et al. (2006). "KAP1, a novel substrate for PIKK family members, colocalizes with numerous damage response factors at DNA lesions." Cancer research **66**(24): 11594-9.

Wightman, B., I. Ha, et al. (1993). "Posttranscriptional regulation of the heterochronic gene lin-14 by lin-4 mediates temporal pattern formation in C. elegans." Cell **75**(5): 855-62.

Wilson, J. B., K. Yamamoto, et al. (2008). "FANCG promotes formation of a newly identified protein complex containing BRCA2, FANCD2 and XRCC3." Oncogene **27**(26): 3641-52.

Winter, J., S. Jung, et al. (2009). "Many roads to maturity: microRNA biogenesis pathways and their regulation." Nat Cell Biol **11**(3): 228-34.

Wong, H. K., R. E. Fatimy, et al. (2015). "The Cancer Genome Atlas Analysis Predicts MicroRNA for Targeting Cancer Growth and Vascularization in Glioblastoma." Mol Ther **23**(7): 1234-47.

Xie, J., S. L. Ameres, et al. (2012). "Long-term, efficient inhibition of microRNA function in mice using rAAV vectors." Nat Methods **9**(4): 403-9.

Yamakuchi, M., M. Ferlito, et al. (2008). "miR-34a repression of SIRT1 regulates apoptosis." Proc Natl Acad Sci U S A **105**(36): 13421-6.

Yang, G., D. Han, et al. (2014). "MiR-196a exerts its oncogenic effect in glioblastoma multiforme by inhibition of IkappaBalpha both in vitro and in vivo." Neuro Oncol **16**(5): 652-61.

Yin, D., S. Ogawa, et al. (2013). "miR-34a functions as a tumor suppressor modulating EGFR in glioblastoma multiforme." Oncogene **32**(9): 1155-63.

Yip, S., J. Miao, et al. (2009). "MSH6 mutations arise in glioblastomas during temozolomide therapy and mediate temozolomide resistance." Clin Cancer Res **15**(14): 4622-9.

Yu, B., H. C. Tai, et al. (2010). "Receptor-targeted nanocarriers for therapeutic delivery to cancer." Mol Membr Biol **27**(7): 286-98.

Yu, F., Y. Jiao, et al. (2012). "MicroRNA 34c gene down-regulation via DNA methylation promotes self-renewal and epithelial-mesenchymal transition in breast tumor-initiating cells." J Biol Chem **287**(1): 465-73.

Zhang, C., L. M. Moore, et al. (2013). "IDH1/2 mutations target a key hallmark of cancer by deregulating cellular metabolism in glioma." Neuro Oncol **15**(9): 1114-26.

Zhang, J., M. F. Stevens, et al. (2012). "Temozolomide: mechanisms of action, repair and resistance." Current molecular pharmacology **5**(1): 102-14.

Zhang, J., M. F. Stevens, et al. (2011). "Certain imidazotetrazines escape O6-methylguanine-DNA methyltransferase and mismatch repair." Oncology **80**(3-4): 195-207.

Zhang, S., Y. Wan, et al. (2012). "MicroRNA-21 inhibitor sensitizes human glioblastoma U251 stem cells to chemotherapeutic drug temozolomide." J Mol Neurosci **47**(2): 346-56.

Zhang, W., J. Zhang, et al. (2012). "miR-181d: a predictive glioblastoma biomarker that downregulates MGMT expression." Neuro Oncol **14**(6): 712-9.

Zhang, X., T. Chen, et al. (2012). "Notch1 promotes glioma cell migration and invasion by stimulating beta-catenin and NF-kappaB signaling via AKT activation." Cancer Sci **103**(2): 181-90.

Zhao, J., P. Lammers, et al. (2013). "TP53-independent function of miR-34a via HDAC1 and p21(CIP1/WAF1.)." Mol Ther **21**(9): 1678-86.

Zhao, T., J. Li, et al. (2010). "MicroRNA-34a induces endothelial progenitor cell senescence and impedes its angiogenesis via suppressing silent information regulator 1." Am J Physiol Endocrinol Metab **299**(1): E110-6.

Zielske, S. P. and S. L. Gerson (2002). "Lentiviral transduction of P140K MGMT into human CD34(+) hematopoietic progenitors at low multiplicity of infection confers significant resistance to BG/BCNU and allows selection in vitro." Mol Ther **5**(4): 381-7.